DESIGN STUDY FOR A GAMMA RAY SPECTROMETER FOR INTENSE GAMMA FIELDS

FINAL REPORT

Prepared under Contract NAS8-25617

for

National Aeronautics and Space Administration
George C. Marshall Space Flight Center
Alabama 35812

Space Sciences Laboratory
GENERAL ELECTRIC COMPANY
SPACE DIVISION
P.O. Box 8555
Philadelphia, Pennsylvania 19101

10 December 1970

DESIGN STUDY FOR A GAMMA RAY SPECTROMETER FOR INTENSE GAMMA FIELDS

FINAL REPORT

Prepared under Contract No. NAS8-25617

for

National Aeronautics and Space Administration
George C. Marshall Space Flight Center
Alabama 35812

Prepared by:

W. E. Austin, Principal Investigator
Applied Physics Section

Space Sciences Laboratory
GENERAL ELECTRIC COMPANY
SPACE DIVISION
P.O. Box 8555
Philadelphia, Pennsylvania 19101

ABSTRACT

This study was conducted for the NASA Marshall Space Flight Center under contract number NAS8-2617 to design a gamma ray spectrometer for use in intense gamma fields of 10^2 R hr^{-1} to 10^6 R hr^{-1}. A literature survey was conducted and the design approach selected uses Compton scatter attenuation to reduce the flux intensity to values suitable for spectral measurements. Other physical interactions are shown to have little effect on the Compton shifted energy spectrum.

Sum-Compton spectral detectors are selected to give pulse height data directly convertable to the gamma spectrum through the detector energy response function and the Compton energy shift. Calculations of the fast neutron flux rate effect on these detectors indicated that flux intensities to 10^9 n cm^{-2} sec^{-1} can be tolerated.

Three Compton targets are used to maintain the count rates between 500 and 10^4 sec^{-1} over the four decades of incident gamma intensity. The electronic functions are specified and a spectrometer head conceptual design is proposed. The design weighs approximately 130 pounds, largely due to the necessary tungsten alloy shield.

Page

TABLE OF CONTENTS

Page

Page

LIST OF FIGURES

SECTION 1.0
INTRODUCTION AND SUMMARY

This report discusses the design of a gamma ray spectrometer capable of gamma spectral measurements in radiation fields of 10^2 R/hr to 10^6 R/hr. The work was performed by the General Electric Company, Space Sciences Laboratory under the National Aeronautical and Space Admistration contract No. NAS8-25617. The study conducted was theoretical, and no experiments were conducted to support the design. The theoretical relationships and the projected designs are based on prior experimental knowledge published in the literature by many contributors, and, therefore, we have every expectation that the designed spectrometer will function as described.

In Section 2.0, we give a brief summary of gamma spectroscopy techniques, the problems associated with the contemplated measurements and the anticipated solution to these problems. Section 3.0 is devoted largely to the physics of Compton scatter, the investigation of competing reactions and the deduction of the effect of competing reactions.

In Section 4.0, we discuss the problems associated with obtaining the spectrum of a continuous gamma source and show the excellent characteristics of the sum-Compton detector system for measuring continuous spectra. We describe computer computations performed to determine the peak to tail ratio of various sum-Compton configurations and give the results for four geometries.

In the fifth section, we examine the effects of fast neutrons on the detectors and the attenuation of fast neutrons in the gamma shield. We conclude that the gamma spectral measurements can be performed in the neutron environment above the liquid hydrogen tank, but not below the tank. In Section 6.0 we derive the gamma shield requirements by computing the detector interaction rate for a fission gamma spectrum through the tungsten shield. The shield thickness largely controls the weight of the spectrometer, and the effects of shield leakage background will be only during the final few minutes of the measurement.

We discuss counting rate effects, including accidental coincidence pulse rates, in Section 7.0.

Section 8.0 considers various aspects of the final design. A need for two detector systems, one for the low energy portion of the spectrum and the other for the high energy portion of the spectrum, with considerable overlap in the spectral coverage, is demonstrated to obtain statistical accuracy. The energy resolution of the total gamma ray spectrometer is shown to meet the contractual design goals. The cooling requirements for the semiconductor sum-Compton detectors is discussed and a solid CO_2 source of cryogenic cooling is proposed. Other detection methods are discussed and an alternate single crystal scintillation detector is suggested as an alternate detector, at a saving of weight and simplified electronics, but at the expense of a definitive measurement.

Section 9.0 indicates the electronic circuitry requirements in functional form and shows the design of the spectrometer head.

SECTION 2.0
GAMMA RAY SPECTROSCOPY

It is not the purpose of this study to present a short course in gamma interaction and spectroscopy and we will only briefly discuss these topics as an introduction to the design philosophy. The reader is referred to the excellent book edited by Kai Siegbahn[1] for a rather complete discussion of spectroscopy techniques and methods.

2.1 INTERACTION OF GAMMA RADIATION WITH MATTER

Gamma photons are removed from a beam individually and in single events and this leads to the familiar relationship

$$I = I_o \exp\left[-\mu_o x\right] \tag{2.1}$$

for narrow beam attenuation.

where I_o is the incident flux

I is the uncollided flux

μ_o is the total absorption coefficient

and x is the absorber thickness.

The product μ_o is dimensionless, and as x may have units of cm, g cm^{-2}, atoms cm^{-2}, or electrons cm^{-2}, the absorption coefficient may be expressed as cm^{-1}, $cm^2\ g^{-1}$, cm^2 $atom^{-1}$, or cm^{-2} $electron^{-1}$. The absorption coefficient is the sum.

$$\mu_o = \sigma_a + \sigma_s + \tau + K \tag{2.2}$$

and σ_a is the Compton absorption coefficient

σ_s is the scattering (mere deflection) coefficient

τ is the photoelectric absorption coefficient

K is the pair production absorption coefficient

All of these coefficients are energy dependent and atomic number (Z) dependent Photoelectric absorption is dominant for low photon energies, the Compton effect is dominant at middle energies (around 1 MeV) and the pair production effect is dominant for high energy gamma radiation.

Evans[2] and many other fine texts discuss these reactions and cross sections in detail, and we only briefly discuss the effects as they pertain to gamma ray spectroscopy. In later portions of the study, we will examine these effects in detail as they pertain to the immediate design effort, particularly the Compton effect.

2.1.1 The Photoelectric Effect

The photoelectric effect consists of the complete absorption of all the energy of a photon by a bound electron. The photoelectron is ejected with an energy equal to the photon energy minus the binding energy of that electron. An X-ray with an energy corresponding to this binding energy, results as the photoelectron vacancy is filled with a free electron or one from a more loosely bound shell. These X-rays may, or may not, escape a gamma spectral detector.

For spectroscopy purposes, the photoelectric effect results in a signal directly related to the photon energy (except for the X-ray escape probability) and total absorption gamma ray spectroscopy is easily achievable for low energy photons.

2.1.2 Scattering Effects

Photons can be scattered by atomic electrons with or without the loss of energy. Coherent scattering results in the mere changing of direction of the photon. The well known Compton effect results in the partial loss of photon energy to an electron as well as a change in the photon direction. The equations relating to the transfer of energy and angle of scatter are well known and have been experimentally verified, and we will discuss them in detail in a later and more appropriate section.

The Compton effect produces a multitude of signal events in a detector system. These may be distinguished from the photopeaks for a single or a few differing monoenergetic gamma lines, but for a continuous gamm spectrum, they lead to a pulse height distribution not easily converted to a gamma spectrum. Mathematical unfolding techniques, based on a matrix of detector response curves, are often employed to unfold a pulse height distribtion into an incident gamma spectrum. Other experimental methods, suppress the Compton contribution by anticoincidence techniques or count only Compton events by two detector coincidence techniques.

2.1.3 Pair Production

Gamma rays, exceeding 1.022 MeV in energy, may create electron-positron pairs in the field of a nucleons or electron. The combined kinetic energy of the pair equals the photon energy minus the rest mass of this pair. This effect becomes increasingly dominant at higher energies.

Pair spectrometers can consist of three detectors with collimated gamma radiation incident on the center detector. The other two detectors, placed diametrically opposing each other about the central detector, can indicate the

occurrence of pair production absorption in the center detector by coincident detection of the 511 keV. positron annihilation quanta. The simultaneous measure of the kinetic energy of the pair indicates the initial photon energy.

2.1.4 Summary of Gamma Interactions

The aforementioned interactions are the most probable processes for gamma ray absorption. A summary and brief description of gamma interactions are shown in Table 2.1.

The three important interactions are photoelectric absorption Compton scattering and pair production. For wide energy gamma ray spectroscopy, the problem is to determine which events were produced by which process, as the fraction of the incident photon energy losses in the detector varies with each process. Various spectrometer designs have been used to recognize the type of event by detector arrangement and electronic circuitry.

2.2 GAMMA RAY SPECTROMETERS

The earliest means of gamma ray spectroscopy was crystal diffraction and the wavelength of radium gamma rays were measured by Rutherford and Andrade[3]. Crystal diffraction is still one of the most precise tools for gamma spectroscopy but the development of the scintillation detector coupled to the photomultiplier in 1944[4] blossomed into a versatile and widely used tool. The development of NaI (Tl)[5] and other alkali halide crystals and techniques for growing large crystals produced simple and excellent spectrometers for general laboratory use. Gas filled counters have long been used[6] for the detection of gamma rays and the proportional counter[7] has superior energy resolution. Gas filled counters suffer from low efficiency for high energy gamma radiation and are also comparably slow in response time.

Table 2.1

Process	Notation	Description	Name	Z Dependent	Remarks
Photoelectric	τ	Full energy to bound electron		$\sim Z^5$	Decreases $\sim E^{-28}$
Electron	σ	Coherent scattering	Rayleigh and Nuclear Resonance	Z^2 to Z^3	Bound electron scattering
	σ	Coherent	Thompson	Z	Energy dependent
	σ	Incoherent	Compton	Z	Decreases slowly with E
Nuclear Scattering	σ	With bulk material	Mossbauer effect		Nuclear resonance at very low energies
	σ	Nuclear resonance		Z^2	Coherent
	σ	Nuclear coherent Scattering	Nuclear Thompson Scatter	Z^4	Independent of E
	σ	Nuclear incoherent scattering	Nuclear Compton Scatter		>100 MeV
Coulomb Field Interactions	K	Pair production	Nuclear	Z^2	>1.022 MeV
	K	Pair production	Electron	Z	>1.022 MeV
Photonuclear Absorption		(γ, P) (γ, n) (γ, f) etc.			

The advent of semiconductor ionization detectors during the past fifteen years has given the experimenter additional tools with unique gamma spectroscopy properties. The ion drift[8] construction technique has increased the intrinsic region so that large volume solid state detectors are available with good efficiency to high energy gamma radiation as well as superior energy resolution.

2.2.1 Scintillation Detectors

Scintillation detectors are composed of a medium in which ionizing particles produce light and a photomultiplier tube which converts the light to electrons and then multiplies the number of electrons to large detectable signals. The scintillation light pulse is nearly directly proportional to the energy lost by the charged particle in the scintillator and as the photomultiplier gain is essentially constant (with fixed operating parameters) resulting in a spectrometer in which the electric charge per pulse is proportional to the particle energy loss. The charge produces a voltage across the capacitance at the output of the photomultiplier tube, and this voltage pulse may be amplified and measured through pulse height analysis circuitry. A pulse height distribution is obtained by observing many such events. A differential pulse height distribution is a graphical plot of the number of events lying between E and $E + \Delta E$ for all values of E. Event with a monoenergetic source of radiation, the differential distribution of pulse heights exhibits a Gaussian shape and the energy resolution is generally expressed as the ratio of the full width of this curve to the mean energy, $\Delta E/E$, measured at the half maximum amplitude. Many factors contribute to the energy resolution of a scintillation detector, but are not the immediate subject of this study.

A concise and thorough review of scintillation counters was written by Matt and Sutton[9] among others. A series of twelve conferences[10-21] have been held over the years on scintillation counter techniques, methods, and measurements

and these conferences have also included semiconductor counter techniques since 1962. Improvements in crystal quality and size and progress in photomultiplier design have maintained a steady advance in the state of the scintillation spectroscopy art.

Scintillation counters are used for all of the charged particles and for neutron detection and spectroscopy, but the widest application is for gamma ray spectroscopy. The gamma rays interact with the three processes briefly discussed above, and this results in a distribution of pulse heights not directly reducible to the gamma spectrum. Experimental techniques have been employed to make the pulse height distribution more readily convertable to a gamma spectrum.

Large single crystals have been used as total absorption spectrometers and have reduced the Compton scatter effect on the pulse height distribution, particularly when the incident photon beam is collimated toward the center of the detector. Nearly complete absorption of multiple Compton events is achieved although the backscatter ($\theta = 180^{o}$) component remains. Large crystals are expensive and exhibit poorer energy resolution than small crystals and has led to the use of coincidence and anticoincident configurations using multiple crystals, arranged as the experiment demanded.

One approach[22, 23] is to surround a small crystal by a larger crystal and to reduce Comtpon and pair production events by anticoincidence circuitry. Hofstadter and McIntyre[24] first developed the two crystal coincidence spectrometer which selects Compton events only. The gamma rays incident on the first crystal from a known direction fixes the scatter angle to the second detector, and measurement of the pulse amplitude from the first scattering crystal allows calculation of the incident photon energy. Later techniques have used pulse

height selection[25] in the second crystal to improve the energy resolution in the primary crystal, and the summing of the energy deposited in coincidence in the two detectors. The sum Compton spectrometer has taken advantage of the superior energy resolution of Ge (Li) solid state detectors and has improved the photopeak to total ratio[26] to 400 to 1 for 66 keV and 360 to 1 for 1120 keV gamma radiation.

The disadvantage of the sum Compton technique is the low efficiency ($\sim 10^{-4}$) but this is of no great concern in the high intensity radiation fields toward which this study is directed. The advantage of the sum Compton spectrometer is the high peak to total ratio obtained so that direct conversion of the pulse height distribution to the gamma spectrum is possible, correcting only for the system efficiency as a function of energy. The energy response is a function of the detector geometry and will be discussed in detail later in this study.

Another spectrometer approach is the three crystal pair spectrometer[27, 28, 29] in which triple coincidence is required, detecting the two annihilation quanta simultaneously with the kinetic energy of the created pair. This approach has been improved[30] for energy resolution by using a Ge (Li) detector as the center detector, and efficiencies are improved by an order of magnitude by requiring capture of only one annihilation quanta, although secondary single escape peaks are thus generated. For NaI (Tl) scintillation detectors, the pair spectrometer is comparable in efficiency to the sum Compton spectrometer, but would be much less for a Si(Ge) detector or other low Z central detector.

Many types of scintillation materials are available and in use, but the most important phosphor is NaI (Tl). Energy resolutions of 7.5% at 662 KeV are common with NaI (Tl) spectrometers of relatively small crystal size. The efficiency and energy response of various NaI (Tl) detector sizes have been

computed and experimentally determined and catalouged by Heath[31]. Other inorganic phosphors include KBr, KI, CsI, CsBr, and LiI. Thallium chloride activated with iodides has recently been studied[32] as a high Z scintillator, but as yet, good energy resolution has not been obtained.

Inorganic phosphors, including plastics and liquids, are available and characteristic phosphor decay times much shorter than the inorganic phosphors is obtainable. This may prove useful in the design of a sum Compton scintillation spectrometer for intense radiation fields, because much faster coincidence circuitry can be employed and thus a system more tolerant of high count rates could be used. The conversion efficiency of the inorganic phosphors is less than for NaI (Tl), however, and this results in a poorer energy resolution.

Radiation damage to scintillators is not as severe as for solid state detectors and for the severe radiation environment addressed by this study, a scintillation detector system may be necessary. On the other hand, the superior energy resolution of germanium and silicon detectors is desirable if the necessary shielding indicates these detectors can survive the environment without serious degradation.

2.2.2 Semiconductor Detectors

Semiconductor detectors have progress rapidly during the past ten years with increased used in particle and gamma ray spectroscopy. They are, in essence, solid state ionization chambers with ionization potentials of the order of three eV, almost and order of magnitude less than gaseous ionization potentials. This fact yields a smaller fractional statistical deviation in the number of electron carriers and thus theoretically gives a better energy resolution.

Silicon and germanium junction diodes have been used as charged particles detectors for some time but until lithium drift compensation techniques[33, 34] were developed, semiconductor devices were not suitable for general gamma ray spectroscopy. The lithium ion compensation allows large volumes (tens of cm^3) of intrinsic[35] material from which the carriers may be collected. Ge (Li) detectors are particularly suitable for gamma ray spectroscopy because of the relative high atomic number. These detectors must be cooled, however, as the band gap of 0.66 eV allows the thermal generation of carriers at room temperatures. Goulding[36] presented a survey of the applications and limitations of these valuable devices, and we will not dwell on detector details at this time.

The three major gamma interactions occur for semiconductors as was outlined for scintillation devices. Similar spectrometers, of total absorption[37], anti-Compton[38, 39] and sum Compton[26] have been experimentally developed to improve the pulse height distribution functions.

A disadvantage of the Ge(Li) detectors is that they must be maintained in a cooled state, even when in storage, to prevent a "dedrift" of the lithium ions. Si (Li) detectors also have a much lower noise figure if cooled during operation, but can be stored at elevated temperatures.

Radiation can produce lattice defects in the single crystals of semiconductor detectors. Little effort has been expended, so far in this study, on a literature search of radiation damage effects. This area will be pursued in the near future, as it is vital in the decision to be made on the types of detectors to be employed. Radiation damage from alpha particles is reported[40] for 2×10^9 alpha particles cm^{-2} resulting in loss of resolution in a surface barrier detector. Klingensmith[41] reports degradation after 5×10^{11} fast neutrons cm^{-2} in junction diodes. On the other hand, p-n junctions have withstood thermal

neutron fluxes of 10^9 n cm^{-2} sec^{-1} and gamma fluxes of 4×10^8 r hr^{-1} for weeks without apparent degradation[42]. The lithium compensated devices should be more sensitive to radiation damage than junction and surface barrier diodes because of the lower electric field strengths and subsequent shorter trapping lengths.

2.3 THE INTENSE GAMMA FIELD PROBLEM AND CONCEPTUAL SOLUTIONS

2.3.1 Intense Field Problem

There are two general methods for performing gamma ray spectroscopy. One method is to measure the energy deposited by each individual photon in a detector of some particular type, and by knowing the absolute efficiency of the detector as a function of energy, corrections to the rate of detection for each energy may be applied to give the incident spectrum. The other method is to employ crystal diffraction wherein the position of the diffracted gamma ray is indicative of the energy. A spectrum is obtained by measuring the flux rate as a function of position.

The stipulated gamma dose rates for this study are:

1) Maximum - 7×10^5 Roentgens per hour

2) Minimum - 1×10^2 Roentgens per hour

The integrated gamma dose over the life of the measurement is expected to be 7×10^6 Roentgens.

The dose rate of 7×10^5 R hr^{-1} is equivalent to a photon flux of 2.6×10^{11} photons cm^{-2} sec^{-1} of 1 MeV photons. The gamma interaction cross sections

are energy dependent, of course, but are of the order of 0.2 cm^2 $gram^{-1}$, and a reaction rate of approximately 5×10^{10} sec^{-1} $gram^{-1}$ for almost any material would be obtained. The present pulse height analysis capability is of the order of 10^5 sec^{-1} (and pulse pile up is a problem at that rate) so a directly immersed detector would need to be of the order of 2×10^{-6} grams in weight, to limit the count rate to 10^5 sec^{-1}. The range of only a 200 keV electron is 4.5×10^{-3} gm cm^{-2}, and we conclude that a directly immersed detector in the gamma field is theoretically impossible.

Thus, the flux must be attenuated while preserving the spectral nature of the attenuated photons. We discuss various concepts for achieving this condition in the following sections.

2.3.2 Crystal Diffraction

Many forms of crystal diffraction spectroscopy have been used, however, they share a common characteristic. Gamma radiation that is scattered elastically, i.e., without loss of energy, by the spatial distribution of electrons from parallel crystalline planes, is in phase only at the angle of incidence $(90^\circ - \theta_B)$ given by the Bragg relationship

$$n\lambda = 2\, dH \sin \theta_B \qquad (2.3)$$

where λ is the wavelength

n is the order of the diffraction

d_H is the spacing between crystal planes

and θ_B is the Bragg diffraction angle

Thus, to perform a spectral measurement, the source to crystal orientation must also be changed simultaneously. This seems too complicated for space flight measurements, and, in addition, only a single energy is measured at a given time, unless multiple detectors are employed. Furthermore, the crystal to detector distance must be large to achieve good energy resolution, and this condition alone would impose a large weight penalty for the necessary shielding of nondiffracted radiation. For these reasons, crystal diffraction spectroscopy is considered inapplicable for the measurements for which this study is directed.

2.3.3 Recoil Beta Measurements

The scintillation and semiconductor counters infer the interacting photon energy by measuring the kinetic energy of the resultant photoelectron, Compton electron, or created pair. It has been suggested[43] that possibly these recoil beta particles from a thin target exposed to the gamma flux could be spectrally analyzed by a beta ray spectrometer, otherwise shielded from most of the primary radiation. It is not apparent to the author how this scheme could be successfully applied for the following reasons.

First, photoelectrons could not be distinguished from Compton electrons, so one would have a complicated unfolding problem associated with the data so obtained. This would be further complicated by the energy loss of some of these electrons within the passive target before entering the vacuum region of a magnetic beta ray spectrometer.

Secondly, considerable shielding would be required to diminish gamma induced electrons from other surfaces of the spectrometer. Thirdly, the magnetic spectrometer can focus monoenergetic beta particles emitted at various

angles, but no spectrometer has been developed that analyzes all energies over large angles of emittance simultaneously. By aperture limiting the angle of emittance, a spatial distribution of electrons by energy can be achieved, but the first and second reasons given seem to make this scheme impractical.

2.3.4 Aperture Limitation

A detector system might be shielded from most of the direct radiation except for a thin collimator. However, it can be shown that this collimator aperture would need to be of the order of 10^{-5} cm^2 in area, in order to reduce the signal rate to the order of 10^5 sec^{-1} at the high dose rate of 7×10^5 R/hr. Shielding is never complete, and in addition becomes a source of radiation from neutron capture. No means of ascertaining this background spectrum for subtraction from the data to yield the incident spectrum is available. In addition, diffraction of unknown magnitude may occur to photoelectric radiation penetrating such a small collimator. This method is therefore not recommended.

2.3.5 The Compton Scatter Attenuation Spectrometer

A more promising technique is to use Compton scattering to reduce the gamma flux to a readibly detectable level. The detector system must be shielded against the bulk of the primary radiation, at least to fluxes less than obtained via Compton scattering from a target. If a small target is employed and the radiation impinging on the target is collimator limited, and the solid angle subtended by the detector to the target is small than a precise relationship exists between the energy of the detected photon and the incident photon striking the target. Furthermore, the target may be removed so that the gamma background, composed of radiation penetrating the shield and originating in the shield, may be subtracted from the data to yield the Compton scattered events.

The energy shift of the photon is given by the well known relationship

$$E' = \frac{E_o}{1 + \alpha (1 - \cos \theta)} \qquad (2.4)$$

where E_o is the incident photon energy which is to be measured with the spectrometer

E' is the detected photon energy, which we assume is measured with the precision of the detector.

α is the incident photon energy in relativistic units (.511 MeV = unity

θ is the angle of Compton scatter

The theoretical energy resolution, i.e. disregarding instrumental resolution effects, is obtained by differentiating (2.4) with respect to θ to obtain

$$dE' = \frac{\alpha (E')^2}{E_o} \sin \theta \, d\theta \qquad (2.5)$$

Thus, to minimize the energy resolution $d\theta$ must be kept small through collimation of the radiation incident on and scattered from the target. In addition, it is desirable to design the apparatus so that θ, and $\sin \theta$, are small. However, one must consider coherent scattering, which is predominantly scattered at small angles, and reduce detection of coherent radiation to a negligible quantity so that the Compton energy shift correction can be applied to the data to yield the incident spectrum.

The author is convinced that the Compton attenuation technique is the simplest method of obtaining the gamma spectrum in radiation fields of 10^2 R hr^{-1} to 7×10^5 R hr. Furthermore, it seems that such a system can be designed to operate at even higher fluxes of 10^8 R hr^{-1} if required.

SECTION 3.0
PHYSICAL PARAMETERS EFFECTING COMPTON SCATTER ATTENUATION

The Compton scatter attenuation spectrometer will consist of a target on which a collimated beam of the incident radiation impinges, and one or two gamma spectral detectors which observe the scattered radiation. The detectors are otherwise shielded from the incident flux, but will see a background signal penetrating this shield. The background may be determined by removing the target and subtracted from the data obtained with the target in place. A definite spectral relationship exists between the scattered and incident radiation, and the flux attenuation may be determined as a function of energy so that the incident spectrum and intensity may be constructed precisely from the scattered spectrum.

In order to proceed with the design of a Compton attenuation spectrometer, all of the gamma interaction effects must be considered in detail. We know that the scatter target should be of a low Z material so that: 1) the scattering cross sections will be relatively large compared to other gamma interaction cross sections; 2) the electron binding energies are small such that the electrons may be considered "free" relative to the photon energies; and 3) X-ray fluorescence from the target will be energetically of low value.

Carbon and beryllium are readily obtainable in pure stable solid forms, and we have selected carbon as the most suitable target material, largely to eliminate possible toxicity problems associated with working with beryllium.

The total cross sections for the four major gamma interactions are plotted in Figure 3.1 for the carbon atom. Data below 1 MeV is from McMaster[44] et al, and the data above 1 MeV is from Grodstein[45]. The cross sections shown are in barns (10^{-24} cm^2) per carbon atom and may be readily converted to cm^2 $gram^{-1}$ by multiplying by 0.050. The Compton scatter cross section curve, C, is large

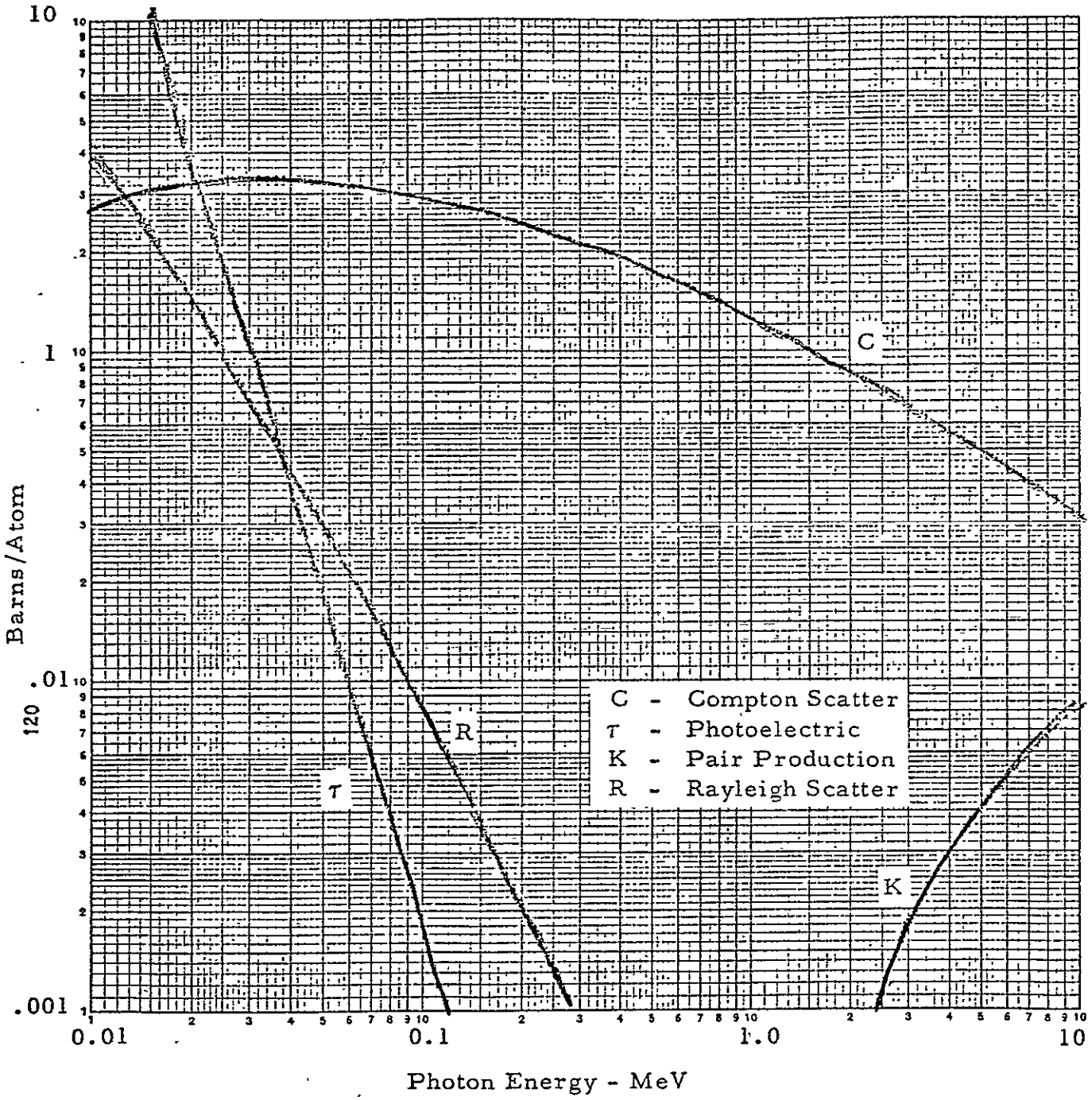

Figure 3.1. Gamma Interaction Cross Sections in Carbon

compared to the other interaction cross sections throughout the range from 50 keV to 10 MeV. The photoelectric absorption, with cross section curve labeled τ, completely absorbs the photon energy (except for the K fluorescence of 283 eV for carbon) and therefore is not a source of interfering radiation to the spectrum produced by inelastic scatter.

The pair production cross sections are shown by the curve K, and these interactions produce annihilation radiation of 0.511 MeV which is interfering in obtaining the incident gamma spectrum. The cross sections are small, however, and the annihilation radiation would be isotropically distributed, whereas, the Compton scatter is very angular dependent and highly dominant in the forward direction at these high energies. This factor will be considered in Section 3.3 of this report.

Rayleigh (coherent) scattering cross sections are designated by curve R. Rayleigh scattering is very angular dependent and can be considered interfering because the elastically scattered radiation will not have the energy shift that results from the inelastic (Compton) scatter process. We show in Section 3.2 that this is not a serious limitation, and that coherently and incoherently scattered radiation are not interfering at low energies (< 100 keV) and that coherent radiation will be a small fraction of the Compton radiation at higher energies.

3.1 THE COMPTON PROCESS

The classical Compton scatter equations are derived in many fine texts but we repeat the equations here as we must use and refer to them in the design of the spectrometer. In the following diagram and discussion, the incident photon energy is termed $E_o = h\nu_o$, the scattered photon energy is $E' = h\nu'$, $\alpha = h\nu_o/m_o c^2$, the recoil electron has momentum p and kinetic energy T, θ is the angle between the incident photon direction and scattered photon direction, and φ is the angle of the recoil electron, as shown.

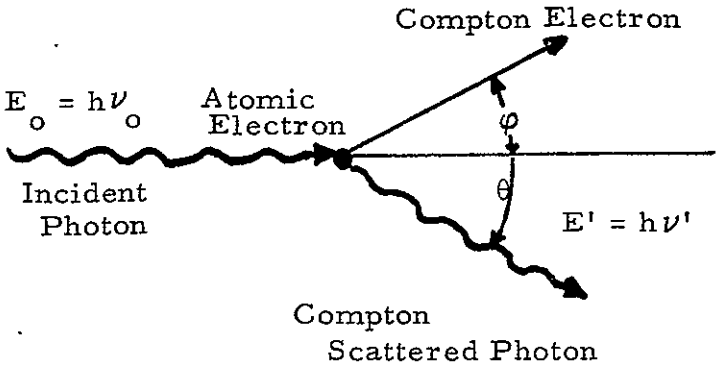

It has been shown, by use of the conservation laws, that the energy of the scattered photon is given by

$$\frac{E'}{E_o} = \frac{h\nu'}{h\nu_o} = \left[1 + \alpha\ (1 - \cos\theta)\right]^{-1} \tag{3.1}$$

The energy of the recoil electron is

$$T = h\nu_o - h\nu' = E_o\ \frac{\alpha\ (1 - \cos\theta)}{1 + \alpha\ (1 - \cos\theta)} \tag{3.2}$$

and

$$\text{cotangent}\ \varphi\ = (1 + \alpha\ )\ \text{tangent}\ 1/2\ \theta \tag{3.3}$$

These relationships are valid for free electrons, and for carbon having a K shell binding energy of only 283 electron volts, the electrons, especially the L shell electrons, may be considered free to photon energies greater than 50 keV.

Figure 3.2 shows graphically the relationship between E' and E_o for various angles of scatter as given by relationship (3.1). It is seen that the maximum energy of the scattered radiation is 0.5 MeV for $\theta = 90^o$ scattering and only 0.25 MeV for backscatter ($\theta = 180^o$). Thus, the sides and back of a gamma detector may be effectively shielded with only a moderate thickness of high Z material.

Klein and Nishina[46] applied Diracs' relativistic theory of the electron to the Compton scatter process in 1928 with brillant success. The differential scattering cross section, per electron, for unpolarized radiation was derived to be

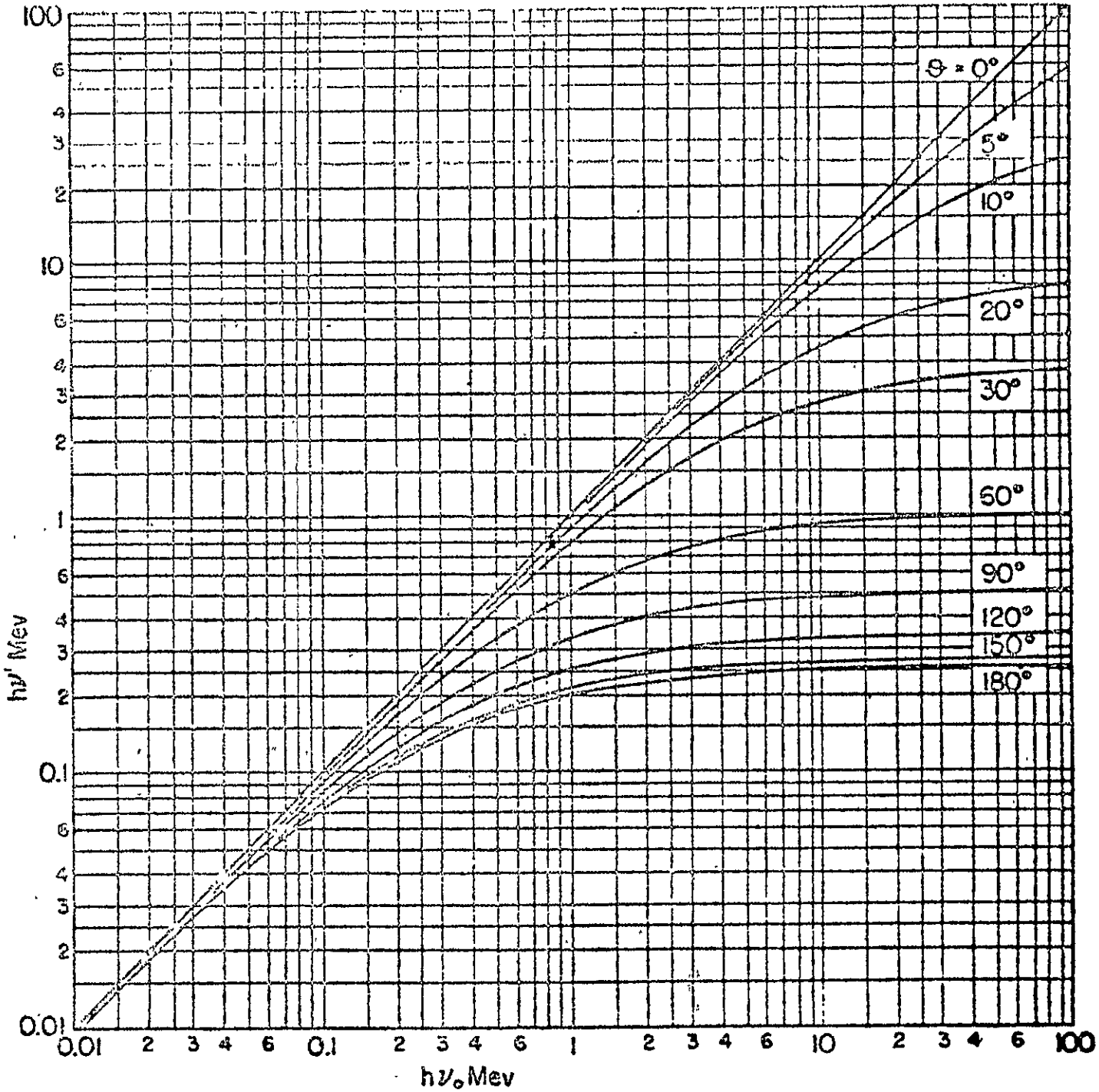

Figure 3.2 The Scattered Photon Energy $h\nu'$ as a Function of Incident Energy $h\nu_o$ and Scattering Angle θ

$$\frac{d_e\sigma}{d\Omega} = \frac{1}{2} r_o^2 \left\{ \frac{1}{[1 + \alpha(1 - \cos\theta)]^2} \left[1 + \cos^2\theta + \frac{\alpha^2 (1 - \cos\theta)^2}{[1 + \alpha(1 - \cos\theta)]}\right]\right\} \quad (3.4)$$

where $r_o = e^2/m_o c^2$.

Figure 3.3 indicates these differential cross sections graphically and, of course, these values may be converted to atomic cross sections by multiplying by the atomic number, Z, of interest. The atomic cross sections for carbon differential with respect to θ, are listed in Table 3.1 from the Klein Nishina relationship.

Table 3.1. Photon Collision Differential Cross Section for Atomic Carbon in Units of 10^{-24} cm^2 steradians^{-1} per Atom

$h\nu_o$ MeV	θ 5°	10°	20°	30°	45°	60°
0.04	.434	.468	.444	.408	.345	.273
0.1	.474	.466	.438	.396	.322	.246
0.2	.472	.463	.427	.376	.289	.210
0.4	.468	.458.	.409	.343	.246	.171
1.0	.467	.442	.361	.270	.166	.106
2.0	.461	.418	.300	.198	.109	.069
4.0	.447	.376	.223	.130	.069	.042
10.0	.408	.280	.127	.066	.030	.020

A cursory examination of Figure 3.3 and the data listed in Table 3.1 shows that we should desire to minimize the angle of scatter in achieving the attenuated flux, so that the differential cross section as a function of energy does not vary widely. As a large angle of scatter would prove relatively insensitive to the higher energy radiation, which is the less abundant in a fission spectrum. In addition,

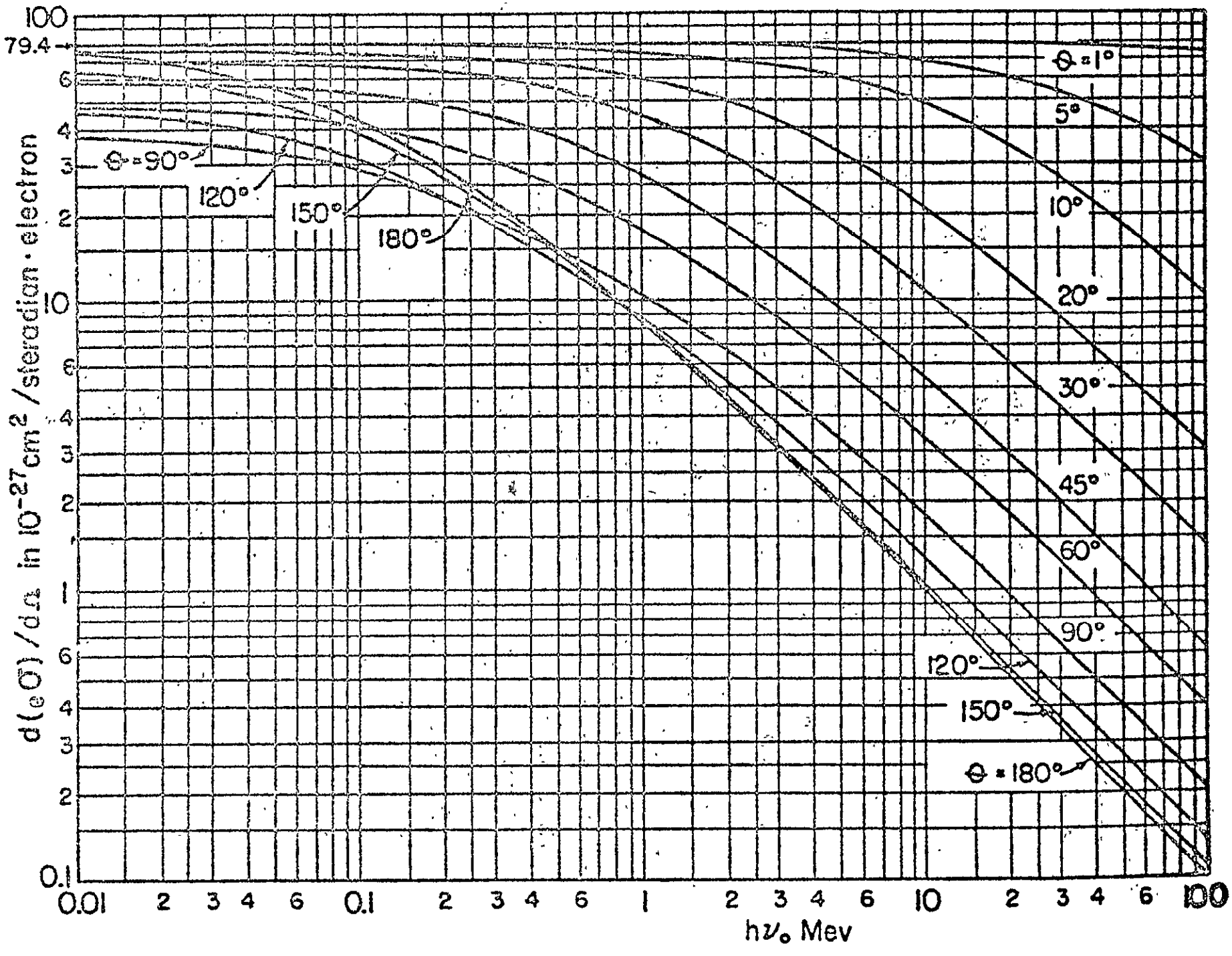

Figure 3.3. The Electron Differential Cross Section for Compton Scattering as a Function of Energy and Angle

Figure 3.2 shows a greater Compton energy shift for the wider angles of scatter, which would exaggerate the non-linearity of the energy response and impair the energy resolution of the Compton attenuation spectrometer.

The preceding discussion was for the limiting case of free electrons, but in the more general case, the binding energy of the electrons to the atoms and their motion and distribution must be considered. Excepting for the hydrogen atom, only approximation distribution theories have been developed and rather poor agreement exists between these theories. These theories express the incoherent scattering cross section differential with respect to angle of scatter as the product of two factors. The first factor is the Klein Nishina differential cross section (3.4) which is the probability that a photon be deflected at a certain angle and transfer a certain momentum to the electron (considered free). The second factor is the probability that the electron will receive a certain amount of energy and become excited or leave the atom, and is denoted by S(q, Z). Although various values of S are obtained with each distribution theory, they each agree that S is unity when the recoil momentum exceeds the orbital momentum, and that S approaches zero as the recoil momentum decreases below the orbital momentum S includes the average effect on all orbital shells. Values of S have been calculated by Bewilogua[47] from equations developed by Heisenberg using the Thomas-Fermi distribution. Using the Bewilogua values we calculate the values of S for carbon as listed in Table 3.2. The binding energy effect is seen to reduce the incoherent scattering cross section only a minimal amount at the energies and angles of interest to this design with carbon atom.

Table 3.2. Incoherent Cross Section Binding Energy Corrections for Carbon - S (q, 6)

Photon Energy	θ 5°	10°	θ 20°	30°	45°
50 keV	.50	.71	.87	.95	.96
100 keV	.70	.89	.96	.97	1.0

Other atomic distributions than the Thomas-Fermi distribution could be employed and differing results for S would be obtained. Thus, there is an uncertainty in the Compton scattering differential cross sections at low photon energies and low scattering angles. This uncertainty is not sufficiently large to cast doubt on the Compton scatter attenuation method, but is sufficiently large to require careful empirical sensitivity calibration of a completed spectrometer design for the energy region of 50 to 100 keV.

3.2 COHERENT SCATTERING

Coherent scattering consists of three types:

1. scattering by bound electrons without excitation;
2. scattering by the nuclear charge;
3. scattering from nuclear resonance

3.2.1 Rayleigh Scattering

The first of these is Rayleigh scattering which is responsible for the success of crystal gamma ray spectroscopy and interference phenomena in the X-ray region. Moon[48] presented the results of calculations by Franz[49] based on the Thomas-Fermi distribution for Rayleigh scattering which show that 75 percent of the radiation is in a forward cone of angle θ_c where

$$\theta_c = 2 \arcsin \left[0.026\, Z^{1/3} (mc^2/h\nu)\right] \qquad (3.5)$$

Excepting at small angles the differential cross section is given by

$$\frac{d\sigma}{d\Omega} = \frac{8.73 \times 10^{-33}}{\sin^3 Y_2 \theta} \left(\frac{Zmc^2}{h\nu}\right)^3 \frac{1}{2}(1 + \cos^2\theta) \frac{cm^2}{\text{steradian}} \qquad (3.6)$$

We have solved (3.6) for the carbon atom at photon energies of 50, 100, and 200 keV as a function of θ and the results are plotted in Figure 3.4 for the curves labeled R(E), denoting Rayleigh scattering. The Compton differential scattering cross sections, curves C, for carbon are also shown with the binding energy correction for 50 and 100 keV photons. We see that the Rayleigh scattering

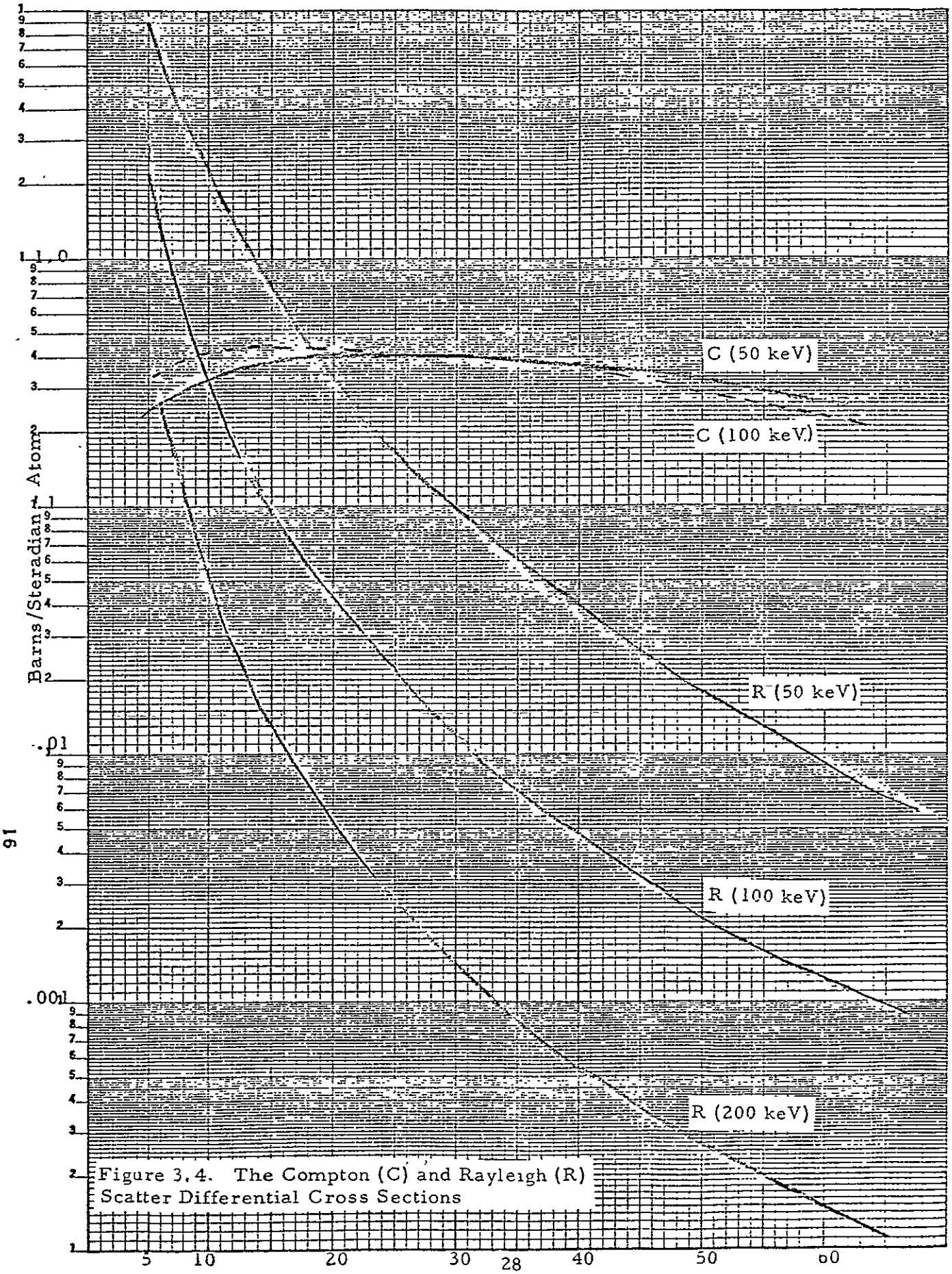

Figure 3.4. The Compton (C) and Rayleigh (R) Scatter Differential Cross Sections

differential cross section for 50 keV radiation is comparable to the Compton cross section, and that a large portion of the low energy photons would be due to elastic scattering. Thus, the gamma detector would be exposed to E' and E_o scattered radiation, and if E' and E_o differ considerably, this would be detrimental in obtaining a precise spectra in the low energy portion of the spectrum.

We have calculated $E_o - E'/E_o$, which is in effect the energy resolution imposed by detecting both elastic and inelastic scattered radiation, as a function of θ and the incident energy, E_o, and list these values in Table 3.3. We also list the ratio of the Rayleigh to Compton (binding energy corrected) differential cross section, which relates the mixture of coherent and incoherent scattered radiation. Fortunately, when the difference in energy between coherent and incoherent scattered radiation becomes large, the relative Rayleigh scattering cross section becomes small (the product of these quantities is always small), and we conclude that Rayleigh scattering will not be detrimental in obtaining a precise spectrum through Compton scatter attenuation. The differential scattering cross sections must be the sum of the Rayleigh and Compton cross sections, however.

Table 3.3. Fractional Energy Spread and Cross Section Ratio of Rayleigh and Compton Scattering

Incident Energy	$\theta = 20^\circ$		$\theta = 30^\circ$		$\theta = 45^\circ$	
	$\frac{E_o - E'}{E_o}$	$\frac{\sigma_R}{\sigma_c}$	$\frac{E_o - E'}{E_o}$	$\frac{\sigma_R}{\sigma_c}$	$\frac{E_o - E'}{E_o}$	$\frac{\sigma_R}{\sigma_c}$
50 keV	.0059	.79	.0129	.29	.0279	.073
100 keV	.0117	.095	.0255	.028	.0542	.009
200 keV	.0231	.0135	.0498	.0035	.1028	.0012

3.2 2 Thomson Scattering

The scattering cross section for gamma radiation by the nuclear charge may be obtained by substituting the nuclear mass M and charge Ze for the electron

mass and charge in the Thomson classical equation. The differential scattering cross section becomes

$$\frac{d\sigma}{d\Omega} = 2.39 \times 10^{-32} \frac{Z^4}{A^2} \cdot \frac{1 + \cos^2 \theta}{2} \quad \frac{cm^2}{steradian} \tag{3.6}$$

which is independent of the photon energy. For carbon, the Thomson scattering cross section is of the order of 3 to 2 x 10^{-31} cm^2 steradian, which is very small compared to the Compton cross sections and can be ignored.

3.2.3 Nuclear Resonance Scattering

At exact resonance, the nuclear scattering cross section is the square of the gamma ray wavelength, and of the order of 10^{-22} to 10^{-20} cm^2. As the spectrometer will view a continuous distribution of gamma ray energies, some of these may be in exact resonance with some of the target nuclei and the cross sections far exceed the Compton cross sections. However, the widths of nuclear resonance are so narrow, probably 10^{-4} electron volts or less, that this process has never been observed except for the famous Mossbauer effect. Nuclear resonance scattering is not a source of interfering radiation from a Compton scatter target because of this extremely narrow resonance.

3.3 TARGET PAIR PRODUCTION EFFECTS

One must make certain assumptions about the gamma spectral distribution in order to estimate the perturbation of pair production in the Compton target on the measured spectrum. This perturbation, of course, is the generation of 0.511 MeV positron annihilation in the process of pair production by high energy (>1.02 MeV) photons. As an approximation, we have taken the fission photon yield of Maienschein et al[50] as shown in Figure 3.5, and computed the relative pair production rate in carbon. The annihilation radiation is emitted isotropically, and as two photons are emitted per event, the .511 relative flux per steradian was determined as $1/2\pi$ times the total relative yield. This value is only 1.6 percent of the relative Compton scattered flux in an energy band of 50 keV around

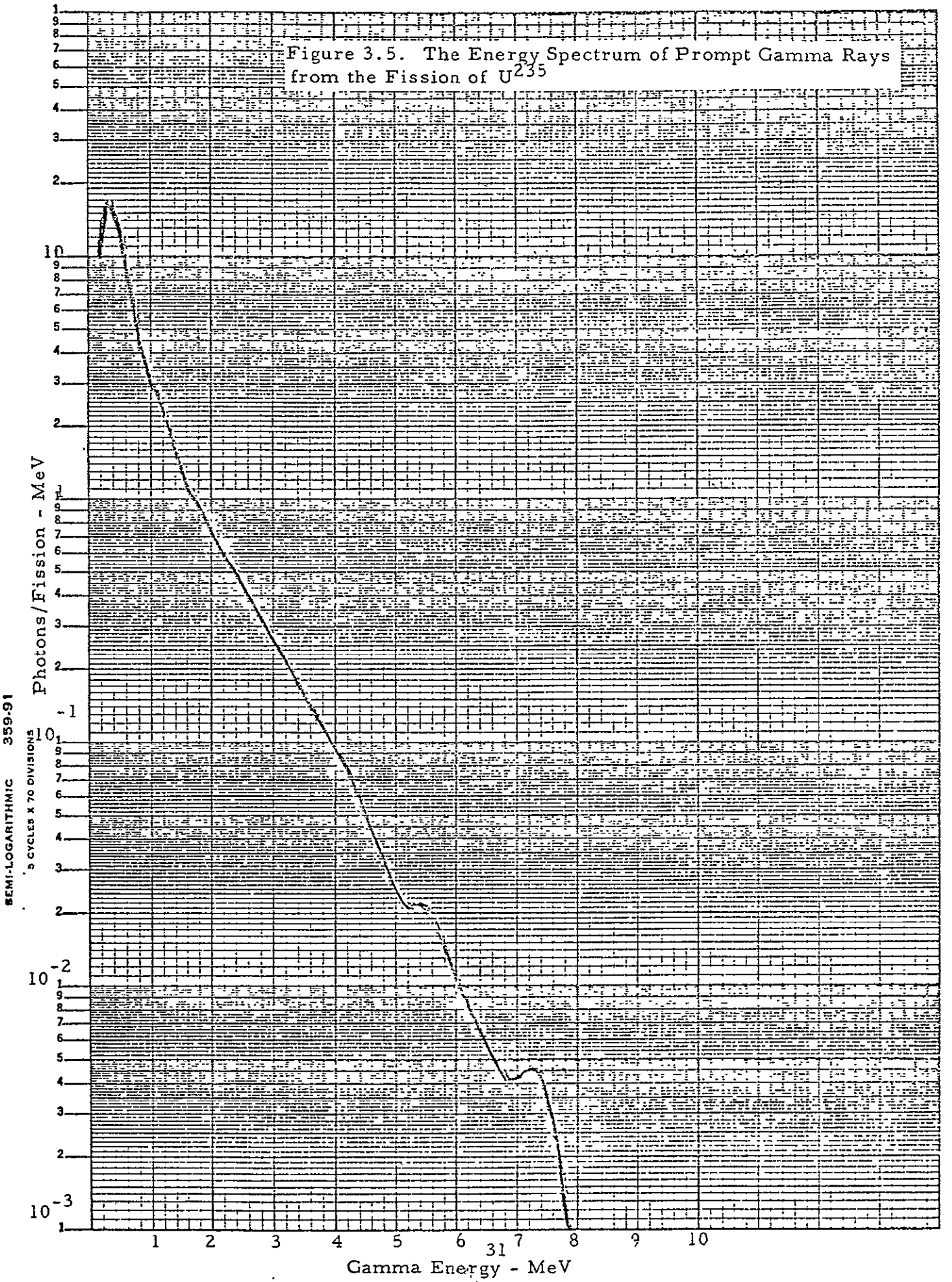

Figure 3.5. The Energy Spectrum of Prompt Gamma Rays from the Fission of U^{235}

500 keV. Thus, pair production in the Compton target does not appear to be a major source of interference in obtaining a spectrum. A reactor spectrum is likely to be harder than a pure fission spectrum, and this would increase the relative pair peak at 0.5 MeV, but if such a peak is observed, the source will be known and corrections can be made.

SECTION 4.0

GAMMA SPECTROMETER DETECTOR DESIGN

We have shown that the gamma flux intensity may be attenuated to a level allowing spectral detection, yet retain the spectral nature of the beam through the energy shift relationship, by using the Compton scatter of a portion of the beam from a suitable target at a suitable angle. The beam intensity at a detector may be written as

$$\left(\Phi_d\right)_E = \left(\Phi_o\right)_E \cdot A_t \cdot N_A \cdot \left(\frac{d\sigma}{d\Omega}\right)_E, \; d\Omega \qquad (4.1)$$

where Φ_o is the incident flux (photons cm^{2} sec^{-1})

A_t is the area in cm^2 of the collimated incident beam

N_A is number of target nuclei per cm^2

$\frac{d\sigma}{d\Omega}$ is the differential scattering cross section

$d\Omega$ is the solid angle subtended by the detector

The subscripts, E, denote energy dependence. The detection rate will be the summation over all energies of the product of the detector efficiency, which is also energy dependent, and expression (4:1). One must, therefore, specify the detector before proceeding with the Compton attenuator design, which fixes A_t, N_A and θ used in expression (4.1).

4.1 THE CONTINUOUS SPECTRUM PROBLEM

The most widely used spectral gamma ray detectors are single crystal detectors such as a scintillation crystal or a Ge(Li) detector. Such detectors record the fractional energy lost per photon within the detector which is approximately 100 percent for photoelectric absorption events but varies from near 0 percent to T_{max} for Compton events. This is no great problem when the detector is

used to identify and quantitatively measure a few radioisotopes or spectral lines, as the several photopeaks are usually distinguishable amidst the Compton events. Quantitative data may be obtained through the stripping of known pulse height spectra for a specific isotope--or, less frequently used, by constructing the photopeak from the known energy resolution of the detector. However, for a continuous spectrum, such as shown in Figure 3.5, no photopeaks are present and the only method of reducing the spectra is to use matrices[51] of the detector response for all energies, and mathematically reduce the data with the aid of a computer. This is a useful technique and is widely applied successfully, however, the problem is complicated and less satisfactory for small detectors. Because the high flux conditions toward which this study is directed will allow the use of inefficient detectors, we have decided to attempt to design a sum-Compton spectrometer to determine the Compton attenuated spectrum. Such a design may not prove feasible over the entire spectral range, but the desired result of obtaining direct spectral data seems worthy of expending the considerable effort required to produce a suitable design. In addition, a judicious choice of detector configuration may allow this same configuration to be employed as a pair spectrometer for photon energies exceeding 2.0 MeV with suitable parallel electronic circuitry.

4.2 THE SUM-COMPTON SPECTROMETER

The sum-Compton spectrometer consists of two or more separate detectors. Only the primary detector, which we will designate as detector A, is exposed to the primary incident photon flux. The secondary detectors, which we designate as B detectors, are largely shielded from the incident photons, but are in close proximity to detector A. We envision detector A to be a small diameter solid cylinder and the incident radiation is incident on the end of this cylinder and collimation restricted to a diameter less than the detector A diameter. Detector(s) B consists of a hollow cylindrical detector whose inside diameter is large enough to surround detector A.

Photons incident on detector A may continue through the detector without any iteration. This is the fraction $\exp\left[-\mu_{a_E} x\right]$ at a particular energy where μ_{a_E} is the total absorption coefficient at energy E, and x is the detector thickness. The fraction $1 - \exp\left[-\mu_{a_E} x\right]$ will interact in some manner within detector A.

Photoelectric events within detector A will not produce events in detector B and will not be analyzed because we will require time coincidence between events in detectors A and B. Coherent scattering will not produce events in detector A and thus will not be recorded even if detected in detector B.

Compton events in detector A may or may not produce events in detector B. The probability of producing events in both detectors is the integral of the product of two factors. The first factor is the probability that a photon will be scattered from detector A into detector B. This probability is expression (3.4) (after correction for the binding energy effect) multiplied by the detector atomic number, Z, integrated over $d\Omega$ of detector B. As detector B is axially symmetric, $d\Omega = 2\pi \sin\theta \, d\theta$ and the integration can be performed over θ. However, this integration is not performed separately as the second factor, which is the probability that the scattered photon will interact in detector B is both energy and angle dependent. This probability is $1 - \exp\left[-\mu_{a_E} x\right]$ with x varying with the angle θ and μ_{a_E} being energy dependent.

These calculations are being prepared and will be available for the next reporting period. Such calculations are sometimes performed using expensive Monte Carlo techniques which can account for secondary scattering within both detectors, however, we do not believe such calculations are justified as the analytical calculations should be sufficiently accurate for the present purpose. These calculations will result in energy response functions for a specified detector geometry. These functions, all of which will be a function of the incident photon energy, will include: a) the fraction of events scattered in detector A and photoelectric captured in detector B; b) the photoelectric absorption in detector A; c) the scattered events in detector A not interacting in detector B; d) the scattered events in detector A that are also scattered in detector B; and e) the pair production in detector A that results in the escape of one or both annihilation quanta.

Only (a) type events are considered signal events and the others are a source of background. The (b) and (c) type are not analyzed excepting for random coincidence. Type (d) and some of type (e) interactions will produce a coincident background in which the total energy of the incident photons is not absorbed and it is desirable to achieve a high ratio of (a) to (d) events. This ratio should be high for low to moderate gamma ray energies and decrease with increasing energy. In addition, the (a) type function will decrease rapidly with energy. It may prove desirable to create a pair spectrometer for the high energy portion of the spectrometer. If detector B is split along the axis into two segments, the coincidence absorption of a .511 MeV photon in each half will be indicative of a pair reaction in detector A.

Coincidence techniques must be count rate limited in order to reduce the accidental coincidence rate to a minimum. The interaction rate, N_A in detector A will be greater than the rate N_B in detector(s) B, and the accidental coincidence rate will be

$$N_{acc} = 2 N_A N_B \Delta t \text{ sec}^{-1} \qquad (4.2)$$

where Δt is the system resolving time. The accidental rate for an incident spectrum, such as shown in Figure 3.5, of various intensities will be calculated in order to determine the maximum incident gamma flux. This will allow computation of the values A_t, N_A, and $d\Omega$ in expression (4.1) for the Compton attenuation spectrometer.

4.3 SUM-COMPTON SPECTROMETER DESIGN STUDIES

Computations of the efficiency and peak to tail ratios of four differing detector configurations for sum-Compton spectrometers were performed. Cases of germanium-germanium and silicon-germanium detector combinations were calculated for each configuration case. These calculations are only approximate, but should be sufficiently accurate to obtain the detector efficiency and peak to tail ratio for design purposes. This inaccuracy is due to simplifying geometric considerations and the non-consideration of multiple scattering and subsequent absorption within the second detector of the configurations. The direction of the errors are indicated in later sections of this report.

4.3.1 The Computation Program

A computer program was written to solve for the events of interest in the sum-Compton configurations. These events are the fraction of incident photons that are: completely absorbed in the primary detector; scattered in the primary detector; scattered in the primary detector and absorbed in the secondary detector; and scattered in the primary detector and again scattered in the secondary detector. To simplify the program, all total and differential interaction probabilities were expressed as analytical functions of one or two variables, the photon energy, E, and the angle of scatter, θ. The cross sections were converted to linear absorption coefficients so that only path lengths need be considered in the probability calculation

The photoelectric absorption coefficient was assumed to have the general form

$$\tau(E) = A\, E^{-n} \tag{4.3.1}$$

where E is the photon energy in MeV and A and n are constants for a specific element. These constants can be determined from published values of the photoelectric cross sections to obtain the best fit to the relationship

$$\log \tau(E) = \log A - n \log E \tag{4.3.2}$$

for two or more values of $\tau(E)$.

Our solutions for germanium and silicon give good agreement with published[44] data from 50 keV to 400 keV and are

$$\tau(\text{silicon}) = 1.32 \times 10^{-4} \; E^{-3.0} \; \text{cm}^{-1} \tag{4.3.3}$$

$$\tau(\text{germanium}) = 1.94 \times 10^{-3} \; E^{-3.1} \; \text{cm}^{-1} \tag{4.3.4}$$

The Compton differential scattering cross section, expressed as linear coefficients, are constants times the bracketted analytical function of E and θ previously shown in relationship (3.4). These constants are 6.85×10^{-2} cm^{-1} steradian^{-1} for silicon, and 12.68×10^{-2} cm^{-1} steradian^{-1} for germanium. Angular integration of the differential cross sections gives the total scattering cross section

$$\sigma = 2\pi \int_0^{\pi} \frac{d\sigma}{d\Omega} \sin \theta \, d\theta \tag{4.3.5}$$

which becomes

$$\sigma = 2\pi \cdot \text{constant} \cdot \left\{ \frac{1+\alpha}{\alpha^2} \left[\frac{2(1+\alpha)}{1+2\alpha} - \ln \frac{(1+2\alpha)}{\alpha} \right] + \frac{\ln(1+2\alpha)}{2\alpha} - \frac{1+3\alpha}{(1+2\alpha)^2} \right\} \text{cm}^{-1} \tag{4.3.6}$$

with the above numerical constants for silicon and germanium.

With analytical expressions for τ, σ, and $d\sigma/d\Omega$ we may now write the probable fraction of the incident photons completely absorbed in detector A as

$$\text{Fraction Absorbed} = \int_0^{X_A} \tau(E) \exp -\left[(\tau + \sigma)_E \; X_A\right] \tag{4.3.7}$$

As we consider the radiation normally incident on the end of detector A, the integration is performed over this length, X_A, to give

$$p = \left(\frac{\tau}{\tau + \sigma}\right)_E \left[1 - \exp -\left[(\tau + \sigma)_E \; X_A\right]\right] \qquad (4.3.8)$$

Where the subscripts E indicate energy dependence and separate solution for p are obtained for each energy. Similarly, the total number of scattered events in detector A is

$$q = \left(\frac{\tau}{\tau + \sigma}\right)_E \left[1 - \exp -\left[(\tau + \sigma)_E \; X_A\right]\right] \qquad (4.3.9)$$

The angular differential scattering is also similarly written as

$$r = \left(\frac{d\sigma}{d\Omega}\right)_{E,\,\theta} \left(\frac{1}{\tau+\sigma}\right)_E \left[1 - \exp -\left[(\tau + \sigma)_E \; X_A\right]\right] \qquad (4.3.10)$$

where $(d\sigma/d\Omega)$ is angular dependent as well as energy dependent.

The scattered photon has an energy related to the incident energy and the angle of scatter as given by relationship (3.1). The probability of the scattered photon escaping detector A is given by

$$s = \exp -\left[(\tau + \sigma)_{E'(\theta)} \; X_A(\theta)\right] \qquad (4.3.11)$$

Where E' denotes the scattered photon energy and $X_A(\theta)$ denotes the scattered path length in detector A, which is also angular dependent. For geometric simplicity and computational ease, we have assumed that all scattering events originate in the center of detector A as shown in Figure 4.1(a), and the subsequent scattered path lengths in detectors A and B are so determined as a function of θ.

The probability of absorption of any scattered photon reaching detector B, which we term, $p(E' X_B)$ is merely the expression (4.3.8) with E' energies rather than E, and $X_B(\theta)$ path lengths rather than X_A. Additionally, the probability of additional scatter for photons reaching detector B is expression (4.3.9) with the same substitution and we term this probability $q(E', X_B)$.

We have not attempted to calculate the probability of absorption of the radiation scattered within detector B. The calculations performed were

1) Those events scattered in detector A and absorbed in detector B. This is given by

$$2\pi \int_{\theta B} r(E, \theta) \times s(E', \theta)\, p(E', X_B) \sin\theta\, d\theta \qquad (4.3.12)$$

where the integration is over the angles intercepting detector B.

2) Those events scattered in detector A and again scattered (first collision) in detector B. This is given by

$$2\pi \int_{\theta B} r(E, \theta)\ s(E', \theta)\, q(E', X_B) \sin\theta\, d\theta \qquad (4.3.13)$$

3) Those events completely absorbed in detector A. This is $p(E, X_A)$ or expression (4.3.8).

4) Those events scattered in detector A whether interacting with detector B or not. This is $q(E, X_A)$ or (4.3.9).

The calculations result in the probability of occurrence or the fraction of photons incident on detector A that result in the particular combination of events.

4.3.2 Calculation Results

Figure 4.1(a) indicates the relationship of the geometrically simplified path lengths for the scattered radiation and the angle of scatter. Figures 4.1(b) through (e) show the four geometric configurations calculated as sum Compton detectors. Cases with both germanium and silicon as the primary detector (detector A) were calculated but only germanium is considered for detector B. These calculations are only approximate, but are sufficiently accurate for the design purposes of estimating the efficiency fraction and the peak to tail ratio as a function of incident energy.

Cases I, II, and III have the primary detector A inside the hollow cylindrical detector B, and the position of detector A is varied by case. Case IV, on the other hand, has less geometric efficiency and consists of a ring shaped detector B positioned forward of detector A. This geometry produces a much less efficient detector system but has an improved peak to tail ratio.

Figures 4.2 and 4.3 show the interaction probability for photoelectric absorption and Compton scattering as a function of incident energy on 0.5 cm thick detectors of silicon and germanium respectively. These are the interaction fractions for detectors A in each case calculated. Note that the ratio of the photoelectric absorption to Compton scatter is approximately the peak to tail ratio that would be obtained with a single detector. For germanium, this ratio is 0.01 at 1.0 MeV and much less for the silicon detector.

The interaction rates may be used to estimate the count rate that would be obtained in detector A for specific incident spectra and gamma flux. Note also, the decrease of the scattering fraction for the germanium detector at energies below 0.1 MeV, this is due to the rapid attenuation of the photon flux through the detector due to photoelectric absorption. For this reason, it may be preferable to use silicon as the detector A in the sum-Compton detector system to retain efficiency at the lower energies of interest.

Figures 4.4 through 4.6 show the efficiency fractions for silicon-germanium detector combinations for Cases I, II, and III. The solid lines represent the fraction of the incident flux that is scattered within detector A and then absorbed within detector B. The dashed lines indicate the fraction that is scattered again in detector B in the first collision. Note that it is probable that a large fraction of the latter events will be absorbed in detector B through multiple interactions. Therefore, the dashed lines are somewhat overstated in magnitude and the solid lines are correspondingly understated. However, the ratio of the solid to dashed lines should be representative of the approximate peak to tail ratio. Note that this ratio improves as detector A is moved toward the rear of detector B.

For Case III, shown in Figure 4.6, the peak to tail ratio at 1.0 MeV is 0.15 compared to 0.01 for a single detector. Note also that the peak efficiency for the Case III configuration is some 15 times greater (.0015 versus .0001) than for the single detector of Figure 4.3, although of course, the total efficiency of the sum-Compton configuration is much less than for the single detector.

Figures 4.7 and 4.8 show the interaction fractions for Case IV configurations with detectors A being silicon and germanium respectively. The peak to tail ratio at 1 MeV is an indicated 0.33 which is a further improvement over Case III, however, this is accomplished at the expense of peak efficiency which shows a marked decline over the Case III configuration.

It is not expected that the sharp decline in efficiency of the germanium-germanium combination (Figure 4.8) would prove to be as severe as indicated. This decline is largely due to the exponential absorption term (4.3.11) assuming that all the scattering occurs in the center of detector A and this assumption over-attenuates the scattering from shallow regions of detector A.

Pulse height discrimination of detector B pulses should improve the indicated peak to tail ratios. Consider that the lowest energy pulse of interest, in detector B is of the order of 40 keV, resulting from the scatter of incident 50 keV radiation. At much higher incident energies, the scattered radiation energy reaching detector

B can not exceed approximately 300 keV because of the large angle (>135°) of scatter required. The scattering cross section exceeds the photoelectric absorption cross section in germanium at 300 keV, but pulse height discrimination set at 40 keV, would negate scattering of 300 keV photons for scattering angles of 35° and less. Wider angle scattering within detector B should result in higher absorption and the peak to tail ratio should far exceed that indicated in Figures 4.7 and 4.8.

In addition, the tail pulse height distribution is much different with a sum-Compton spectrometer than with a single detector. For instance, consider a 1.0 MeV incident photon on detector A, the Compton recoil electron would deposit 0.8 MeV in detector A and the scattered photon could be totally or partially absorbed within detector B. In any event, the coincident sum must be within 20% of the peak energy. Thus, the tail obtained in a sum-Compton spectrometer is largely just below the peak energy and, therefore, the unfolding of continuous spectra data obtained with a sum-Compton spectrometer is much easier than unfolding the data from a single detector.

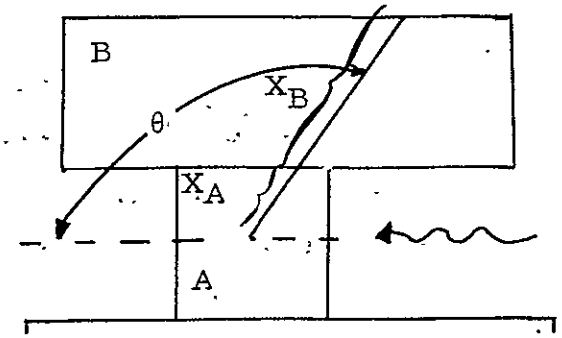

(a) Relationship of X_A (θ), X_B (θ), and θ .

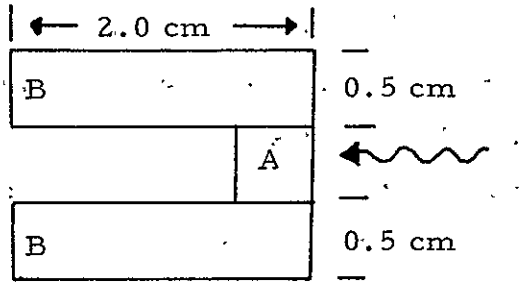

(b) Case I

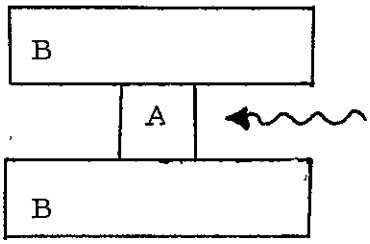

(c) Case II

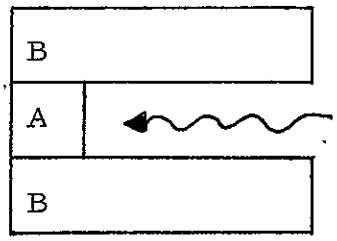

(d) Case III

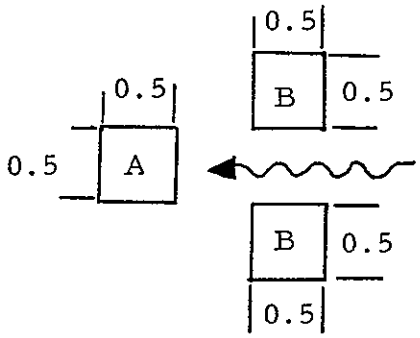

(e) Case IV

Figure 4.1.

Figure 4.2. The Interaction Fractions in 0.5 cm Thick Silicon

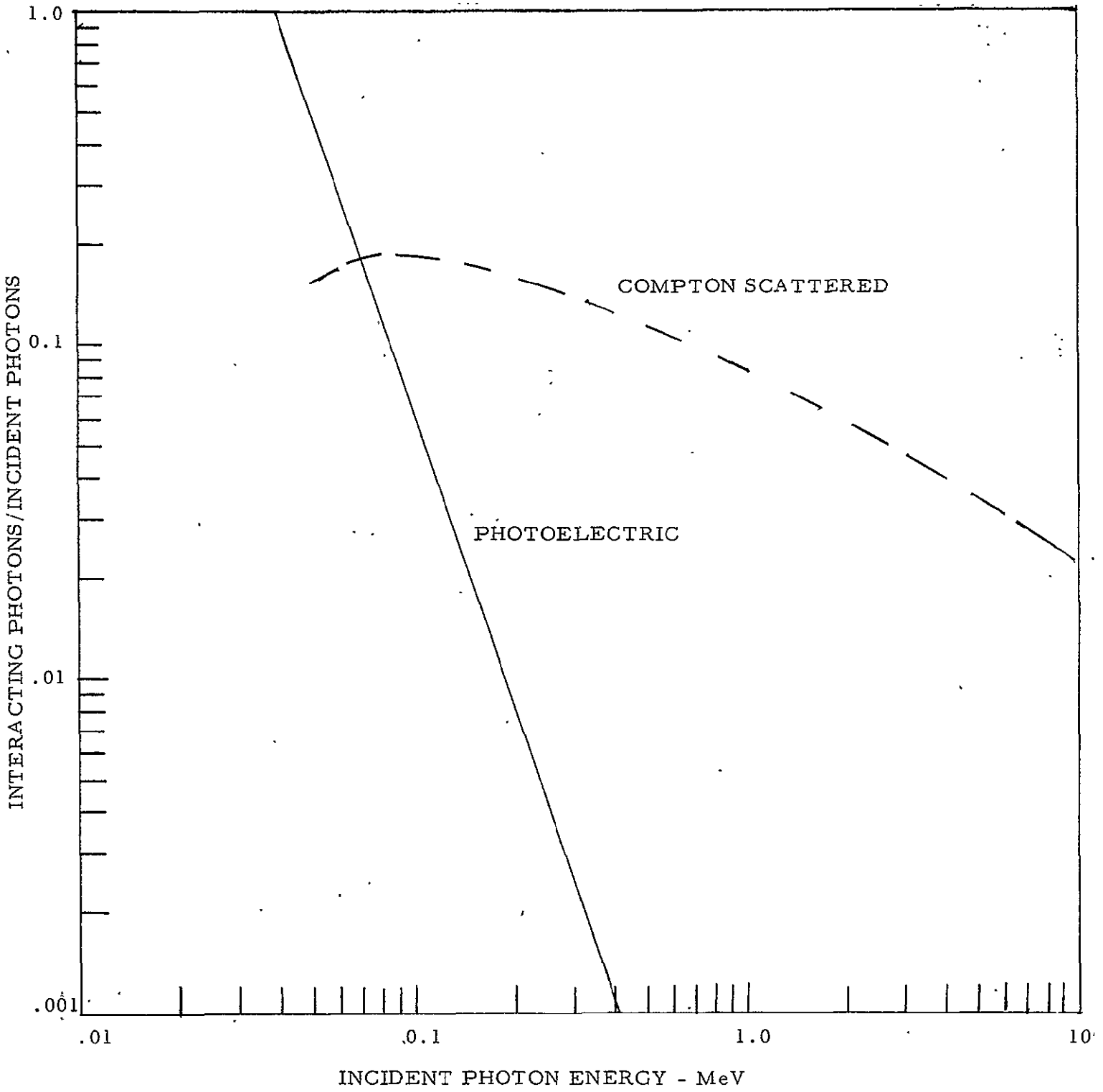

Figure 4.3. The Interaction Fractions in 0.5 cm Thick Germanium

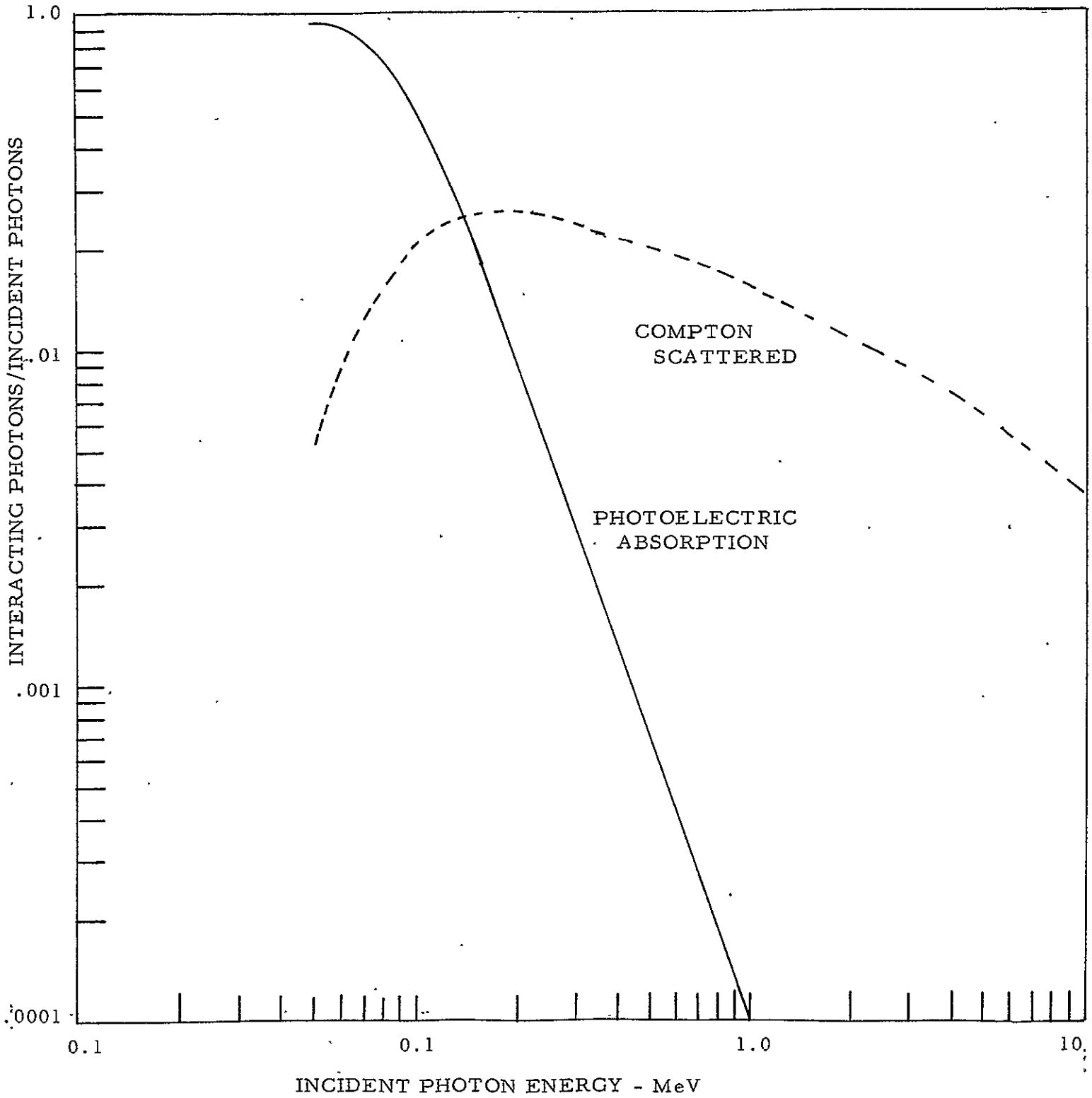

Figure 4.8. Case IV Configuration, Detector A - Germanium, Detector B - Germanium

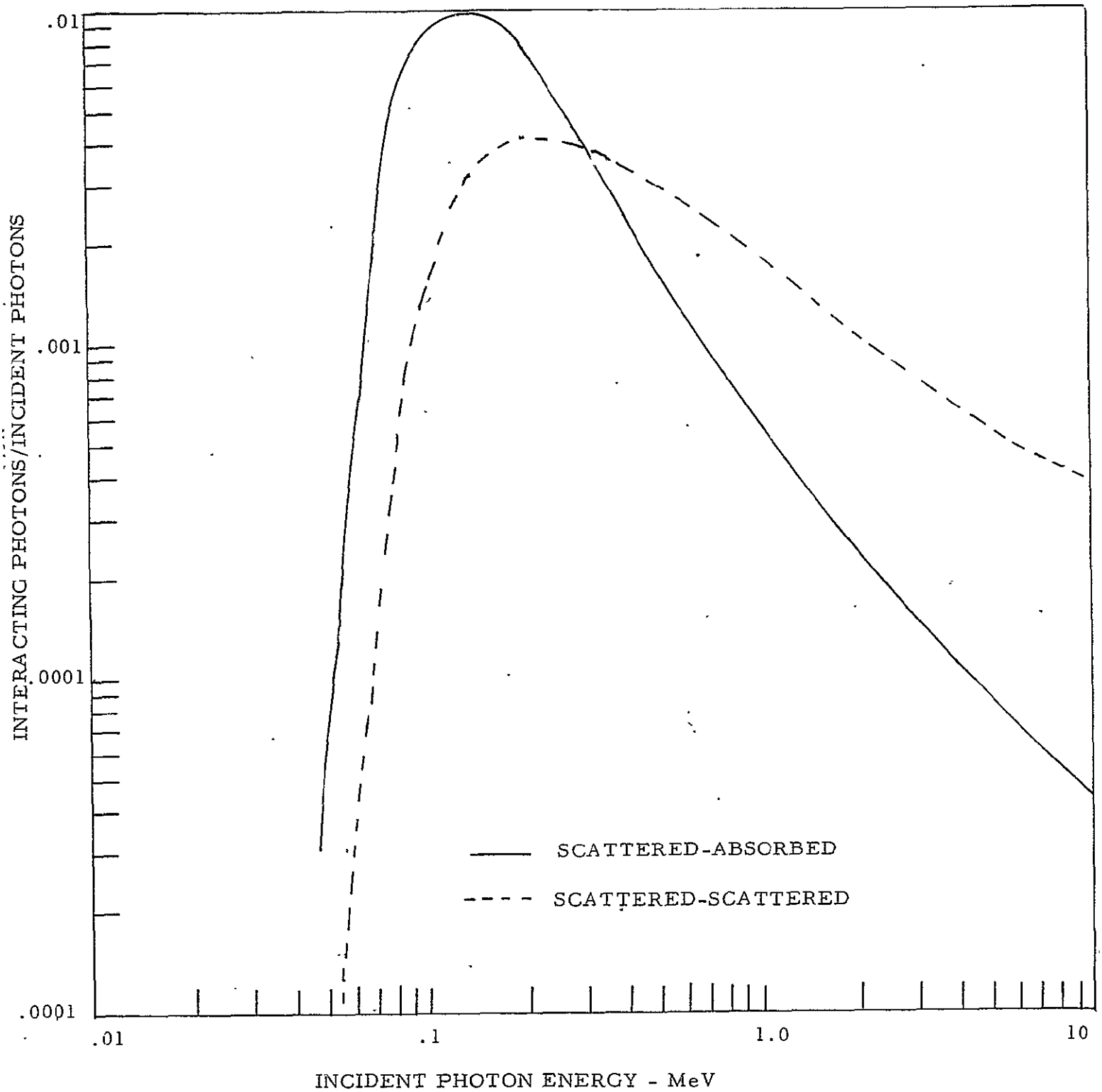

SECTION 5.0
FAST NEUTRON RADIATION EFFECTS

The signal observed from semiconductor radiation detectors is due to ionization, i.e., the displacement of electrons from the lattic structure. The free electrons migrate to the positive electrode and the holes (electron vacancies) migrate to the negative electrode. These carriers recombine at the detector electrodes, and thus the radiation effects of ionization disappear rapidly and do not permanently effect the detector. Nuclear radiation can also displace atoms from their equilibrium sites within the lattice structure, and this leaves vacancies and interstitial atoms resulting in permanent damage (unless the detector is reprocessed). It is the effects of this type of permanent damage that is first noticeable in a mixed gamma and neutron environment. Other damage mechanisms include the transmutation of the constituent isotopes through nuclear reactions in the detector, but these effects are less noticeable unless the thermal neutron field is very predominent. For this study, we anticipate shielding the detector system with boron, which has a high thermal neutron capture cross section, and therefore only fast neutron effects on the detectors need be considered. Fast neutron radiation effects the detectors by a degrading of the detector characteristics with accumulated or integrated neutron flux and also produces a background rate in the detector that is related to the instantaneous neutron flux rate. The integrated effects impose a time limitation for operation in a specific neutron flux and the instantaneous induced background rate imposes a maximum for the neutron flux rate in which reliable gamma spectral measurements can be obtained.

5.1 INTEGRATED FAST NEUTRON EFFECTS

The knock on atom from a neutron elastic collision creates a vacancy and an interstitial atom a short distance away where the recoil atom comes to rest, and the vacancy and interstitial atom are called Frenkel pairs. A recoiling atom may create several such Frenkel pairs by additional collisions and the threshold energy for these displacements are of the order of 15 to 80 electron volts.

An incident particle of mass M_1 and energy E_1 colliding with a mass M_2 can transfer to the struck particle a maximum energy of

$$W_{max} = \frac{4 M_1 M_2}{(M_1 + M_2)^2} \cdot E_1 \qquad (5.1)$$

for a head on collision. Lesser energies from zero to the above value are equally probable, and the average value for monoenergetic particles will be one half of that indicated in (5.1). Equation (5.1) shows that for incident electrons, which may be internally generated by gamma radiation, the maximum transfer of energy is less than 10^{-4} of the electron energy. On the other hand, a fast neutron can result in a maximum transfer of energy of 13.3% for a silicon recoil and 5.5% for a germanium recoil. Thus, it is expected that a germanium detector will be more immune to fast neutron damage than a silicon detector, and this is substantiated by experimental results. In addition, (n, p) and (n, α) reactions are much more common in silicon than in germanium. Thus, germanium is the better of the two semiconductor detector materials for gamma spectral measurements in mixed neutron and gamma fields.

The integrated fast neutron radiation effects in lithium drifted germanium detectors has been studied experimentally by Kramer[53] et al. Changes in the leakage current, detector capacitance, pulse rise times, and energy resolution were reported. The most sensitive degradation in detector performance is the loss of energy resolution. For instance, the energy resolution at 1.33 MeV was initially 6.3 keV, as reported in reference 53, deteriorated to 16.5 keV (fwhm) with an integrated neutron flux of 6.7×10^{10} n cm^{-2}. This change is not noticeable until the integrated flux exceeds 10^{10} n cm^{-2}, but determination proceeds rapidly above that level. The referenced study shows that the determination in energy resolution is largely due to hole trapping, and that the energy resolution can be improved in a neutron irradiated detector, by observing only those pulses with

92

the proper rise time. However, this would lead to unduly complicated electronic circuitry, and in addition, we can show that the background signal rate due to fast neutrons presents a greater challenge in the present study. We will arbitrarily stipulate that an integrated fast neutron flux of 10^{11} n cm^{-2} is the maximum tolerable flux, as the energy resolution is degraded by a factor of four at that flux level, and probably would not give spectral information at integrated flux levels only two or three times greater than that value.

5.2 FAST NEUTRON RATE EFFECTS

The rate at which signal pulses are produced in the detector by fast neutrons is important and limits the maximum neutron flux density in which a particular detector system can be satisfactorily operated. Chassman[54] et al have determined the fast neutron induced signals in single germanium (lithium drifted) detectors for various neutron energies. These signal events are due to elastic and inelastic scattering of neutrons within the detector, and to a lesser extent, reactions in the materials composing the cryostat and surrounding materials. Specific spectral pulses were observed corresponding to the various excited states of the germanium isotopes. Use of the coincidence sum Compton spectrometer would reduce the detected rate except for random coincidences. If the single rate in each detector is large, than this random coincident rate can be large and, in addition, may add to the pulse observed from true coincident signals. Thus, we must calculate and determine the rate at which neutrons interact with the detectors so that this background effect may be estimated.

Any neutron collision, within the detector, whether elastic or inelastic will produce a signal. The total neutron cross section for germanium is between 3.2 and 4.2 barns for neutrons of 1 to 10 MeV in energy. As there are 4.41×10^{22} germanium atoms per cubic centimeter, the neutron reaction rate becomes

$$N_n = 4 \times 10^{-24} \text{ cm}^2/\text{atom } 4.4 \times 10^{22} \text{ atom/cm}^3 \varphi \qquad (5.2)$$

$$= 1.7 \times 10^{-1} \Phi \text{ cm}^{-3} \text{ sec}^{-1}$$

where Φ is the fast neutron flux in neutrons cm^{-2} sec^{-1}.

5.3 THE ATTENUATION OF FAST NEUTRONS

A dense shield of a high atomic number material is necessary to shield the detector system from direct gamma radiation. We anticipate that this shield will be largely tungsten, and we, therefore, need to calculate the fast neutron attenuation in such a shield. To do this, one must consider the neutron removal cross section for tungsten, and this removal cross section is actually geometry dependent. This is because most of the fast neutron interactions are scattering reactions, and the neutron continues to exist until captured. The scattering absorbs a portion of the neutron energy, but for heavy nuclei such as tungsten, the neutron fractional loss of energy is small in each encounter.

Consider a thin rod of material with the length of the rod parallel to the fast neutron propagation direction. Any collision will effectively remove a neutron because it would be scattered out of the narrow beam shielded by the rod, and we assume no surrounding material exists to scatter neutrons back into the beam. Therefore, the total neutron collision cross section can be used as the removal cross section for such geometry. On the other hand, consider a plate of tungsten, neutrons scattered out of a volume is partially compensated by neutrons scattered into that volume from other regions of the plate. The fast neutron flux is diminished only by scattering in the back direction and by absorption. Thus, the removal cross section is less than the total cross section.

The total fast neutron cross section for tungsten is 7 barns above 1 MeV according to BNL 625. The fast neutron removal cross section for tungsten is 2.5 barns for fission neutrons as determined by ORNL[55]. As there are 5.5×10^{22} tungsten atoms per cubic centimeter, the neutron removal coefficient is .137 cm^{-1} and the total interaction coefficient is .385 cm^{-1}. The fast removal theory shows that the fast neutron flux density will decrease exponentially with material thickness and the proper coefficient. Using the above coefficients, we

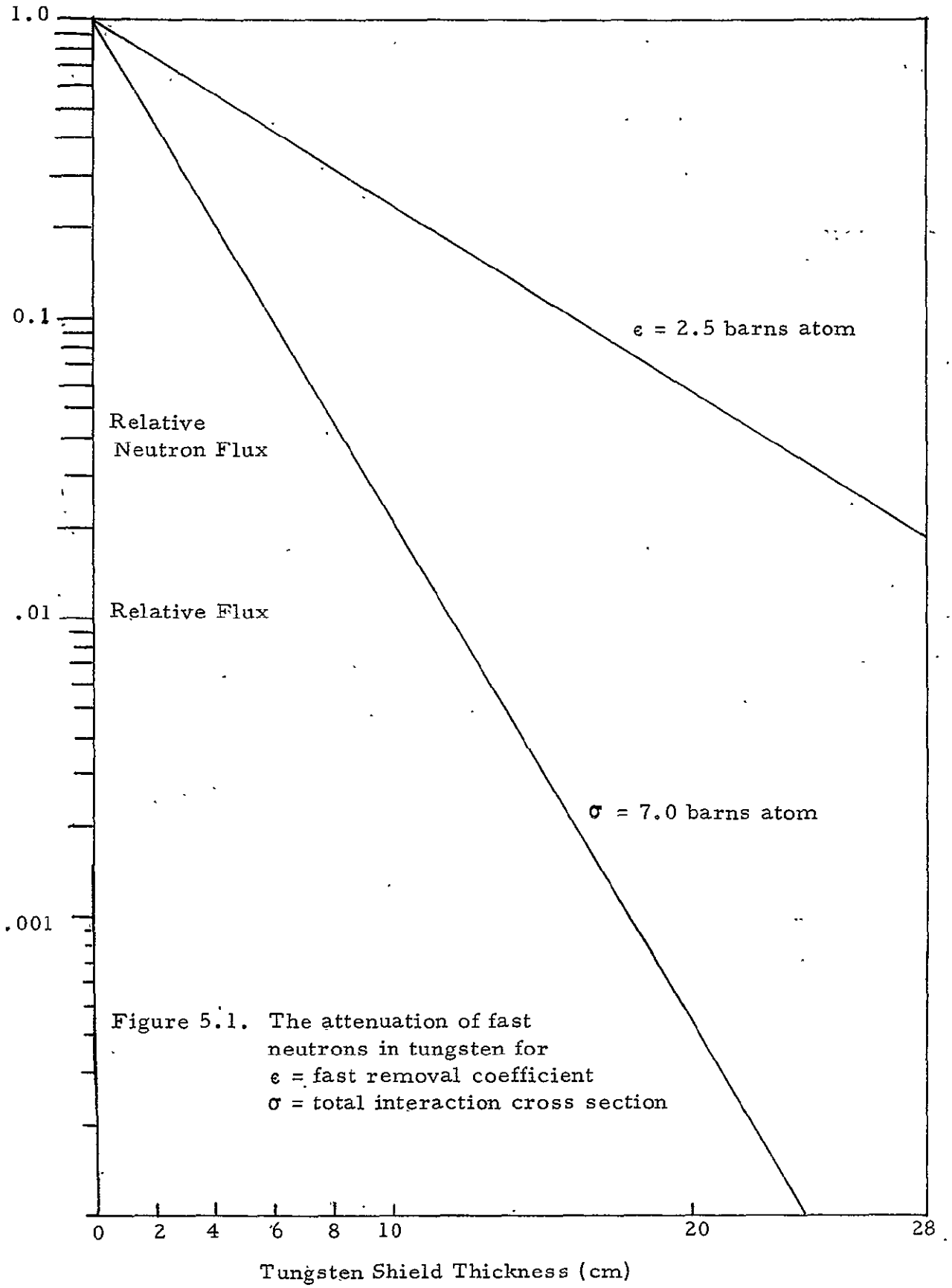

Figure 5.1. The attenuation of fast neutrons in tungsten for
ε = fast removal coefficient
σ = total interaction cross section

have plotted the fast neutron attenuation in tungsten in Figure 5.1. The upper curve is that obtained by using the slab fast neutron removal coefficient, and the attenuation will be at least that great. The lower curve uses the total interaction cross section, and the fast neutron attenuation can not exceed these values. Thus, we have bracketted the true attenuation, but conservatively consider it to approximate the upper curve.

5.4 THE NEUTRON ENVIRONMENT

The neutron and gamma ray environment has been calculated by the Lockheed Aircraft Corp. and reported in reference 56. We have taken the neutron dose rate, at the top of the LH_2 tank, and as a function of time prior to emptying of this tank, and have converted this dose rate to a fast neutron fluence (n cm^{-2} sec^{-1}). This rate is shown in Figure 5.2 along with the time integrated neutron flux (n cm^{-2}) as the upper curve. Note that the integrated neutron flux is only slightly above 10^9 n cm^{-2}, and thus no deterioration of the germanium detector energy resolution would result. The tungsten shielding will provide attenuation of about two decades and therefore the maximum neutron flux rate in the detectors is of the order of 2×10^6 n cm^{-2} sec^{-1}. This would induce a signal rate of 2×10^5 sec^{-1} per cubic centimeter of detector volume. This signal rate will produce a random coincident rate and effect the true coincident spectrum that is measured as discussed in Section 7 of this report.

For a fast neutron flux of 10^{11} cm^{-2} sec^{-1} as would be obtained at the bottom of the LH_2 tank and close to the reactor, a neutron induced signal rate of 10^8 sec^{-1} per cubic centimeter of detector would be obtained, assuming that no additional neutron shielding was provided. This high rate would prohibit gamma spectral measurements to be obtained unless the additional bulky shielding was provided. Note also, that with the attenuation of a factor of 100 calculated for 30 cm of tungsten, the detector energy resolution would limit the time of the measurement to only 100 seconds. This should be more than sufficient to determine the spectrum, but as previously stated, the neutron rate signal would probably be too large to allow precise gamma spectral measurements.

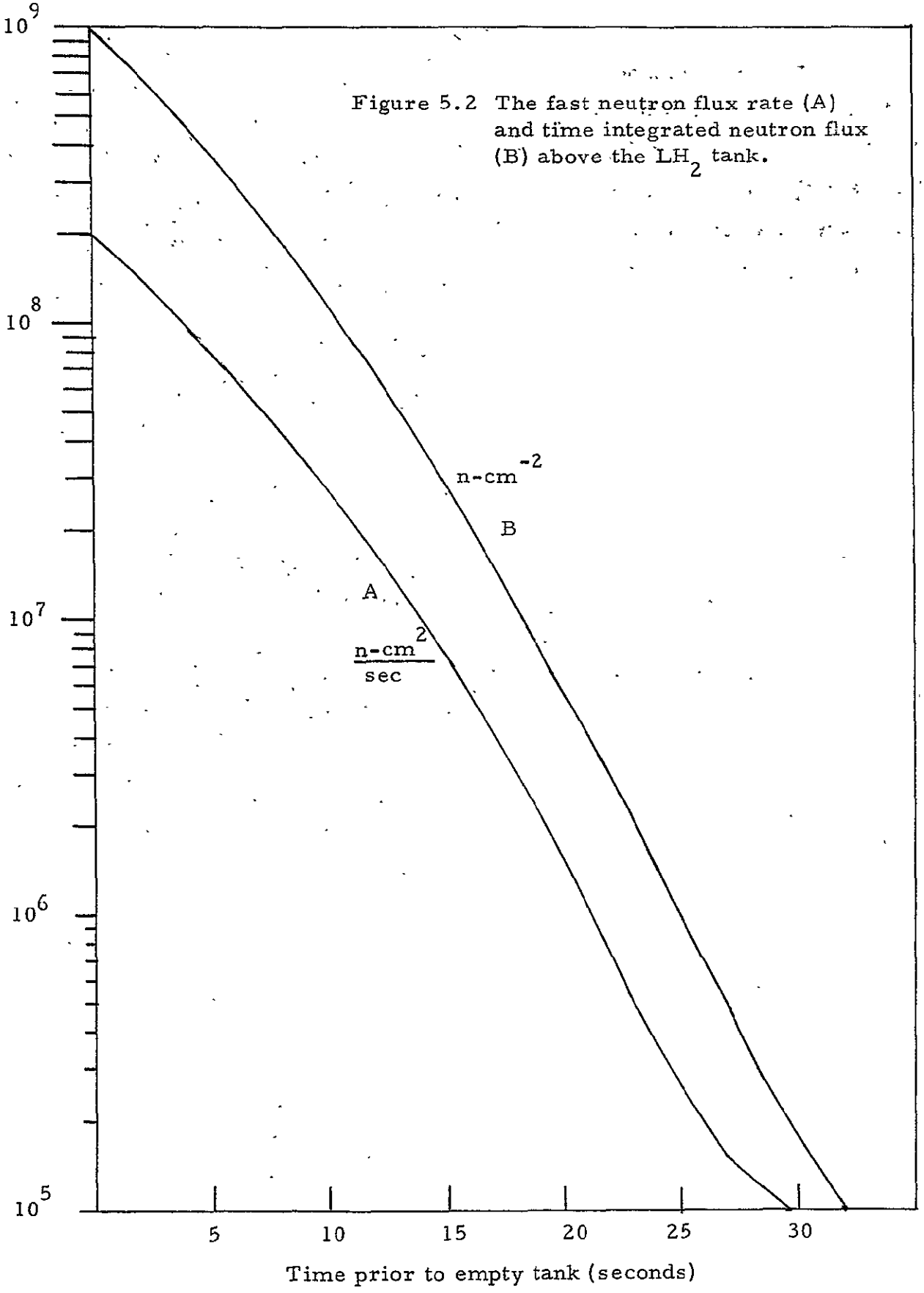

Figure 5.2 The fast neutron flux rate (A) and time integrated neutron flux (B) above the LH_2 tank.

Note also that fast neutrons having inelastic collisions with the tungsten will produce high energy inelastic scatter gamma radiation which may interact with the detector. As 90% of the neutron flux is removed in the first 15 cm of the tungsten, and the tungsten gamma absorption coefficients are relatively large at these high energies, it is thought that this signal source would be small. Calculations will be made to determine the magnitude of this background.

SECTION 6.0
GAMMA SHIELDING REQUIREMENTS

We have stated previously that a gamma shield is necessary to protect the detectors from the intense direct radiation. In this section we describe how the shield thickness is determined.

6.1 CHOICE OF MATERIALS

The shielding problem is simplified by the conditions of the measurement, i.e., the photon flux is nearly unidirectionally away from the reactor. Thus, the maximum shield thickness need only be placed between the detectors and the reactor and need only be large enough in diameter to shadow shield the detectors from the reactor.

Other radiation may be scattered into the detector from the side, but it can be shown that the maximum energy of such radiation is 0.5 MeV, and, therefore, only minimum shielding is required on the sides of the detector to provide sufficient attenuation.

The most efficient gamma shield material for continuous spectrum gamma rays is always obtained with the most dense material with the highest atomic number. This is because the mass absorption coefficients increase with atomic number and the linear attenuation coefficient is the product of the mass absorption coefficient and the density of the material. In addition, the fissile materials must be excluded because the neutron fission reaction would produce a large gamma background. Furthermore, we should select a material that is inexpensive and readily available. These selection guides result in the elimination of most high Z materials excepting lead and tungsten. Although lead is a higher Z material than tungsten, the lead density of 11.3 grams cm^{-3} is much inferior to the tungsten density of 19.3 grams cm^{-3}.

In addition, a large fraction of the inelastic neutron scattering gamma radiation produces a 115 keV gamma ray in tungsten and this radiation is readily absorbed within the tungsten.

The total gamma ray absorption coefficients for tungsten are shown in Figure 6.0.

6.2 METHOD OF CALCULATION

One must assume a specific gamma spectrum in order to calculate the leakage flux through the gamma shield. We have taken the fission spectrum of Figure 3.5 as the basis of the calculations although it is recognized that the NERVA spectrum may be very dissimilar. The spectrum was broken into 15 intervals of 0.5 MeV width, and the average photon density per interval was determined. The sum of the result was used to normalize the data in the form of the percentage of all photons falling within each energy group. Table 6.1 shows the steps and results of the calculations. Column 1 in Table 6.1 lists the energy interval for the listing in columns 2 through 8. Column 2 shows the relative number of photons from a fission gamma spectrum falling in each energy group. The sum of the numbers in column 2 is unity.

Column 3 lists the mean linear absorption coefficient for each energy group. These numbers were obtained by taking the mean mass absorption coefficient for tungsten over each energy interval and multiplying by the tungsten density of 19.3 grams cm^{-3}. Column 4 is the attenuation of the photons through 20 cm of tungsten. This is merely $\exp\left[-20\bar{\tau}\right]$ where $\bar{\tau}$ is given in column 3.

Column 5 is a listing of the buildup factors for each energy interval. Buildup factors are necessary because the absorption coefficients include scattering, i.e., all the photons are not absorbed. The buildup factor, B, is defined as the ratio of the actual gamma flux to that which would be calculated using basic exponential attenuation, as in column 4. A technique of numerical solution of the transport equation for gamma penetration in its fully accurate form has been developed by

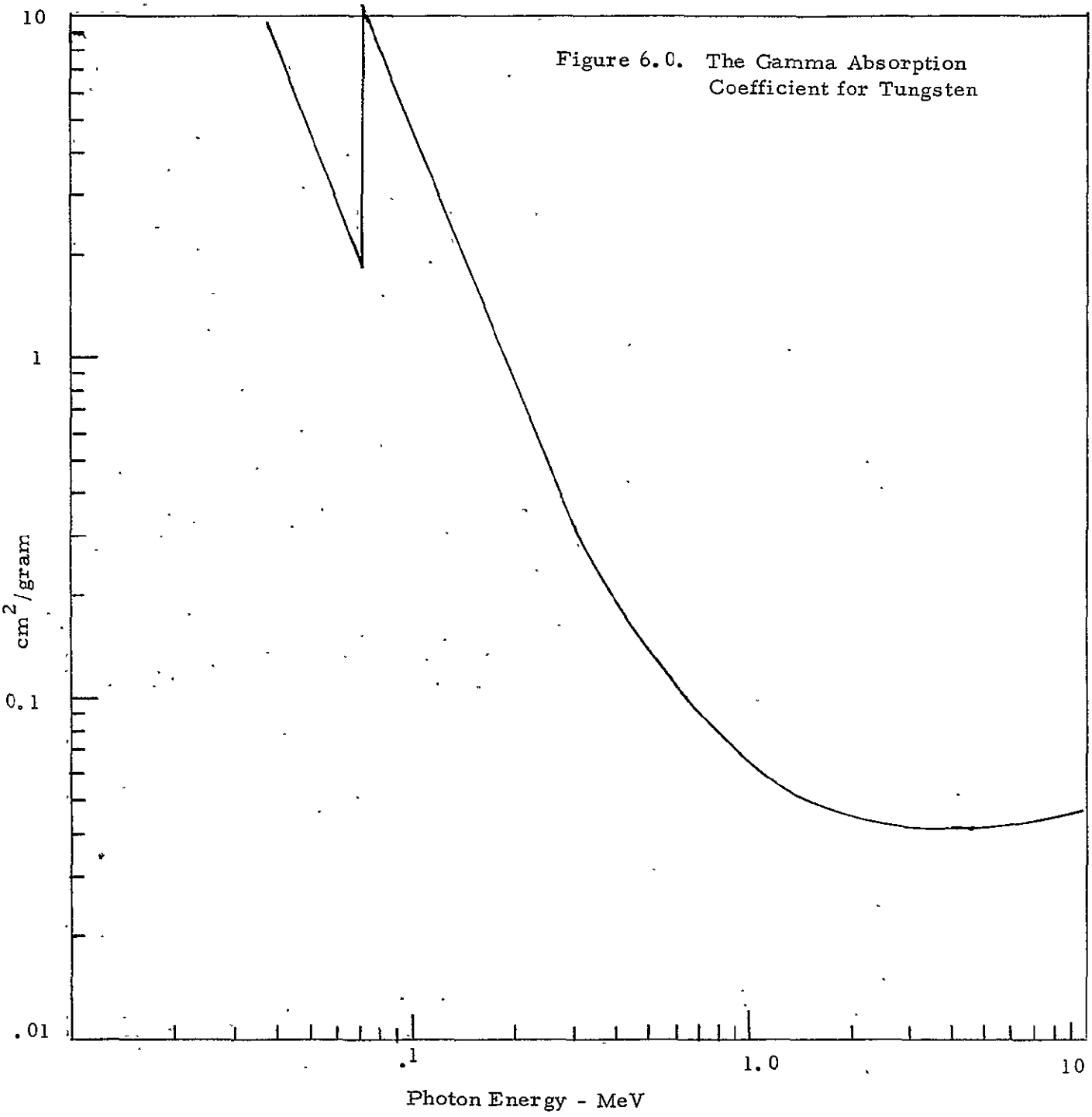

Figure 6.0. The Gamma Absorption Coefficient for Tungsten

Table 6.1

1 Energy Interval	2 Photon Fraction	3 Tungsten Linear Absorption Coefficient	4 20 cm Attenuation	5 Buildup Factor	6 Leakage Photons per R/hr^{-1}	7 Germanium Absorption Coefficient	8 Germanium Interaction per cm^3 per $R\ hr^{-1}$
< .5 MeV	.495	2.56 cm^{-1}		1.1			
1.0	.321	1.48	1.6×10^{-13}	1.1	2.8×10^{-8} cm^2		
1.5	.100	0.78	2.2×10^{-7}	2.1	2.8×10^{-2}	.31 cm^{-1}	9×10^{-3}
2.0	.064	0.73	4.9×10^{-7}	2.1	3.3×10^{-2}	.254	8.3×10^{-3}
2.5	.03	0.58	3.0×10^{-5}	4.4	1.95	.222	.435
3.0	.0173	0.58	3.0×10^{-5}	4.4	1.14	.202	.230
3.5	.01	0.58	3.0×10^{-5}	5.4	.81	.190	.145
4.0	.0075	0.59	2.7×10^{-5}	5.4	.53	.186	.100
4.5	.004	0.63	3.3×10^{-6}	4.5	.03	.175	.005
5.0	.0017	0.67	1.7×10^{-6}	4.5	.0065	.170	
5.5	.00125	0.73	4.9×10^{-7}	8.6	.0008	.166	
6.0	.00075	0.77	2.0×10^{-7}	8.6	.0008	.166	
6.5	.00035	0.82	9×10^{-8}	5.4	9×10^{-6}	.164	
7.0	.0002	0.86	2.6×10^{-8}	5.4		.1	
7.5	.0002	0.86	2.6×10^{-8}	5.4			

Spencer and Fano.[57] These calculations require a large scale computer, but curves for computing the buildup factor, which corrects the simple exponential calculations, are given in reference 55. These relate the buildup factor to three variables A_1, α_1 and α_2 by

$$B(E_o, \mu_x) = A_1 \exp\left[-\alpha_1 \mu_x\right] + A_2 \exp\left[\alpha_2 \mu_x\right] \quad (6.1)$$

where $A_2 = 1 - A_1$. These relationships were used to compute the buildup factors shown in column 5 of Table 6.1. Note that the buildup factors become constant after a few mean free paths and need not be recalculated for other shield thicknesses of the same material.

Column 6 indicates the leakage photon flux through 20 cm of tungsten with an incident flux of 5×10^5 photons cm^{-2} sec^{-1} which is equivalent to 1 R hr^{-1} of a fission spectrum. The data in column 6 is the product of 5×10^5, the buildup factor (column 5), the basic attenuation (column 4) and the photon fraction (column 2). The sum of column 6 is 4.5 photons cm^{-2} sec and represents the photon leakage of 1 R hr^{-1} through 20 cm of tungsten.

Column 7 is the linear absorption coefficients for germanium and is obtained by multiplying the mass absorption coefficients in cm^2 $gram^{-1}$ by the density of germanium. Column 8 is the photon interaction per cubic centimeter of germanium and is the product of columns 6 and 7. The sum of column 8 is .91 photons cm^{-3} per R/hr. Figure 6.1 shows the leakage spectrum and germanium interaction rate through 20 cm of tungsten.

6.3 SHIELD THICKNESS CALCULATION

The gamma spectrometer is to be designed to operate in 7×10^5 R hr^{-1}. Thus, the interaction rate in the germanium detectors with 20 cm of tungsten shielding would be 6.3×10^5 sec^{-1} cm^{-3} with an incident field of 7×10^5 R hr^{-1}. Our previous work showed that the detector volume would be approximately 3 cm^3.

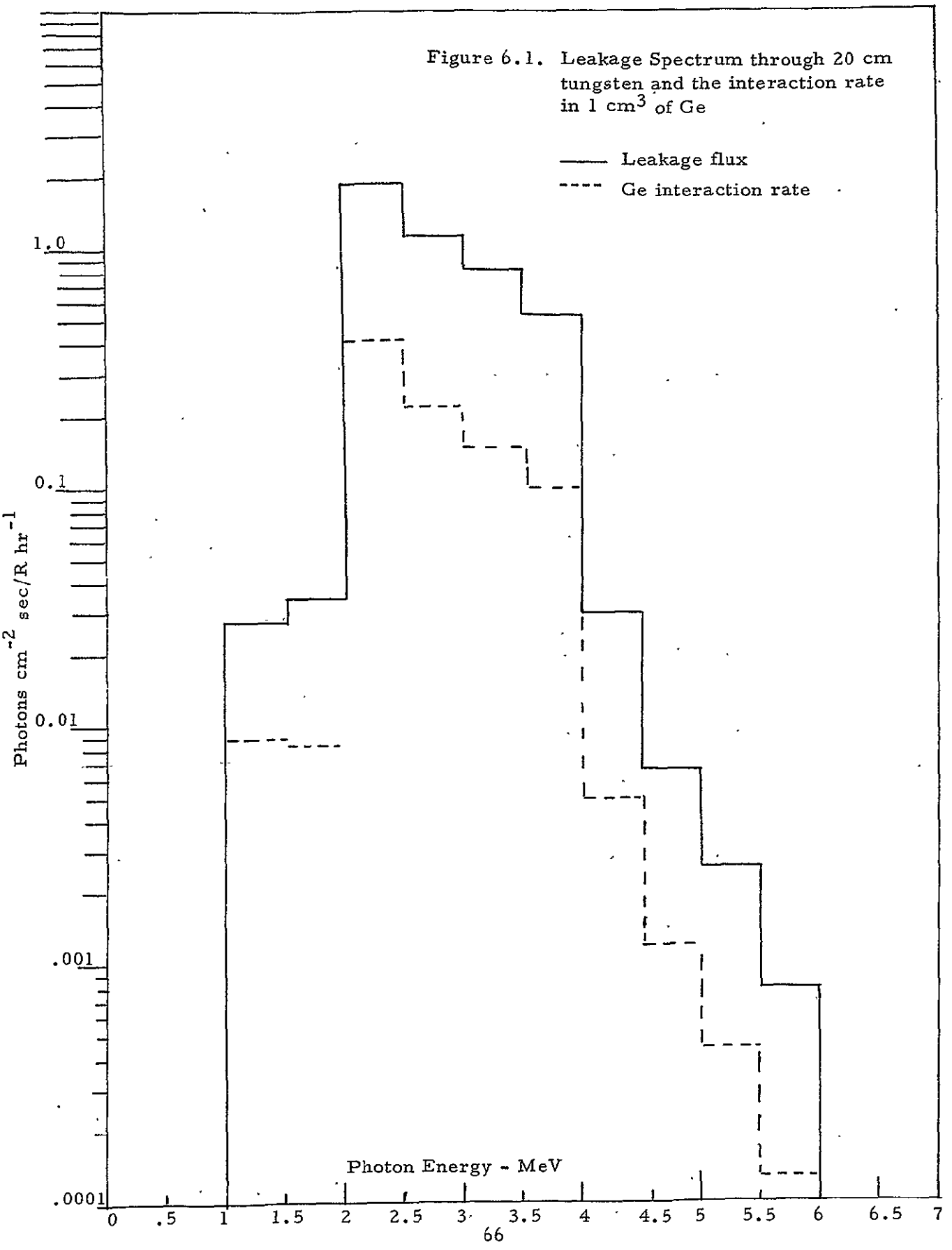

Figure 6.1. Leakage Spectrum through 20 cm tungsten and the interaction rate in 1 cm^3 of Ge

for a sum-Compton spectrometer, for a background rate of 1.9×10^{6} sec^{-1} at 7×10^{5} R hr^{-1}. We stipulate that this background should not exceed 10^{3} sec^{-1} to give a good signal to background ratio, as is discussed in the next section, and thus additional attenuation of $.5 \times 10^{-3}$ is required over that obtained with 20 cm of tungsten. The basic attenuations are listed in column 4 of Table 6.1 and the maximum value is 3×10^{-5}, whereas we require $(3 \times 10^{-5})(.5 \times 10^{-3}) = 1.5 \times 10^{-8}$ in attenuation. The increase length factor, n, can be solved for from the relationship

$$(1.5 \times 10^{-8}) = (3 \times 10^{-5})^{n} \tag{6.2}$$

or

$$\log 1.5 \times 10^{-8} = n \log 3 \times 10^{-5}$$

which follows from the power term of the exponential attenuation factor. Solving this, we obtain n = 1.7, or a total tungsten thickness of 34 cm is required to provide the attenuation required for 7×10^{5} R hr^{-1}.

The Lockheed calculations[56] indicate that the maximum dose rate at the tank top is only 2×10^{4} R hr^{-1} and if this is the maximum gamma flux that will be observed, than less tungsten shielding would be required. This is clearly a NASA decision, but from the preceding discussion of the neutron environment effects, it appears that gamma spectral measurements can not be anticipated below the LH_2 tank unless one is prepared to provide additional neutron shielding. Thus, Table 6.2 has been prepared to give the tungsten shield thickness requirements for three maximum dose rates.

Thus, we see that a considerable saving in tungsten thickness and overall weight can be obtained by designing the spectrometer head for the exact conditions to be expected, rather than for a general specification.

Table 6.2

Maximum Dose Rate	Tungsten Thickness Requirement
7×10^5	34 cm
10^5	30 cm
2×10^4	24 cm

SECTION 7.0

COUNTING RATE EFFECTS

The sum Compton spectrometer requires coincident pulses in detectors A and B to register a signal event. The energy deposited in both detectors is summed and is largely indicative of the incident energy. However, at high count rates in the individual detectors, random coincidence pulses will produce false signal events.

7.1 RANDOM COINCIDENCE RATES

The sum output is to be observed only if pulses are received "simultaneously" from the two detectors. Let N_A be the average true rate of events in detector A and N_B be the average true rate of events in detector B. Let N_{AB} represent the true coincident rate, which is the result of photons scattered from A into B. Note that if no background exists, detector B will see only those gamma rays scattered from detector A, as no direct radiation is incident on detector B. In this case, $N_B = N_{AB}$. However, a background due to neutrons and the attenuated gamma flux will be incident on detector B, and $N_B > N_{AB}$.

Within detector A, those pulses not associated with true coincident pulses is $N_A - N_{AB}$ and the coincident A gate is open for a fraction of the running time $(N_A - N_{AB})\ \Delta\tau_1$, where $\Delta\tau_1$ is the resolving time of the fast coincident circuitry. In detector B, the pulse rate not associated with the true coincident rate is $N_B - N_{AB}$ and the random coincident rate may be written as

$$N_R = 2\ (N_A - N_{AB})(N_B - N_{AB})\ \Delta\tau_1 \tag{7.1}$$

where the factor 2 comes from the fact that N_B pulses may precede or follow the N_A pulses to produce a random coincidence. Typically, a fast coincident circuit can given resolving times of the order of 10^{-7} seconds or better. We note that as N_{AB} approaches either N_B or N_A, that N_R becomes small, and it is necessary

to have $N_R << N_{AB}$, if an accurate gamma ray spectrum is to be obtained.

7.2 RANDOM SUM EVENTS

Although fast coincidence circuitry can give resolving times of 10^{-7} seconds or less, the pulse length requirement for collecting all the charge of an event is of the order of 1 to 2 x 10^{-6} seconds. Thus, if a fast coincidence gates "on" the sum pulse height analysis, the "on" time is of this duration. If another event occurs in either detector A or B during this "on" time, the additional event will add energy to the sum of the true coincident events. The true coincident events will have the gate "on" for the fraction of time $N_{AB} \Delta\tau_2$, where $\Delta\tau_2$ is the pulse duration. The chance of increasing the energy sum greater than the true coincidence sum is

$$2 \left[(N_A - N_{AB}) + (N_B - N_{AB}) \right] \quad N_{AB} \Delta\tau_2 \tag{7.2}$$

To insure that the observed spectrum is not unduly warped by random sum events, then

$$2 \left[(N_A - N_{AB}) + (N_B - N_{AB}) \right] \quad \Delta\tau_2 << 1 \tag{7.3}$$

The conditions impose an upper limit on the counting rates that can be tolerated in the detectors if reliable gamma spectra are to be observed. Thus, the maximum neutron flux rate and other sources of background in the individual detectors must be limited to insure compilation of an accurate spectrum.

7.3 MISCELLANEOUS TOPICS

7.3.1 Trip to Marshall Space Flight Center

A visit to the Marshall Space Flight Center was completed in mid-October. The purpose of the visit was to hold a technical conference on the state of the study. A brief review of the study was conducted by the author and comments from the

NASA technical staff were appreciated. It appears that the requirement for cooling semiconductor radiation detectors is objectionable. We will study the use of scintillation detectors for performing the measurements to alleviate the cooling requirement, and a report of this will be included in next month's technical report. It is certain that a single scintillation detector may be used for gamma spectral measurements, but in such a design, mathematical unfolding techniques will be required. A coincident sum spectrometer using scintillation detectors does not appear feasible at this time because of certain technical difficulties which will be discussed later in detail.

7.3.2 Papers for Review

A Georgia Tech Research Proposal dated July 15, 1969, was sent to the author for review. The proposal was for the design of a sum Compton spectrometer for certain biomedical radiographic uses. The sum Compton gamma ray spectrometer is an ideal spectrometer for identifying radioisotopes quantitatively amidst a background of other gamma radiation because of the excellent peak to tail ratio and superior energy resolution. Thus, spectral lines can be identified and measured quantitatively under conditions where other gamma spectrometers can not even resolve the spectral lines due to Compton interactions of other gamma radiation. For instance, the sum Compton spectrometer has been used to measure the quantity of specific fission products in nuclear reactor fuel elements, and thus provide a means of indicating the percent of burnup of the fuel element. Whether such good peak to tail ratios are required for the controlled biomedical studies is not known to the author, however.

The Monte Carlo calculation techniques developed at Georgia Tech specifically for determining the peak to tail ratio and efficiency of the sum Compton spectrometer should be a useful and valuable tool for predicting these values for a specific design. However, such computer techniques for designing a geometry would be rather expensive because of the large number of calculations required.

The other paper on the Apollo 16 gamma ray spectrometer was interesting but thought to offer no application to the present study.

SECTION 8.0

VARIOUS DESIGN CRITERIA

Most of the preceding sections have largely discussed basic physical and instrumental relationships necessary to the gamma spectrometer design. In this and later sections, we will be more concerned with detail design calculations and decisions.

8.1 REQUIREMENT FOR TWO DETECTOR SYSTEM

We can demonstrate that two separate detector systems are required to cover the entire energy band of 50 keV to 10 MeV. The demonstrative reasons are:

1) due to statistical accuracy over the entire spectrum

2) limitations due to detector size and the range of high energy recoil electrons.

8.1.1 Statistical Limitations

The statistical limitation is compounded by the short measuring interval ($\sim$5 seconds), the natural decrease of detector sensitivity at higher energies and the decrease in the photon flux of the spectrum at higher energies.

To demonstrate this effect, we have taken the fission spectrum shown in Figure 3.5 and multiplied each energy by the detector energy response shown in Figure 4.6. The total efficiency, i.e., the sum of the dashed and solid lines of Figure 4.6 was used. The result is plotted in Figure 8.0 and shows a five decade change in count rate per unit energy interval from 50 keV to 7 MeV.

The design goal is to achieve an accurate spectrum in each five second interval from start up to shutdown of the flight reactor. We have previously indicated that a maximum detection rate of the order of 10^4 sec^{-1} exists, and thus a 5 second interval would provide only that order of magnitude of total counts. For most intervals of measurement time, the count rate would be less as the flux rate is

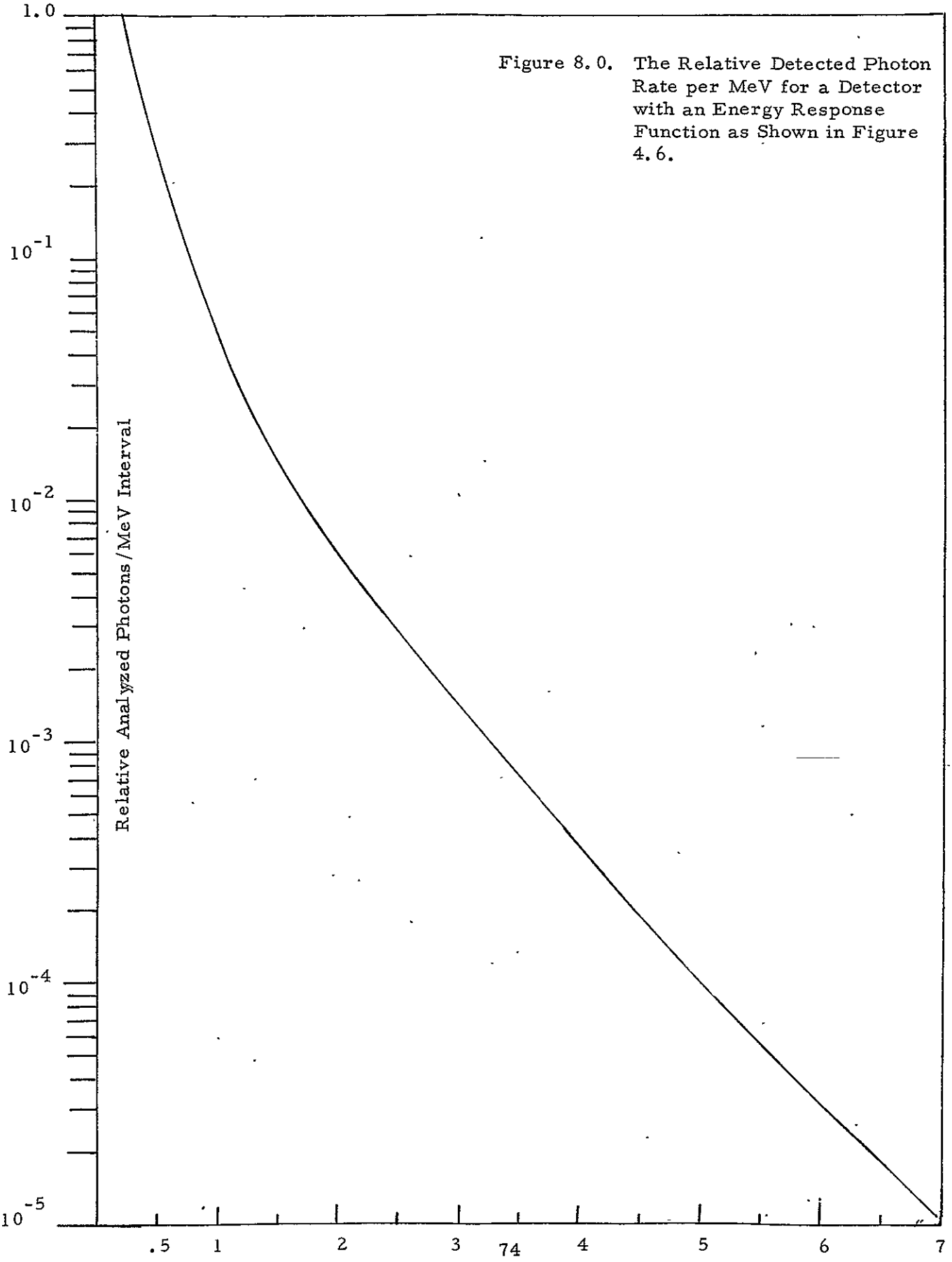

Figure 8.0. The Relative Detected Photon Rate per MeV for a Detector with an Energy Response Function as Shown in Figure 4.6.

constantly changing, and only a few discrete changes in overall sensitivity can be made by switching the mass of the Compton target. Thus we see from Figure 8.0, that with a total spectrum consisting of approximately 10^4 events, very good statistics will be obtained below 2 or 3 MeV, but the statistics at higher energies would be very poor, and an actual total event rate of one event per MeV per spectrum would occur at 7 MeV.

Therefore, to meet the time and accuracy requirements stipulated, we must divide the spectrum into energy intervals and take simultaneous measurements. The high energy detector system should be more sensitive above 1 MeV than the other system, and should not be subjected to the low energy photons existing in the environment. This can be accomplished by introducing a shielding plug between the target and the high energy detector.

The actual spectrum from the NERVA reactor will probably be harder than that used for illustrative purposes, but the statistical problem would still be very severe and will require two detector systems.

8.1.2 Detector Size Limitations

Most of our attention has been directed toward a sum-Compton detector system because this type of detector approaches a total absorption spectrometer more closely than any other small detector system. By total absorption, we mean that those photons recorded lose all or nearly all of their energy in the detector system. Thus, data reduction is much simplified and complicated mathematical unfolding techniques need not be applied. In addition, the coincidence necessary to provide a signal reduces the background from neutrons provided the detector system is small.

The latter stipulation of detector size is in conflict with the range of recoil electrons induced by high energy gamma radiation. Consider that the range of electrons is approximately 0.5 grams cm^{-2} per MeV of energy. Most of the energy of high energy photons is given to the recoil electron in the Compton scatter process, provided the angle of scatter is $\geq 90^{\circ}$ as stipulated by the Case III and Case IV

configurations previously discussed. Thus, a 7 MeV photon would result in at least a 6.5 MeV electron and the electron range would be 3.25 gram cm^{-2}. If detector A were of silicon with a density of 2.33 grams cm^{-3}, a length greater than 1.4 cm to absorb the recoil electron would be required. As the recoil electrons are produced throughout the volume, the detector would need to be at least twice that length to achieve a peak to tail ratio of unity. Such large detectors would increase the neutron induced count rate and lower the neutron flux in which the system could operate. In addition, if detector A is a silicon detector, it would be diffiult to obtain such a long depletion region, although an alternative of orienting the detector such that the radiation is incident across the applied field might possibly be used.

The high energy detector can circumvent the recoil electron path length by using a more dense and higher Z material for detector A, because the necessity for detecting low energy photons will not exist. This is discussed in more detail in another section of this report.

8.2 SENSITIVITY CALCULATIONS

We stated the relationship for the scattered beam intensity previously in equation (4.1). In this section we will indicate the magnitude of the various variables which must be established for a completed design. We will do this for two detector systems; the first for the low energy spectrometer and the second for a high energy spectrometer.

8.2.1 General Calculations

The scattering cross section for $\theta = 20^{o}$ is approximately 7×10^{-26} cm^{-2} per steradian per electron for moderate energy gamma radiation. The electron density is $N_o \times Z/A$ for materials, where N_o is Avogadros number, Z is the atomic number, and A the atomic weight of the material. This gives 3×10^{23} electrons per gram for most materials. The product of these two numbers is 2×10^{-2} cm^{2} $(steradian)^{-1}$ $(gram)^{-1}$ of the target material. The solid angle

subtended by the detector to the scattering target is simply $\pi r^2/R^2$, where r is the exposed radius of the detector and R is the separation distance of the detector and the scattering target. We have taken the product of the above scattering cross section and the geometric terms and plotted the results in Figure 8.1 with r and R as parameters for design purposes. If both r and R are specified, the counting rate may be determined by multiplying the appropriate value from Figure 8.1 by the incident beam cross sectional area, the gamma flux, the target mass per unit area and the detector efficiency for the spectrum.

The specifications require that the gamma ray spectrometer operate from 10^2 R hr^{-1} to 7×10^5 R hr^{-1} with good accuracy and statistics over the entire dynamic range. This is a range ratio of 7×10^3. Additionally, we desire to cover this range with three sizes of Compton scattering targets, one in each quarter of a rotatable wheel. The other quarter of the wheel is intended to have no target so that background subtraction may be programmed when desired. Thus, there will be two abrupt changes in sensitivity, from the heaviest to the middle target, and from the middle to the lightest target. Additionally, the count rate will vary from some minimum rate to a maximum rate for each target. If we set the allowable count rate change for each target equal to the abrupt change from target to target, we will maximize the average count rate over the total dynamic range. As three changes in count rate will occur, one gradual for each target and two abrupt, this maximum is the cube root of the dynamic range, which is numerically 19.1. We round this off to a factor of 20.

We have previously determined that a maximum coincident count rate of 10^4 sec^{-1} is a limit for the sum-Compton spectrometer. This was based on an efficiency of 4% and a maximum singles rate of a little more than 10^5 sec^{-1} in detector A. Thus, one range in count rate is from 500 sec^{-1} to 10^4 sec^{-1}, and the following table indicates where a target size shift is necessary.

Table 8.0. Design Count Rates

R/hr	Relative Target Mass	Counts/sec
10^2	1	5×10^2
2×10^3	1	10^4
2×10^3	.05	5×10^2
4×10^4	.05	10^4
4×10^4	.0025	5×10^2
8×10^5	.0025	10^4

The changes of Compton target mass would occur at 2×10^3 R/hr and 4×10^4 R/hr. The necessity for the change can be sensed by observing the count rate, either the singles rate or the coincident rate. Obviously, an inhibit signal must be available to prevent the change from occurring during a five second data accumulating period.

8.2.2 Low Energy Detector Sensitivity Calculations

We have shown that two separate detector systems are highly desirable to obtain good statistical accuracy over the entire spectrum and to limit the size of the detectors and consequently the neutron effects. We have also stated that a natural division of the spectrum would be of the order of 1 to 2 MeV, and a large region of overlap will naturally occur.

The preferred detector material for detector A in the low energy spectrometer is silicon. This preference is because response down to 50 keV gamma radiation will be obtained, whereas with germanium or a NaI(Tl) scintillator, the energy response falls off greatly below 200 keV in a sum Compton spectrometer. This roll off is caused by the high photoelectric cross section of the higher Z materials. In addition, silicon is sufficiently weighty in nuclear mass to reduce the neutron elastic collision recoil effect, whereas a plastic scintillator would be very susceptible to neutron recoil pulses because of the high hydrogen content.

Assuming that silicon will be used for detector A, and the dimensions of the detector are 5 mm diameter by 5 mm in length, this represents 1.16 grams cm^{-2} of absorber. Thus, a 1 MeV photon will create Compton recoil electrons whose path lengths are short compared to this length, and a good peak to tail ratio will be obtained. Higher energy gamma radiation would have reduced peak to tail ratios, as the recoil electron path lengths approach and exceed the detector dimensions. Therefore, we desire to limit the energy of the photons incident on the detector to energies of the order of 1 MeV. This can be accomplished by selecting a large angle of scatter from the Compton target to the detector as shown in Figure 3.2. We must not degrade the energy resolution too severely, however, and examination of Figure 3.2 indicates that a good compromise would be of the order of 60°.

We list the benefits of such a scattering angle for the low energy detector system.

1) The peak to tail ratio will be improved for a given incident photon energy. For instance, an initial 1 MeV photon will arrive at the detector as a 0.5 MeV photon with a correspondingly higher peak to tail ratio.

2) Photons of energy greater than 1 MeV will not be incident on the detector and thus will not generate the non-totally absorbed pulses which complicate spectral analysis.

3) Spectral data to 2 MeV can be obtained with detected photons of less than 700 keV, and pulses exceeding 700 keV can be stored in a single channel to correlate with the results of the high energy detector.

From the desired count rate (500 sec^{-1}) at 5 x 10^{7} γ cm^{-2} sec^{-1} (10^{2} R/hr) and the spectral efficiency of the case III spectrometer, we derive the desired efficiency of 2.5 x 10^{-4} for the Compton attenuator. This efficiency is the product of the collimated beam area and the factors plotted in Figure 8.1, and almost any combination yielding this product should be satisfactory. However, as we know the energy resolution of the scattered radiation is proportional to $d\theta$, we should have R relatively large because $d\theta$ is inversely proportional to R for a given size detector. However, as R is made larger, the dimensions of the necessary shielding will increase with a corresponding increase in weight. The author has arbitrarily selected R = 4 cm as a compromise of weight and energy resoluting and assuming a collimated detector radius of 2 mm, this gives a maximum $d\theta$ of slightly less than 6^{o}. That is, the scattering angle can be stated as $60^{o} \pm 3^{o}$. From Figure 8.1, the above values give a Compton attenuation of 1.6 x 10^{-4} cm^{+2} $gram^{-1}$ of target.

Graphite has a density of slightly more than 2 grams cm^{-3}, and if the large target is to have a thickness near that of the detector, we are limited to about 1 gram cm^{-2} (5 mm thick). We, therefore, require a collimated beam of area 1.57 cm^{2} to achieve the calculated sensitivity. There is nothing sacred about any of the above numbers excepting the sensitivity, and the exact sensitivity will require empirical determination.

8.2.3 High Energy Detector Sensitivity Calculations

For two detector systems to be worthwhile, the sensitivity of the high energy detector must be much greater than the low energy detector to the high energy region of the spectrum. Provided little low energy radiation reached the detector and nearly the same counting rates were obtained, much better statistics would be obtained for the high energy portion of the spectrum. The increased sensitivity may be achieved in several ways. A larger detector with greater density is necessary to absorb the high energy recoil electrons and this will increase the sensitivity. In addition, the detector may be placed closer to the scattering target for better geometric sensitivity. Also, a more massive scattering target can be of

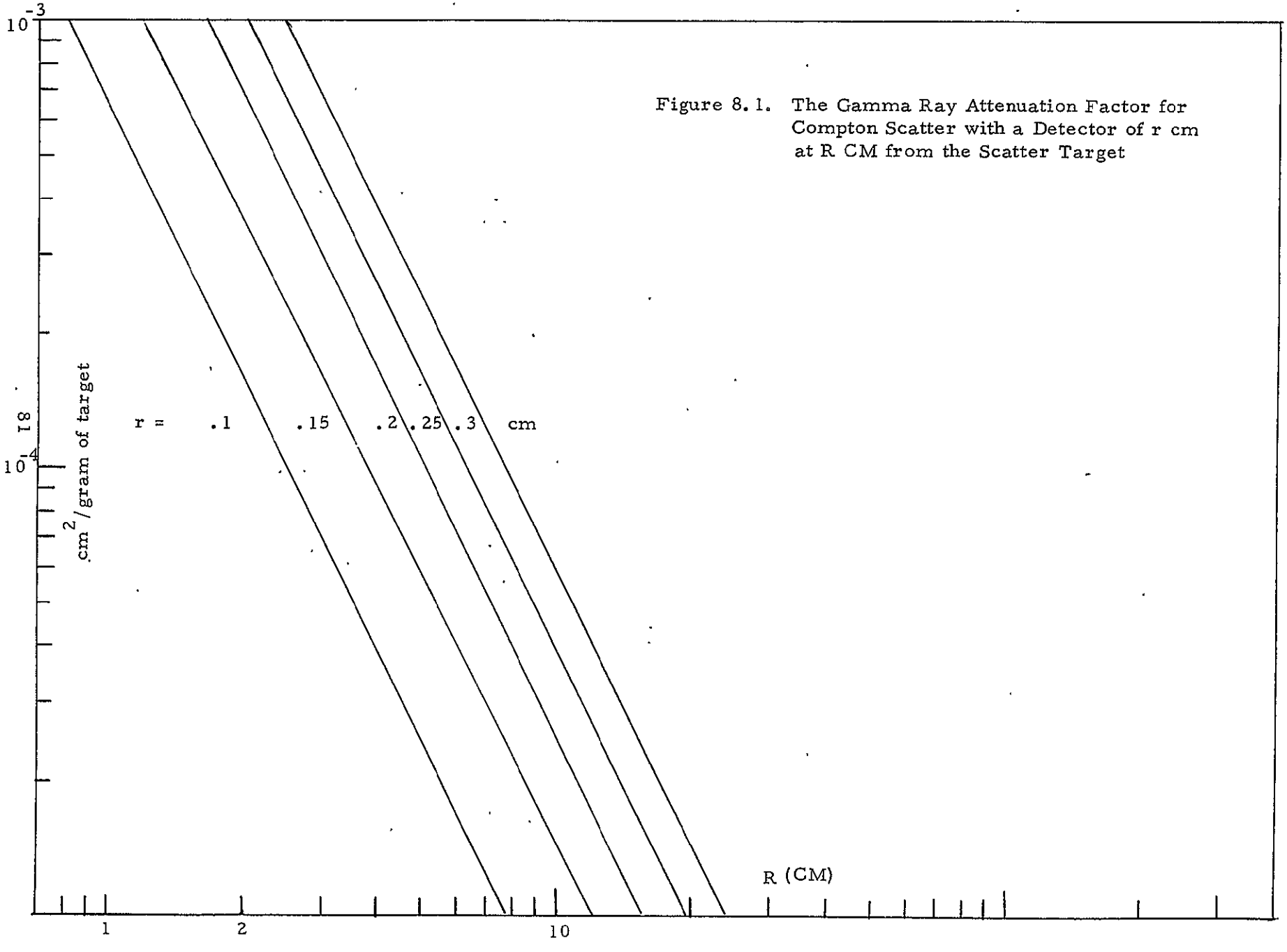

Figure 8.1. The Gamma Ray Attenuation Factor for Compton Scatter with a Detector of r cm at R CM from the Scatter Target

a rather high Z material as absorption of low energy photons is not critical and, in fact, is desirable.

A filter plug may be placed in the beam to remove most of the low energy gamma radiation. This plug will decrease the sensitivity of the system somewhat. The fractional transmission of gamma radiation through a 1 cm thick lead filter is shown in Figure 8.2 and we see that the transmission is relatively flat above 2 MeV, and gradually rolls off to 0.5 MeV below which the attenuation becomes dramatic.

The use of a 1 cm thick lead filter reduces the assumed fission spectrum intensity to 26% of the incident flux. However, 63% of the unfiltered flux is below 600 keV, while only 11% of the filtered flux is below 600 keV. The following table lists the fraction of the filtered and unfiltered flux below the listed energies, with both columns normalized to 100% through 7 MeV of a fission gamma spectrum.

Table 8.1

Gamma Energy	Fraction of Flux Below Listed Energy	
	Unfiltered	Filtered
.1 MeV	.07	0
.2	,164	0
.3	.352	.004
.4	.470	.024
.5	.564	.068
.6	.634	.115
.7	.693	.222
.8	.746	.280
.9	.781	.316

Sixty-eight percent of the filtered spectrum lies above 0.9 MeV while only 22% of the unfiltered flux is above 0.9 MeV and this partially meets one design goal of increased high energy sensitivity.

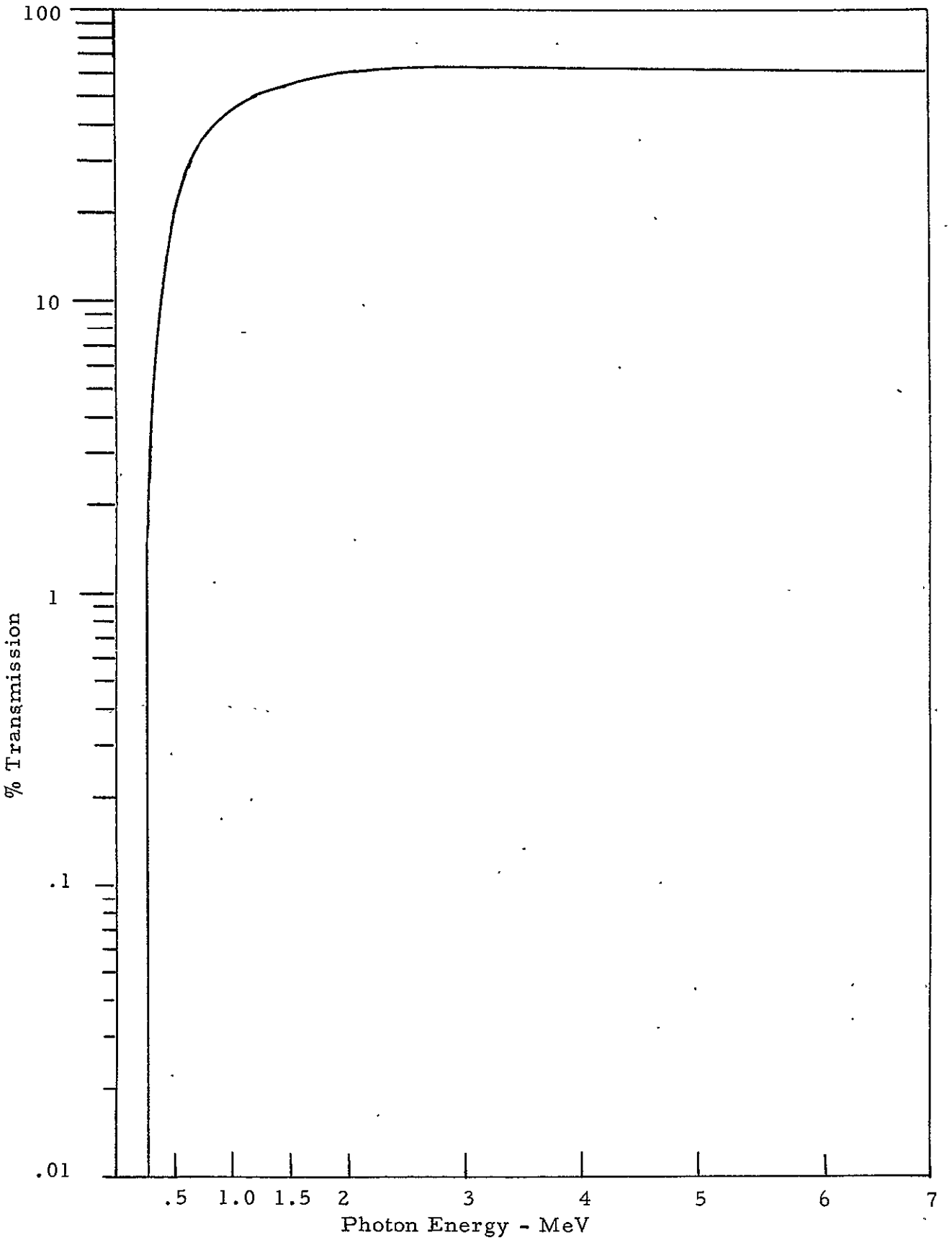

Figure 8.2 Transmission of Gamma Radiation Through 1 cm of Lead

We have previously indicated that the high energy spectrometer must be sufficiently large to absorb the high energy recoil electrons and that the electron range is of the order of 0.5 gram cm^{-2} per MeV. We may use dense and high Z materials for detector A because the detector scattered radiation of interest is higher in energy, and less likely to be absorbed within detector A than for the low energy spectrometer. Likely detector materials include germanium and cadmium telluride semiconductors and sodium iodide scintillators. The following table lists some pertinent data on these materials.

Table 8.2

	Ge	Cd Te	NaI
density	5.33 gr cm^{-3}	6.20 gr cm^{-3}	3.67 gr cm^{-3}
atomic number	32	48, 52	11, 53
atomic weight	72.6	112, 127	22.9, 126.9

CdTe cannot provide adequate depletion depths at the present state of development and we consider therefore only Ge and NaI as possible detector materials. Either detector material can be used as a high energy sum Compton spectrometer, but because of its lower density, a NaI detector would need to be 45% larger to have identical efficiency and peak to tail ratios as a germanium detector. It would, therefore, be more susceptible to neutron and gamma ray background effects, and we recommend a germanium-germanium sum Compton detector configuration. The dimensions of the detector system must be larger than those comptemplated for the low energy detector to absorb the high energy recoil electrons.

The detector system will also respond to pair production interactions, where one or both of the annihilation photons escape detector A and are absorbed in detector B. These reactions will tend to keep the detection efficiency high above

2 or 3 MeV. Since the pair production cross section increases proportional to Z^2, even higher Z detectors would be desirable but, at the present are unsatisfactory or unavailable.

The recoil electron angle of scatter for high energy photon Compton scatter is always small. For instance, a 7 MeV photon which is scattered 90° provides only a three degree angle of scatter for the recoil electron. Thus, the length of detector A must be sufficient to absorb the full energy of the recoil electrons. Those recoil electrons whose range extends beyond the detector limit, will produce a signal less than the incident photon energy and contribute to the tail of a mono-energetic spectrum. The attenuation of high energy photons within the detector is not great and the interaction rate along the axis is almost constant. Thus, the peak to tail ratio, for a given photon energy is nearly

$$\left(\frac{\text{peak}}{\text{tail}}\right)_E = \frac{L}{2r_E} - 1 \qquad (8.1)$$

Where l is detector length and r_E is the recoil electron range, both expressed in units of grams cm^{-1}. Note that relationship 8.1 applies only to the peak to tail ratio of the recoil electron contribution to the sum Compton signal, other tail pulses are generated if the scattered photon is not completely absorbed in detector B.

The energy response of a germanium-germanium sum Comtpon and sum-pair production detector was calculated and is shown in Figure 8.3. Detector A was considered to be 2 cm in length and 0.5 cm in diameter, and detector B was considered to be 2 cm in length with an O.D. of 1.5 cm and an I.D. of 0.5 cm encompassing detector B. The curve S-A implies those events scattered in detector B and completely absorbed in detector A. Curve S-S is those events scattered in detector A and scattered again with the first collision in detector B. Most of the latter events will be completely absorbed with multiple scattering and and the peak to tail ratio is higher than implied.

Figure 8.3 The Energy Response of a Case V Sum Compton and Sum-Pair Spectrometer.

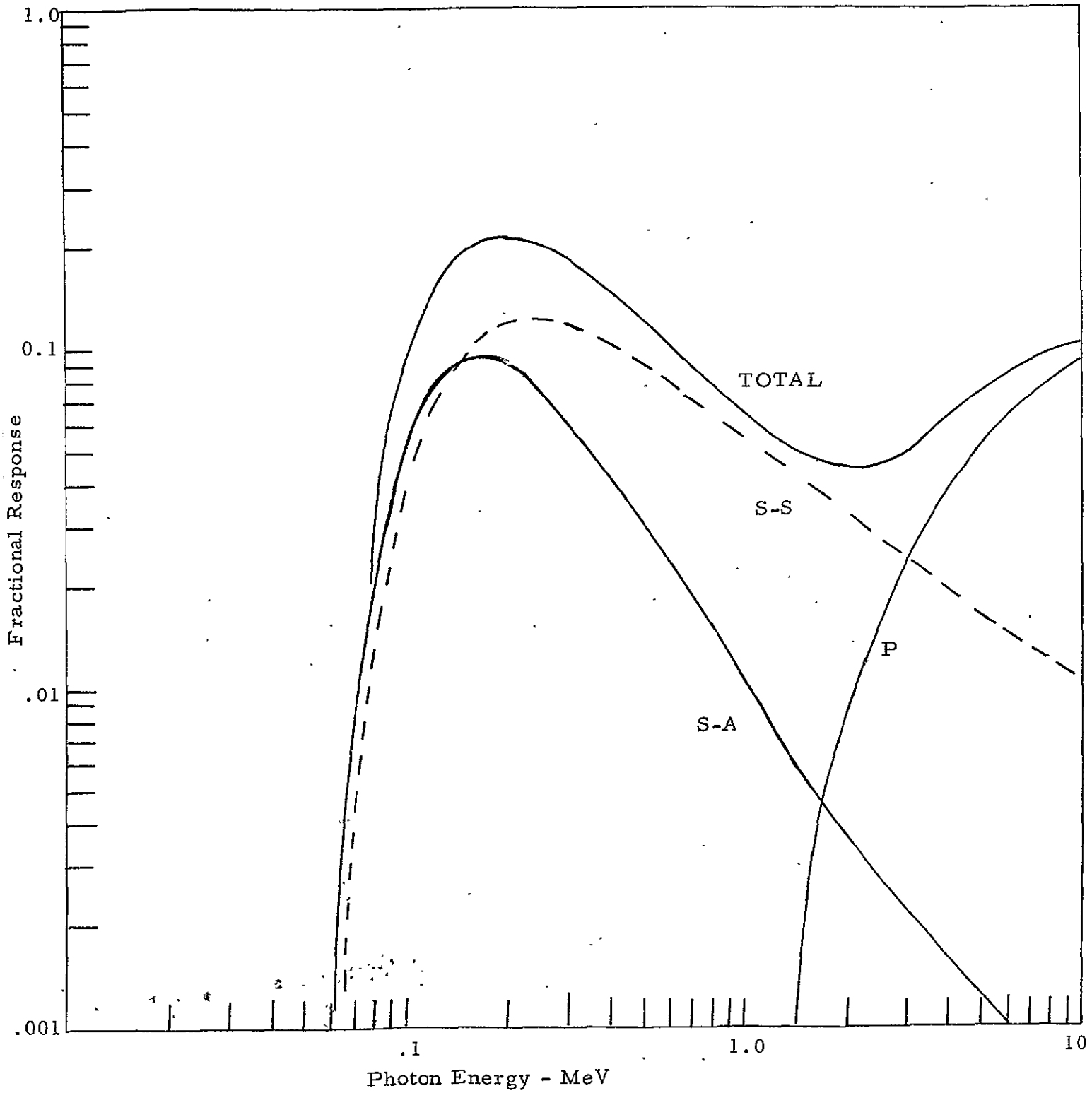

In addition, the scattered photons from incident high energy gamma rays are only a small fraction of the incident energy, so the tail is packed close to the peak in energy. The low energy decrease in response is due to the self absorption of scattered photons in detector A and is the reason that a germanium detector A cannot be employed in the low energy detector system.

The P curve indicates the pair production interactions wherein either annihilation quanta is detected in detector B. The sum of the energies will be obtained, and electronically will be identical to sum Compton events.

Note that a larger diameter detector can be used without changing the fractional energy response significantly except for more attenuation at the low energies. A slight decrease in the pair production response will also occur as detector A is increased in diameter, because a greater portion of the annihilation quanta will be absorbed within detector A.

Construction of such a long detector system will require coaxial electrodes in both detector A and detector B. The radial plane separating the two detectors can be the "p" or grounded junction for the two back biased detectors.

The sum pair production response of the detector system increases dramatically for the higher energies. This is convenient to our design goal as it will increase the statistical accuracy for the high energy portion of the spectrum.

We have taken the standard gamma fission spectrum, modified and attenuated by a 1 cm thick filter whose transmission characteristics are shown in Figure 8.2, and multiplied each energy interval by the total energy response curve shown in Figure 8.3. This gives an overall efficiency of .018 for this particular spectrum. Thus, 1.8% of the incident photons in a fission spectrum will be analyzed. With knowledge of this overall counting efficiency, we may proceed with determining the geometric factors and the scattering target mass.

Unlike the low energy Compton scattering target, the target for the high energy spectrometer may be of a high Z material such as copper, as we are not concerned with the attenuation of low energy photons (< 500 keV) within the target. Furthermore, an increase of pair production within the target should not be too detrimental as the 500 keV annihilation photons are below the prime region of interest and this portion of the spectrum will be obtained with the other detector. The lead filter is another source of annihilation radiation.

We desire to keep the angle of scatter small so that the energy shift of the high energy photons is not significant with the attending loss of energy resolution. An angle of 20^{o} seems appropriate, producing little energy shift and allowing placement of the detector system outside of the primary photon beam, yet inside of the low energy detector.

The desired geometric scattering attenuation is 5×10^{-4} if we are to obtain comparable count rates simultaneously in both the high energy and low energy detector systems. Note that the relative count rate in the two systems will be a function of the incident spectrum, and the design goal of nearly equalizing the count rates in the two systems is subject to wide error. The attenuation factor of 5×10^{-4} is based on our presupposed fission gamma spectra.

Several design layouts of the detector systems, shields and Compton targets indicate that a target to detector distance of 6 cm is necessary. With a 4 mm diameter beam incident on detector A, the geometric efficiency is 8.4×10^{-5} cm^{2} $gram^{-1}$ of target. As the primary beam area was established at 1.57 cm^{2} in the design of the low energy detector system, a target thickness of 3.8 grams cm^{-2} for the target is computed to provide the 5×10^{-4} Compton scatter attenuation. This may be achieved with a copper target .43 cm in thickness for the most massive target. The second and third targets could be .21 mm thick copper and 0.45 mm thick carbon respectively.

8.3 ENERGY RESOLUTION CALCULATIONS

The energy resolution of a detector, measure as the full width at half maximum amplitude, of a Gaussian distribution of pulse heights is a function of three components. It may be expressed as

$$(FWHM)^2 = \Delta_{EL}^{\ 2} + \Delta_{COLL}^{\ 2} + \Delta_{GEN}^{\ 2} \qquad (8.2)$$

where

Δ_{EL} is the electronic noise line width

Δ_{COLL} is due to inefficient charge collection

Δ_{GEN} is the electron-hole pair creation statistics

Relationship (8.2) is the theoretical minimum energy resolution and other instrumental effects, such as a variation in count rate, can produce poorer energy resolution than the theoretical minimum.

The Δ_{GEN} term which is the largest term at high energies, is dependent on the primary energy E, the average energy to create an electron hole pair, ϵ, and the Fano factor, F, by the well known relationship

$$\Delta E\ (FWHM) = \left[8\ (\ln 2)\ F\epsilon E\right]^{1/2} \qquad (8.3)$$

$$= 2.35\ (F\epsilon E)^{1/2}$$

The Fano factor has been measured by several investigators and is of the order of 0.1 for germanium.

In any event, the energy resolution obtainable with modern silicon and germaniur detectors is very good, and is much better than required for this study. However, the Compton scatter attenuation technique degrades the energy resolution because of the finite differential angle of scatter and the Compton energy shift.

The energy resolution obtained by the Compton attenuation technique may be written as

$$\Delta E_o = \Delta E' \left[1 + \alpha (1 - \cos \theta)\right] + \frac{\alpha E_o \sin \theta \, d\theta}{\left[1 + \alpha (1 - \cos \theta)\right]} \qquad (8.4)$$

where

ΔE_o is the incident spectral energy resolution

$\Delta E'$ is the detector instrumental energy resolution

The first of the two terms on the right hand side of the equality sign represents the detector resolution magnified by the Compton energy shift. The second term represents the resolution due to the finite angle of scatter, and this second term is the more dominant term at moderate and high energies.

We show the calculated energy resolution of the two detector systems in Figure 8.4. The lower curve represents the intrinsic detector resolution, which we have conservatively plotted it about twice as large as is generally obtained with a good germanium or silicon detector.

The 60° curve represents the energy resolution of the low energy spectrometer as calculated from expression 8.4. The 20° curve represents the high energy spectrometer. The dashed lines represent the contractual energy resolution (FW HM), and it should be noted that the derived energy resolution for the two spectrometers is the total theoretical line width, not the width at half maximum. The logarithmic scale compresses the increase in energy resolution with energy, but the spectrometer will fundamentally meet the specifications over their respective energy ranges.

Performance of the detector system to reasonably high count rates is of paramount importance. A feedback resistor to the input of the first FET in a charge sensitive amplifier is generally employed to compensate for the average

Figure 8.4. $\theta = 60^{\circ}$ Low Energy Spectrometer
$\theta = 20^{\circ}$ High Energy Spectrometer

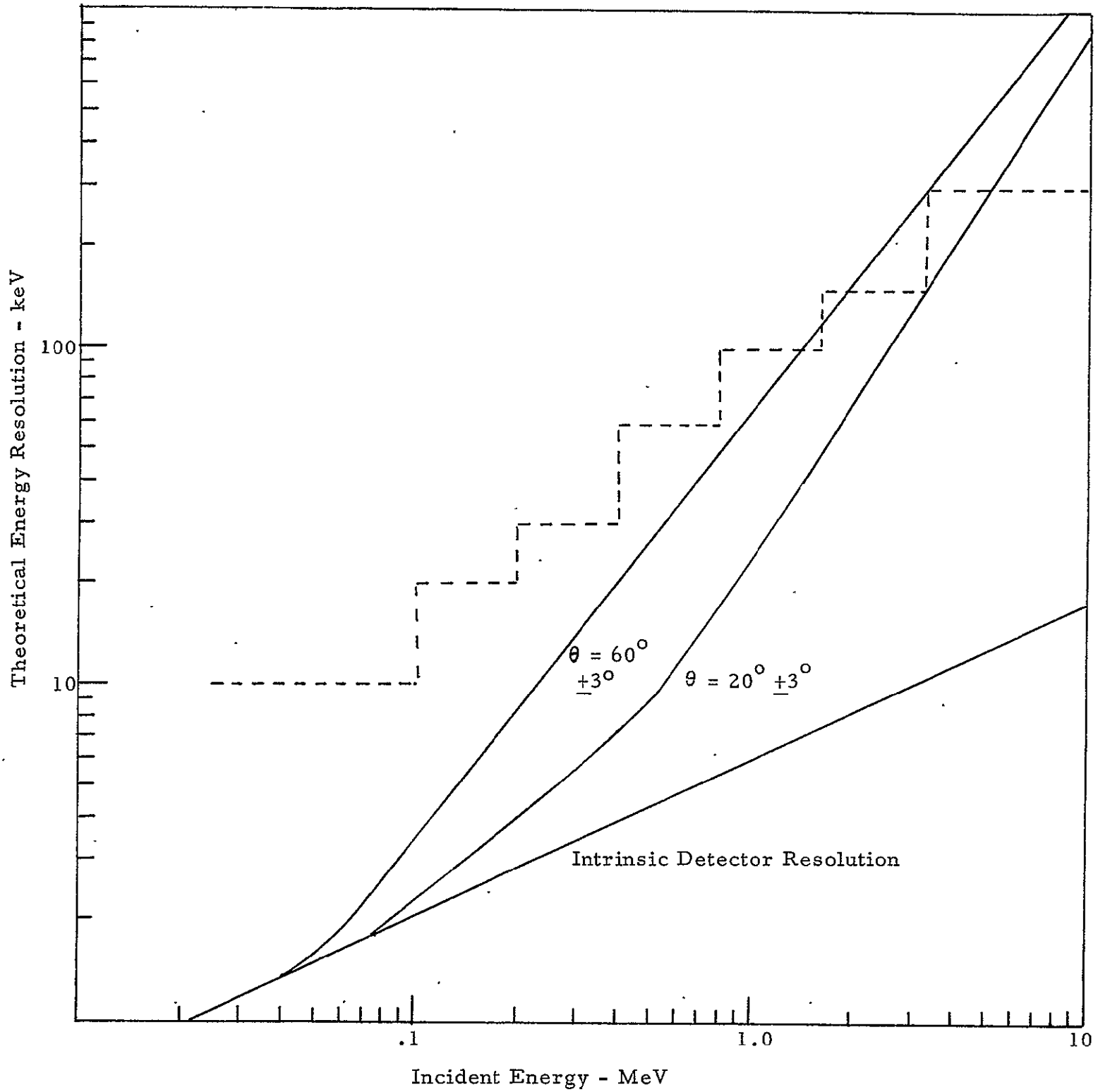

Figure 8.5. A Typical Energy Resolution vs. Count Rate Curve (ORTEC 117 Preamp)

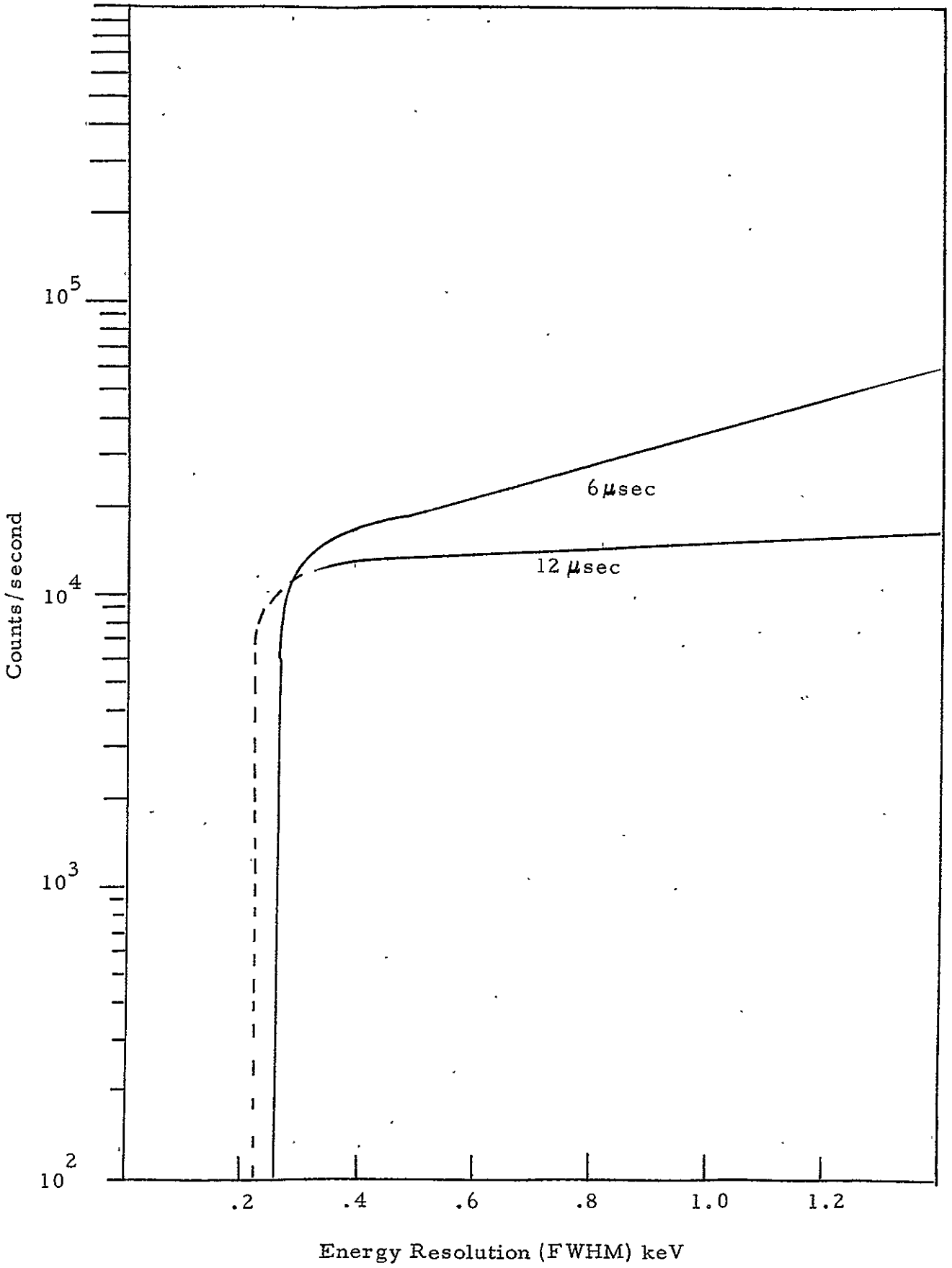

radiation induced current. This stablizes the operating point of the FET and the gain of the amplifier. The required feedback is proportional to the count rate and the average photon energy. Thus, a smaller feedback resistor is required for high count rates and spectral energy content and this leads to more instrumental noise. There is a definite trade-off of good energy resolution at low count rates and a high count rate capability. Other effects due to pulse on pulse and pulse on pulse tail pile up increases resolution broadening. The superior energy resolutions frequently reported in the literature are obtained with very long integration time constants and are directly opposed to high count rates.

It is necessary to return the amplifier base line promptly to the quiescent level after processing an event to prohibit spectral distortion. Figure 8.5 shows the change in energy resolution as a function of count rate for a good (ORTEC 117) laboratory preamplifier with two different time constants in the feedback loop. Note that the design spectrometer will have count rates up to 2×10^5 sec^{-1}, although the coincident signal rate will be limited to about 10^4 sec^{-1}. Fortunately, with the small detectors of the contemplated design, we anticipate time constants of less than 0.5 microseconds to be utilized. This will broaden the energy resolution but should allow good spectral data to be obtained at single count rates exceeding 10^5 sec^{-1}, and the increase in instrumental noise should be small compared to the Compton attenuation broadening shown in Figure 8.4.

8.4 EFFECTS OF OPERATING TEMPERATURE ON SEMICONDUCTOR DETECTORS

We briefly discuss the pertinent experimental results of temperature effects on semiconductor radiation detectors. Martini[58] et al presented a summary of the subject with theoretical and experimental considerations. Other sources of data are in references 59, 60 and 61.

8.4.1 General Considerations

There are several factors that determine the observed performance of semiconductor radiation detectors with variation of temperature. These factors include:

8.4.1.1 Leakage Current - Leakage currents are composed of surface leakage and bulk generated leakage, both of which vary widely from device to device. The surface leakage current is complex but generally increases with temperature. The bulk current generally increases exponentially with temperature corresponding to the decrease in resistivity. High resistivity is necessary to obtain large depletion depths without undue leakage currents and subsequent current generated noise.

8.4.1.2 Carrier Drift Velocity - The drift velocity is related to the product of the electric field and the mobility, which in turn is related to electric field and the temperature. Mobility is not constant with high electric fields in such a way that the drift velocity becomes constant with varying electric fields. As the temperature is increased, the drift velocity decreases for a given field, and increases the probability of trapping.

8.4.1.3 Trapping - Trapping results in the loss of an energy resolution and pulse height. The cross section for trapping increases for lower temperatures but, in an electric field, the carriers have a much higher effective temperature (from the applied electric field) which can be supplied better at low temperatures. Detrapping can occur from thermal agitation or from the electric field forces.

8.4.1.4 Electron-Hole Pair Energy - Because of the temperature dependence on the forbidden energy band gap, the energy required to create an electron-hole pair decreases slightly with increasing temperature. Thus, for accurate calibration, a semiconductor detector should be operated at a single temperature. The energy shift is approximately 0.02% per ^{o}C for both silicon and germanium and, therefore, temperature stability need not be precise.

8.4.1.5 Lithium Mobility - Lithium migration is a problem only with lithium drifted germanium detectors in which the lithium ions tend to diffuse out of the detector at temperatures above -20 ^{o}C. Lithium drifted silicon may be used to +60 ^{o}C even with applied electric fields.

8.4.2 Lithium Drifted Silicon and Germanium

The most widely used semiconductor detectors for X-ray and gamma radiation spectroscopy are lithium drifted silicon and germanium, and consequently more studies of the temperature effects on these materials are available than for other materials. It seems likely, however, that the same general effects would be observed in intrinsic silicon and germanium. Martini[58] shows the energy resolution of Si(Li) and Ge(Li) detectors from 30 to 200 °K. In general, the energy resolution degrades only moderately at 200 °K if a reasonably high (> 450 volts) bias voltage is applied. The charge collection time also increases by about a factor of two from 77 °K to 200 °K. We conclude from the referenced paper that operation of both Si(Li) and Ge(Li) detectors are feasible at temperatures of near 200 °K, with little determination of performance from that obtained at the usual 77 °K operating temperatures.

8.4.3 Intrinsic Germanium Temperature Effects

Intrinsic germanium has recently become available for detector manufacture but a large amount of experience with these detectors has not been accumulated. The only advantage of intrinsic germanium detectors over lithium drifted germanium detectors is that the detectors need not be stored at low temperature, and, in fact, the detectors may be cycled to room temperature repeatably without degradation. A short study of a single small intrinsic germanium detector was conducted at liquid nitrogen and dry ice temperatures. The detector did not have as good energy resolution as is generally expected from Ge(Li) detectors.

Summary of Intrinsic Germanium Temperature Effects

Temperature	77 °K	195 °K
Leakage Current	5×10^{-13} amps	2×10^{-8} amps
FWHM		
22 keV	.45 keV	2.0 keV
122 keV	1.5 keV	3.7 keV

A pulser was used to determine the current generated noise and gave .36 and 3.5 keV FWHM at 77 ^{o}K and 195 ^{o}K. The above study supports the more detailed work of Martini and shows that if the ultimate in energy resolution is not required, that operation at dry ice temperature is available for a semiconductor spectrometer design. It is the author's experience that the parameter of energy resolution varies more from detector to detector than is realized from temperature variation from 77 ^{o}K for a given detector.

8.5 COOLING METHODS FOR SPACE USE

Liquid nitrogen (LN_2) at 77 ^{o}K is widely used in the laboratory for semiconductor radiation detector cooling because LN_2 is economical and readily available. However, liquid nitrogen presents an engineering problem for zero gravity uses in that it must be vented and loss of liquid through the vent is possible. Although this problem may be solved, other solutions seem desirable.

The use of a solid cryogenic material which sublimes on evaporation appears as a most attractive alternative. Although venting is also necessary, unless unduly heavy container walls were used, the loss of solid material through the vent seems unlikely. Another advantage, at least for CO_2, is the higher heat of vaporization over that of LN_2, so that considerably less cryogenic material is required for a specific length of mission. We have already indicated that both germanium and silicon should give satisfactory performance at dry ice temperatures. We list below the few pertinent cryogenic properties of LN_2 and dry ice.

	N_2	CO_2
Vaporization temperature	77 ^{o}K	195 ^{o}K
Heat of vaporization	1.33 k cal/moles	6.0 k cal mol
Heat capacity	17.3 cal/mol/degree	30.9 cal/mol degree

Only one fourth as much CO_2 would be required for a mission as would be required for LN_2.

The dry ice can be formed within a cryostat by supplying CO_2 gas through the vent and cooling the chamber by flow of liquid nitrogen. LN_2 could also be used to hold the CO_2 for periods preceding launch and removed prior to launch. Perhaps, for unduly long missions, a portion of H_2 gas vented from the LH_2 tank can be used to extend the time period further.

8.6 OTHER DETECTOR POSSIBILITIES

We have proposed silicon-germanium and germanium-germanium sum-Compton spectrometers as the preferred detector systems for the gamma spectral measurements. This selection was largely due to superior energy resolution and minimum neutron induced signals, and the sum-Compton technique is proposed so that little ambiguity would be obtained in the spectral results. Other detector materials and detector systems can be employed, perhaps quite satisfactorily, and we briefly examine these detectors.

8.6.1 Single Scintillation Detectors

The simplest detector system would be a single crystal detector to which the gamma radiation is scattered. This crystal could be either a germanium semiconductor detector or a scintillation crystal. A single crystal spectrometer would be much more efficient than the sum-Compton spectrometer, as it would detect each event, rather than only those scattered between the detectors. However, the data would require elaborate mathematical treatment to obtain the incident spectrum as most of the photons would only be partially absorbed within the detector. Because of the high neutron flux, the detector must be small to reduce neutron background, and this small size reduces the peak to tail ratio to values less than obtained with most laboratory gamma ray spectrometers.

We show in Figure 8.6, which was supplied by Prof. R. Pepelnik, the large improvement of the peak to total ratio obtained by the sum-Compton technique. Note that a peak to total ratio of unity is a peak to tail ratio of infinity. The photopeak-spectrometer curve represents a single crystal spectrometer and the peak fraction is as low as 1 percent at 2.5 MeV.

Figure 8.6. Peak to Total Ratios for Several Spectrometers

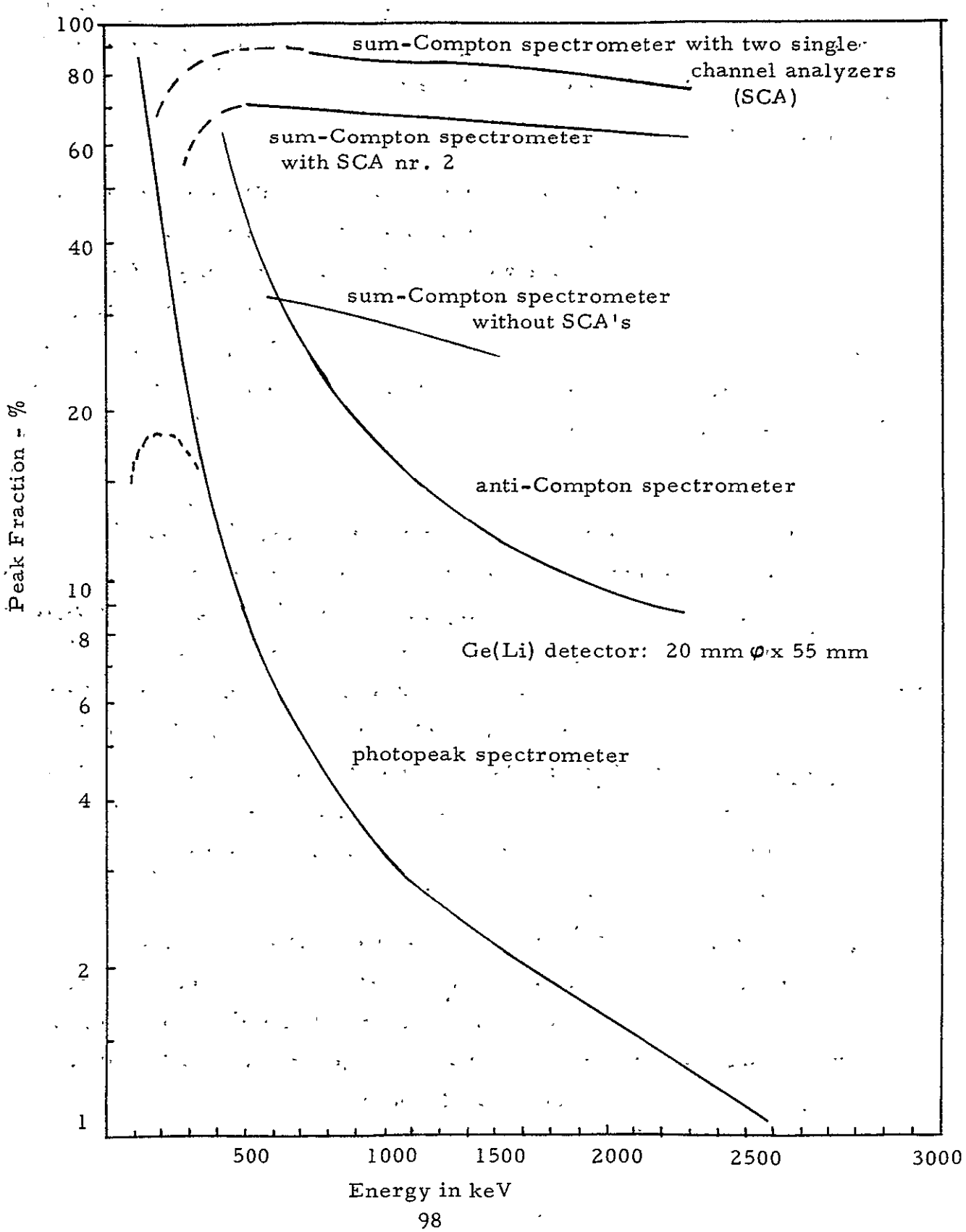

The anti-Compton spectrometer uses a large scintillation detector surrounding a small semiconductor or scintillation detector. The signals are in anticoincidence and with the gamma radiation collimated onto the small detector, a large fraction of the Compton events are negated, and the peak to total ratio is improved. This type of spectrometer is unsitable for the subject measurements because the anti-coincidence annulus detector must be large.

The peak to total ratio of various sum-Compton spectrometers is also shown with various degrees of single channel energy selection for each single detector before slow coincidence is obtained. The peak to total ratio is obviously a function of the detector geometry also, but, in general, improvements of factors of 30 to 90 can be expected over the peak to total ratio of a photopeak spectrometer. We have also implied that most of the tail in a sum-Compton spectrometer is close to the energy of the peak, and consequently the effective peak to total ratio is larger than indicated provided the energy resolution requirement is not too restrictive.

The sum-Compton spectrometer has the above advantage but this is achieved at the expense of overall efficiency. The efficiency is reduced because only scattering events registering in both detectors are recorded. We have shown that geometric changes to increase the peak to tail ratio always decrease the total efficiency. We have also indicated that a sufficiently high efficiency is required to perform spectral measurements in short intervals once to overshadow the neutron induced accidental coincidence background. Even with a rather high efficiency of 4 percent to a gamma fission spectrum, the coincident count rate of a sum-Compton spectrometer is limited to about 10^4 sec^{-1}, because the singles rates would exceed 10^5 sec^{-1}, which approaches the maximum capability of present day gamma spectral analysis. Therefore, a single photopeak spectrometer would have the advantage of being able to count at perhaps a rate of ten times faster, with subsequently better statistics at the high energy part of the spectrum. In addition, if the single detector was a scintillation detector, cryogenic cooling would not be required. However, some cooling is beneficial in reducing the

photomultiplier table noise. Temperature stability is required as typically, a photomultiplier response change is -0.2 percent per degree Centigrade.

A list of a few scintillation materials and their properties is shown in Table 8.6. Of these, CsI (Na) is superior for this study application. First, the cesium iodide is a high Z material and with high density will be closer to a total absorption gamma spectrometer, although low peak to tail ratios would be obtained above 500 keV. Secondly, less energetic neutron recoil pulses would be obtained because of the massive nuclei. Thirdly, the short light pulse duration will enable one to accumulate data a a rate limited by the electronics and not the detector.

Table 8.6. Selected Scintillator Detector Materials

Scintillator	Density	Relative Light Output (%)	Light Decay Constant (sec)
NE102 plastic	1.03	65	2.2×10^{-9}
NE901 glass	2.6	28	7.5×10^{-8}
Anthracene crystal	1.25	100	3×10^{-8}
NaI (Tl) crystal	3.67	230	2.3×10^{-7}
CsI (Na) crystal	4.51	150	0.65×10^{-9}
CsI (Tl) crystal	4.51	95	7.0×10^{-7}

Use of a single CsI (Na) scintillator is entirely feasible for the Compton attenuation spectrometer and is suggested as an alternate dtection method. Data unfolding will be necessary, but the total weight of the spectrometer head will be considerably less, and the electronic circuitry would be simplified and minimized.

We envision a cylindrical detector approximately 2 cm in length and 1 cm in diameter. Because of the much higher efficiency than the sum-Compton spectrometer, the collimated beam striking the Compton targets can be reduced to 0.2 cm^2 rather than the 1.5 cm^2 and only one detector system could be used. The widths of the tungsten shield can be reduced to 5 cm by 8 cm with the length comparable

to the present design (25 cm). This would weigh approximately 33 pounds, which is considerably lighter than the primary design. Thus, if the gamma spectral measurements are to be conducted in a space flight, the single crystal scintillation detector system should be given consideration. On the other hand, if the flight is a test flight requiring ballast, or a ground test is conducted at the Neveda test site, than the more precise but heavier sum-Compton spectrometer system should be considered.

8.6.2 Sum-Compton Scintillation Spectrometers

Sum-Compton spectrometers may be designed using scintillation crystals. In particular, a high energy spectrometer employing a CsI(Na) crystal as detector A and the annular detector B. The energy response should be similar to the germanium detector although slightly less efficient for the same detector length up to 2 or 3 MeV. Above 3 MeV, the CsI(Na) system should increase to about three times that of the germanium detector, because of the higher pair production cross section. As previously mentioned, CsI will have little response due to fast neutron recoils within the detector.

A low energy sum-Compton spectrometer composed of scintillators does not appear as favorable, however. Use of CsI, NaI or the other alkali halide scintillators as detector A would result in little energy response below 100 keV because of the high photoelectric cross sections. The use of a plastic scintillator as the detector A would yield good energy response down to low incident photon energies, but such a detector would be very sensitive to fast neutron proton recoil pulses. The hydrogen content in plastic scintillators is generally over 50 percent, and as the plastic recoils can have energies up to the incident neutron energy, many high energy neutron induced pulses would be observed.

The glass scintillators have mean atomic numbers and densities comparable to silicon, and therefore good energy response to low energies would be obtained and the neutron recoil induced signals would be comparable to silicon also. However, to detect incident 50 keV radiation by the sum-Compton technique, detector

A must resolve 8 keV recoil electrons. This is easily accomplished by most alkali halide scintillators, but is probably not practical with glass scintillators which produce in the order of only ten percent of the NaI(Tl) light output, and the 8 keV pulses would be buried in the phototube noise.

However, with exception to the low energy response, sum-Compton spectrometers can be designed using photomultiplier scintillator detector combinations. Because of the fast phosphor decay time of CsI(Na) and typical glass scintillators, fast coincidence circuitry ($\sim 10^{-8}$ sec) could be used and high count rates could be tolerated.

The rate response to fast neutrons for these scintillators would be similar to that indicated for semiconductor detectors. Assuming the same tungsten thickness and neutron attenuation as discussed in Section 5.4, sum-Compton scintillation detectors should be capable of operation in fast neutron fluxes up to 10^{9} cm^{-2} sec^{-1}. The fast neutron permanent damage to scintillation detectors has evidently not been studied. We have searched the literature, talked to various scintillator vendors and personnel at the ONRL, without obtaining any significant information in this area. We believe that the damage to be less severe than for semiconductor detectors by at least an order of magnitude.

The activation of CsI(Na) by thermal neutrons is computed to be some ten times greater than the thermal neutron activation of germanium. However, this is not considered a problem for either detector material for use in the design application.

Two photomultiplier tubes are required for each scintillation sum-Compton spectrometer. The RCA 8644 or 8645 are 0.755 inch diameter ten stage tubes of 3.8 inch total length. The General Electric Company has successfully flown these type tubes in radiation ablation measurements during reentry in the earth's atmosphere. However, for precise spectral measurements, the gain of the system must be maintained to more precision than in those measurements. The sensitivity of the photomultipliers is approximately one percent per volt, and with a supply

voltage of 1200 volts, one percent regulation could produce a 12 percent variation in overall gain, which is not considered sufficient.

The Harshaw Chemical Co. can supply scintillation detectors with traces of Am^{241} in the crystal. The Am^{241} produces an alpha peak corresponding to a gamma energy of 3.15 MeV, and this peak may be used to electronically regulate the gain of the entire detector system. The Am^{241} source produces only a small background in other regions of the spectrum. Other isotopes producing peaks elsewhere could also be considered for imbedding in the crystals. The Am^{241} source is practical for a low energy sum-Compton spectrometer, but the peak would be in the center of a high energy spectrometer spectrum.

We believe that satisfactory sum-Compton spectrometers could be designed using scintillation detectors, although response down to 50 keV may not be achieved. However, it is not anticipated that any weight saving would be accomplished over the semiconductor design described in this report. The need for cryogenic temperature operation would be eliminated, but it is thought that the semiconductor design is the better choice.

8.6.3 Cadmium Teluride Detectors

There is great interest in semiconductor materials for gamma radiation detectors that can be operated at room temperature and also provide higher atomic weights than germanium and silicon. Cadmium teluride is the most promising of the several materials that might some day meet these requirements. Much progress has been made in improving the CdTe response in the last couple of years, but as yet, the properties are not suitable for good gamma spectroscopy.

CdTe may be operated at temperatures from -100 °C to +100 °C, and with an effective atomic number of 50, resembles the familiar NaI(Tl) scintillation crystal in absorption coefficients program. The density is greater than NaI, and a larger overall efficiency is, therefore, obtainable than with NaI.

The difficulty with present grade CdTe is that the mean free path of the created holes is essentially zero, and the mean free path of the electron carriers is relatively short. Thus, two conditions arise depending on the depletion depth of the detector. If the depletion depth is shorter than the electron mean free path, than signal pulses are generated with amplitudes proportional to the depth of the interaction as well as the radiation energy absorbed. On the other hand, if the depletion depth is longer than the mean free path, only those events farther than one mean free path from the anode will create full energy peaks and those closer will contribute to a tail. This is all due to the fact that the holes and the electrons do not together traverse the full depletion depth of the detectors. In addition, depletion depths of perhaps 2 mm is the present state of the art for CdTe, although with continuing improvements, these detectors may some day be suitable for gamma ray spectroscopy.

SECTION 9.0
THE SUGGESTED DESIGN

This study has concluded that the Compton attenuation technique is the only practical method of performing the gamma ray spectral measurements. Several detector types may be used in the Compton attenuation spectrometer, but we have designed around semiconductor sum-Compton detectors. This selection is in accordance with exhibit "A" II-g of the study contract, "The accuracy obtained must be greater than that obtainable by the present methods of measuring gamma photon spectra."

9.1 THE SUM-COMPTON SPECTROMETER CIRCUITRY

The essential functions of the electronic circuitry are shown in block diagram form in Figures 9.1 and 9.2

Detectors A and B for the sum-Compton configuration are dc biased to approximately 500 volts through a resistance (not shown) to the bias supply. A capacitor, also not shown, is used to ac couple the FET charge sensitive preamplifier to the detector, and the detector to preamplifier distance should be as short as practical. The conventional feedback loop of preamplifier is through R_1 and C_1; and for good stability at high counting rates, $t = R_1C_1$ should be approximately 10^{-5} seconds. Additional wave shape clipping is obtained from the reflected pulse from the shorted delay line D_1. D_1 is not intended to provide a dc path to ground, and the reflected pulse should terminate in approximately 5×10^{-7} seconds after the pulse rise. Note that this time interval is determined by the charge collection time for the detectors, which should approximate 2×10^{-7} seconds for the detector sizes under consideration. This delay line clipping is normally accomplished in the main linear amplifier, but is thought necessary for preamplifier stability at high count rates. Additional voltage and power gain, other than the charge to voltage conversion, will be provided in the preamplifier, so that the linear amplifier may be located some distance away.

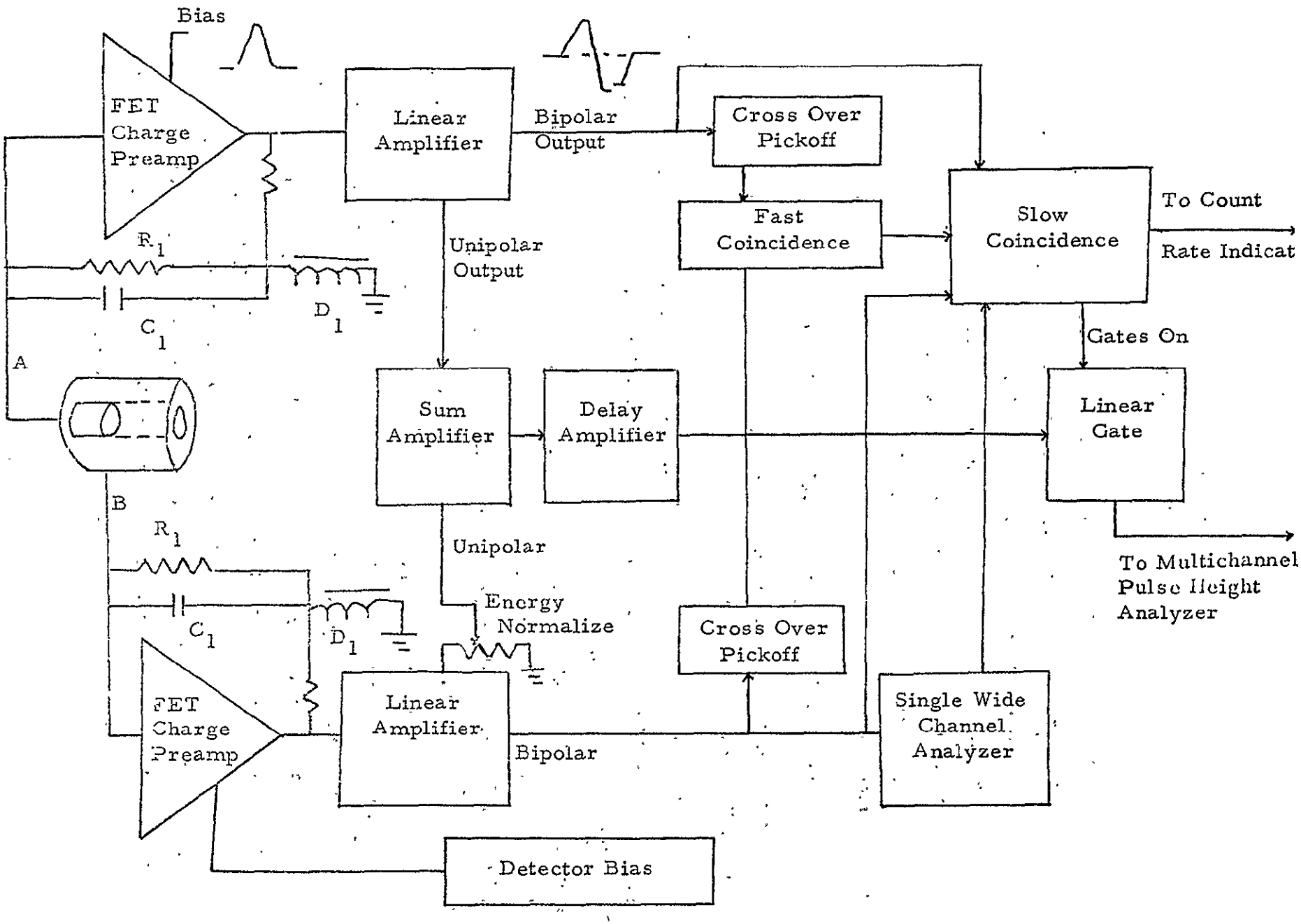

Figure 9.1. Sum-Compton Gamma Spectrometer Functional Diagram

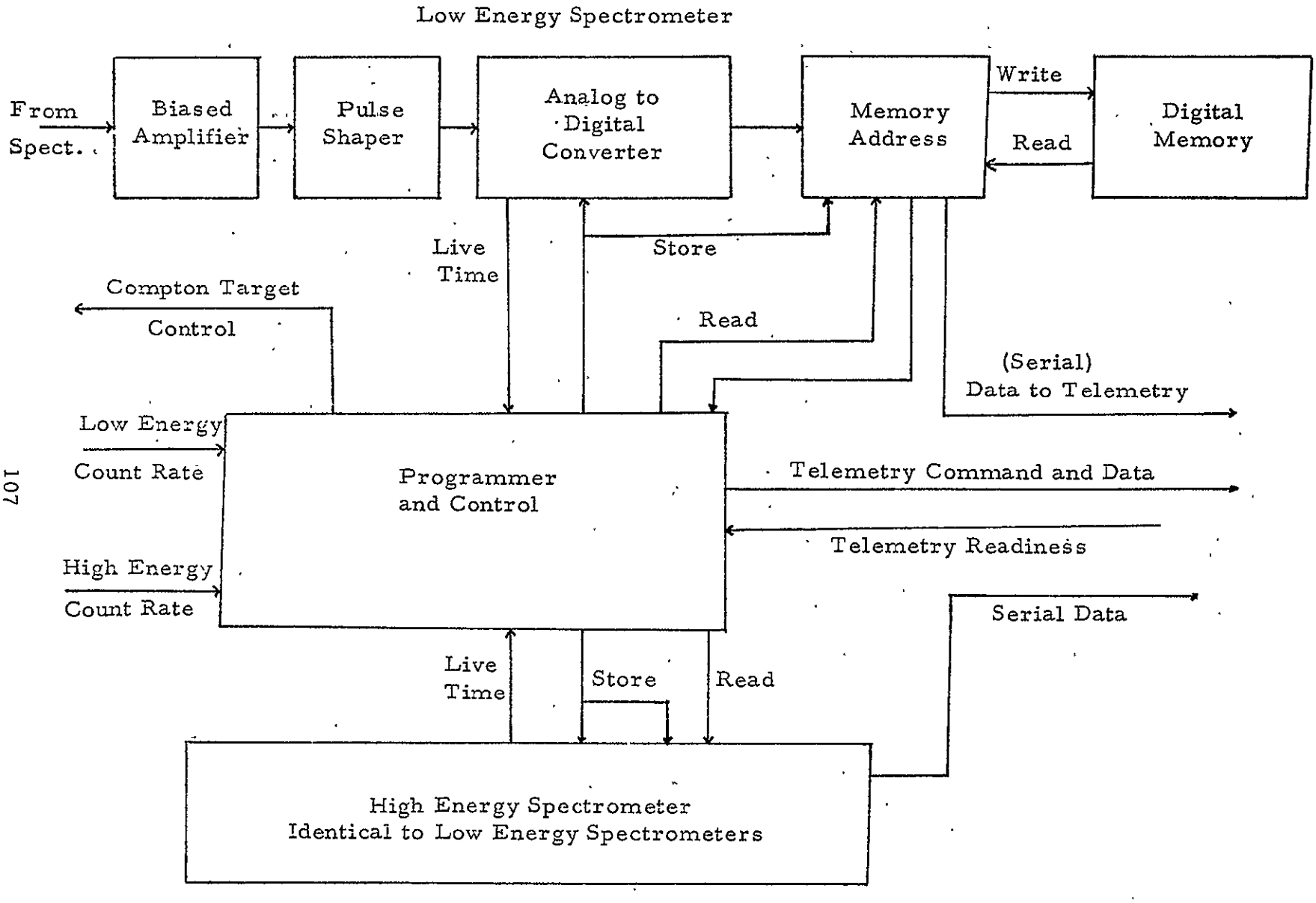

Figure 9.2. Data Acquisition and Telmetry Control Functional Diagram

The linear amplifier is considered a standard delay line nonoverloading type, although the first delay line is incorporated in the preamplifier. The unipolar pulse is amplified in the first stage and routed to the sum amplifier. The later stage of the linear amplifier uses an identical delay line to D_1 to provide a bipolar output. Bipolar pulses are provided to a cross over pickoff for precise timing, and fast coincidence timing.

The unipolar output of the detector B linear amplifier is gain adjustable so that differences in the electron-hole pair creation energy of detectors A and B may be normalized. This is particularly necessary if the detectors are silicon and germanium. This is a laboratory adjustment, and once established for a given detector pair, should not be changed.

The sum amplifier performs the addition of the energy pulses from the two detectors. This sum is delayed and presented to the linear gate. The linear gate passes the summed pulse provided all conditions of fast and slow coincidence are met, and does not pass the pulses of these conditions are not fulfilled.

A single channel analyzer is provided in the detector B chain of electronics. The scattered radiation has a particular energy band, and this permits reduction of accidental coincidence signals. For instance, the low energy spectrometer energy width would be 40 keV to 400 keV and the high energy spectrometer 150 to 550 keV, for the B detector.

The output of the linear gate consists of the summed energy pulses and are analyzed. The count rate from the slow coincidence circuitry may be used to determine the Compton target mass and to trigger the multichannel pulse height analyzer for accepting pulses from the linear gate.

Figure 9.2 shows functions of data analysis and control circuitry. The bias (threshold) amplifier may be set to reject pulses below a particular amplitude, such as 50 keV for the low energy spectrometer and 500 keV for the high energy spectrometer. The pulse shaper is used to stretch the pulses, occurring at a

maximum rate of 10^4 sec^{-1}, to shapes more easily analyzed. The analog to digital converter, address circuitry and digital memory are conventional components of multichannel analyzers. A live time clock is also conventional and assures that the data accumulated is proportional to the flux rate by compensating for time last in analysis.

The programmer is similar to conventional types found in most MCPHA equipment. The additional functions of measuring the count rates and selecting the Compton target from these rates is necessary. Rotation of the permanent magnet stepping motor is commanded digitally as described by Chlarella[64]. Other functions of the programmer include telemetry interfaces.

It is suggested that commercially available electronic circuitry be used in the development model of the spectrometer. These could include, but are not limited to, modified ORTEC 117 preamplifiers, ORTEC 410 bipolar amplifiers, ORTEC 415 sum amplifiers and TMC 353 detector bias supplies. Zero crossing pickoff units, fast and slow coincidence circuitry, and linear gates are all readily available.

9.2 THE MECHANICAL DESIGN

The mechanical design of a Compton attenuation spectrometer utilizing two sum-Compton spectrometers is shown in Figure 9.3. Each detector configuration is mounted on a tungsten cold finger to reduce scattered radiation from the back. A single CO_2 cryostat is shown.

The total weight of the spectrometer head is expected to weigh 130 pounds. This is rather large, but presumably the gamma measurements would be made only on a test flight, where ballast may be necessary.

The boral shield is to absorb the major portion of the thermal neutrons. Note that this shield terminates beneath the plane of the low energy spectrometer. This is so the boral is not a source of gamma scatter into the detectors. The shield design is to present a shadow shield to the gamma and neutron radiation,

and ever attempt to confine structure inside the shield perimeter. The cryostat is the single exception, and the tungsten cold fingers should reduce the scattered gamma radiation from this source.

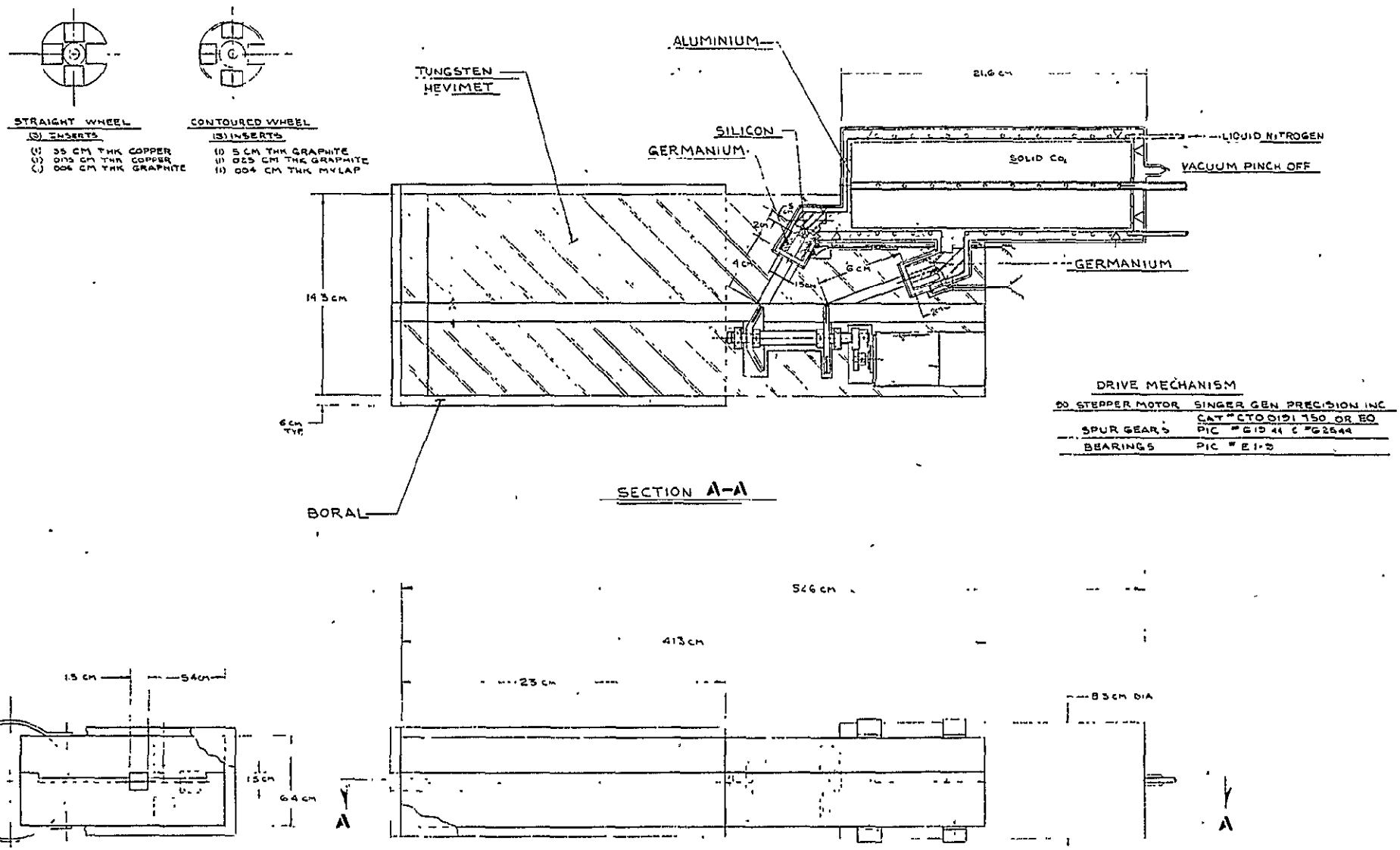

Figure 9.3

REFERENCES

1. Siegbahn, Kai, ed. Alpha, Beta and Gamma-Ray Spectroscopy, Vol. I and II, North-Holland Publishing Co., Amsterdam, 1965.

2. Evans, R. D., The Atomic Nucleons, McGraw Hill Book Co., New York, 1955.

3. Rutherford, E. and Andrade, E., Phil. Mag. 27 (1914).

4. Rutherford, Chadwick, and Ellis, Radiation from Radioactive Substances, Cambridge Union Press, 1951.

5. Hofstader, R., Phys. Rev. 74, p 100 (1948).

6. Geiger, H. and Muller, W. Phys. Zeit 29, p 839 (1928).

7. Geiger and Klemper, Zeits f Physik 36, p 364 (1926).

8. Mann, H. M. and Haslett, J. W., ANL 6455, 23 (1941), Lithium Drifted p-i-n Junction Detectors.

9. Handbuck Der Physik, XLV, p 86, Springer Verlac, Berlin, 1958.

10. First Conference in Scintillation Counters and Crystal Counters, Univ. of Rochester (1948) AECU-137.

11. Second Scintillation Counter Symposium, Oak Ridge (1949), AECU-583.

12. Third Scintillation Counter Symposium (1952), Nucleonics 10.

13. Fourth Scintillation Counter Symposium (1954), Nucleonics 12, No. 3.

14. Fifth Scintillation Counter Symposium (1956), IRE Trans. on Nuc. Sci., NS-3, No. 4.

15. Sixth Scintillation Counter Symposium (1958), IRE Trans. on Nuc. Sci., NS-5, No. 3.

16. Seventh Scintillation Counter Symposium (1960), IRE Trans. on Nuc. Sci., NS-7, No. 2, 3.

17. Eighth Scintillation and Semiconductor Counter Symposium (1962), IRE Trans. on Nuc. Sci. NS-9, No. 3.

18. Ninth Scintillation and Semiconductor Counter Symposium (1964), IEEE Trans. on Nuc. Sci., NS-11, No. 3.

19. Tenth Scintillation and Semiconductor Counter Symposium (1966), IEEE Trans. on Nuc. Sci., NS-13, No. 3.

20. Eleventh Scintillation and Semiconductor Counter Symposium (1968), IEEE Trans. on Nuc. Sci. NS-15, No. 3.

21. 1970 Twelfth Scintillation and Semiconductor Counter Symposium, IEEE Trans. on Nuc. Sci. NS-17, No. 3.

22. Albert, R. D., Rev. Sci. Inst. 24, p 1096 (1953).

23. Bell, P. R., Science 120, p 625 (1954).

24. Hofstadter, R. and McIntyre, J., Phys. Rev. 78, p. 619 (1950).

25. Weinzierl, P. and Tisljar-Lentula, G., Nuc. Insts. and Methods 3, p 177, (1958).

26. Hick, H. and Peplink, R., Nuc. Inst. and Methods 68, p 240 (1969).

27. Ewan, G. and Tavendale, A., Nuc. Inst. and Methods 26, p 183 (1964).

28. Johansson, S., Nature 166, p 794 (1950).

29. Bair, J. and Mucenschein, F., Rev. of Sci. Inst. 22, p 343 (1951).

30. Sicmisson, F. and Kantele, J., Nuc. Inst. and Methods 58, p 229 (1968).

31. Heath, R. L. TID-4500 (31st ed.) Phillup Petroleum Co., Idaho Falls, Idaho.

32. Rosetta, K., Farukh, M., Kramer, Swinehart, and Hofstadter, IEEE Transactions on Nuc. Sci. 17, p 89 (1970).

33. Pell, E., Nat. Acad. of Sci. Report NAS-NSS-32, p 136 (1961).

34. Mayes, J., IEEE Trans. on Nuc. Sci. NS-9, p 135 (1969).

⊕3

35. Elliot, J., Nucl. Inst. and Methods 12, p 60 (1961),

36. Goulding, F., IEEE Trans. on Nuc. Sci. NS-11, No. 3, p 177 (1964).

37. Kramer, H., and Chase, R. L., IEEE Trans. on Nuc. Sci. NS-15, No. 3, p 381, (1968).

38. Sayres, A. and Baicker, J., ibid, p 393.

39. Palms, J., Wood, R., and Puckett, O., ibid, p 397.

40. Dearmaley, G., and Whitehead, F., Nuc. Inst. and Methods 13, 1 205 (1961).

41. Klingsmith, R., IRE Trans. on Nuc. Sci. NS-8, p 112 (1961).

42. Gibson, W., Thomas, and Miller, Phys. Rev. Letters 7, p 65 (1961).

43. Jones, C., NASA/Marshall, private communication.

44. McMaster, H., Kerr, N., Mallett, J., Hubbel, J., Compilation of X-Ray Cross Sections, UCRL-50174, Sec. II (TID-4500)

45. Grodstein, G., X-Ray Attenuation Coefficient from 10 keV to 100 MeV, Nat. Bur. Std. Cir. 583.

46. Klein, O., Nishina, Y., Z Physik 52 (1929), p 853.

47. Bewilogua, L., Physik K, 32, (1931) 740.

48. Moon, P., Proc. Phys. Soc. 463 (1950), p 1189.

49. Franz, W., Z Physik 95 (1935), p 652.

50. Maienschem, F., Peele, R., Zubel, W., Love, T., Proc. of the 2nd U.N. Int. Conf. on the Peaceful Uses of Atomic Energy 15, P670 (Geneva, 1958), p 366.

51. Crold, R., Nuc. Inst. and Methods, 84.

52. Hall, R., IEEE Trans. Nuc. Sci. 17, 3 (1970), p 235.

53. Kramer, H., Chassman, C., and Jones, K., Nuclear Inst. and Methods, 62 (1968), 173.

54. Chassman, C., Jones, K., and Ristinen, R., Nuclear Inst. and Methods, 37 (1963) 1.

55. Rockwell, T. ed., Reactor Shielding, D. VanNostrand Co., Princeton, N.J., p 7.

56. Modular Nuclear Vehicle Study, Phase IV, LMSC/A960352, Dec. 1969.

57. Spencer, L. and Fano, U., J. Research National Bur. Standards, 46, p 446 (1951).

58. Martini, M., McMath, F., and Fowler, I., IEEE Trans. on Nuc. Sci., N517, 3, p 139 (1970).

59. Sakai, E., and Malm, H., Applied Phys. Letter, 10, p 268 (1967).

60. Sakai, E., Malm, H., and Fowler, I., Semiconductor Nuclear Particle Detectors and Circuits, Eds. Wil. Higgenbotham, G. L. Miller, and R. L. Chase, Nat. Acad. Sci. Pub. 1593 (1969).

61. Martini, M., and McMath, T., Nuc. Inst. and Methods, 76, 1 (1969).

62. Mayer, J., Zanio, K., Martini, M., and Fowler, I., IEEE Trans. on Nuc. Sci. NS17, No. 3, p 221.

63. Bell, R., Hemmat, N., and Wald, F., IEEE Trans. on Nuc. Sci. NS17, No. 3, p 241.

64. Chlarella, L. J., Machine Design, 42, 29, November 24, 1970, p 84.